Electrical characterization of polymer-PCBM solar cells

Kramer, J.M.

Award date:
2005

Graduation report

Electrical characterization of polymer-PCBM solar cells

Jan Maarten Kramer
431205
M2N, August 2005

Supervisors:
M.Kemerink
H.H.P.Gommans
R.A.J.Janssen

Summary

Polymer solar cells look promising but have only an efficiency of 5%. The PPV/PCBM solar cell is electrically characterized in this research.

PPV is a conjugated material that conducts holes. Under illumination the light will cause electron-excitation in the PPV from the HOMO to the LUMO. Because of the lower LUMO of PCBM, the electrons will be transferred to the PCBM, decreasing the chance of recombination. With the contact materials aluminum and PEDOT:PSS the electrons and holes will drift to the electrodes.

Samples are made of an ITO layer, a PEDOT:PSS layer, an active layer of PPV, PCBM or a blend of these, an optional 1nm LiF layer and an aluminum layer. The samples are reproducible. Research is done with IV-measurements and impedance spectroscopy, in the dark and under illumination at different temperatures.

A cell consisting of pure PPV is still working as a solar cell. At high voltages double carrier injection occurs. PCBM does not react on light. Double carrier injection is possible above the built-in voltage.

Some of the properties of the blend can be understood from the properties of the pure materials. For the permittivity, the blend is higher than both the components. For the mobility, the blend is more than the sum of the components, bipolar conduction.

The behavior of the blend on traps and double carrier injection for different temperatures cannot be understood from the behavior of the pure materials. Only the effect that double carrier injection occurs up to higher frequencies can be expected because PPV is expected to conduct better in the blend.

In terms of the injection barriers the blend is the combination of the pure materials. LiF does not change the possibility in describing the blend as a sum of the PPV and the PCBM. LiF does decrease the Fermi-level of the Al, making the band-gap smaller.

Combining the drift-diffusion equation, Poisson's equation, the Einstein relation and detailed balance we can determine an analytical model for the temperature dependent built-in potential. Measured built-in voltages fit very well with this model.

Contents

Chapter 1: Introduction

1.1: Polymer solar cells

The demands for energy are still increasing. This while it will get a problem to satisfy even today's demand with fossil sources[1,2]. Therefore other sources of energy are explored. Solar cells are available yet but do not contribute more than a few percent of the demand. The manufacturing of the cells is expensive. Better cells are needed. A promising direction for cheap solar cells are the polymer solar cells, made of conjugated polymers[3]. Therefore, and because of scientific interest, research is done on a specific polymer solar cell.

Since the discovery of the luminescent properties of PPV (poly (p-phenylene vinylene)) there has been an increasing interest for its application in devices as light emitting diodes and solar cells. This is because of a unique combination of properties that has demonstrated its potential in a number of applications that is still increasing[4]. Its most important feature is the combination of solubility and the semi-conducting or metallic electronic structure.

Today, one of the best polymer solar cells consists of poly (phenylene vinylene) PPV in combination with the conducting PCBM. The research will be done on this solar cell. The efficiency of this cell however is only 3%[5], what is less than inorganic solar cells. To compete with inorganic cells, the efficiency must be improved. PPV is the photoactive material in the PPV/PCBM solar cell. Under illumination the light will cause electron-excitation from the highest occupied molecular orbital (HOMO) to the lowest unoccupied molecular orbital (LUMO). Because the LUMO of PCBM lies below that of PPV, the electrons will be transferred to the PCBM. Once an electron is transferred to the PCBM, the chance that it will recombine with a hole has become very small. With well-chosen contact materials, in this research aluminum and PEDOT:PSS, the electrons and holes will drift to the electrodes because of the resulting built-in field.

1.2: Research goal

Up till now, many investigations have been done to optimize this particular cell[6]. The transport on the micro level is yet not fully understood. A series of questions arise from the way the PPV/PCBM solar cell works. What are the effects of the mixing of PCBM and PPV? What effect does this have on the permittivity and the mobility? Will traps be filled and if so, how is this a sum of those two materials? With PPV a hole conductor and PCBM an electron conductor, the blend conducts both. But is this simply a sum of those two? What will happen to the band-alignment, that is the level and course of the HOMO and LUMO? Adding LiF has an improvement on the performance. How does this happen?

To answer these questions, this research is done. IV-measurements are done at different temperatures to learn about the mobilities and band alignment via the built-in potential. To determine the permittivity and traps impedance spectroscopy is done. With impedance spectroscopy the different effects like trapping and double carrier injection can be discriminated for all have their specific reaction times. All these measurements are done with and without LiF so they can be compared.

This report is set up in a similar way: chapter two discusses the theory, chapter three explains the experimental set-up and chapter four discusses preliminary measurements about the reliability of the set up and some interesting effects that are caused by the set-up. Chapters five and six deal with the measurements of the cell with only PPV and only PCBM respectively, followed by chapter seven that deals with the blend. Chapter eight is about the effect of LiF. The IV-measurements of chapters five to eight led to a theory of the temperature dependence of the built-in potential. This theory is discussed in chapter two, and compared with the measurements in chapter nine. Chapter ten gives a short discussion on in what extend the blend can be assumed as the sum of the materials.

The characterization as described above will give quantitative results about the mobilities and more qualitative trends.

Chapter 2: Theory

2.1: Conjugated polymers

An introduction will be given about the properties of conjugated materials. The C atom in the ground state has an electron-configuration of $1s^2 2s^2 2p^2$. This means that there are four electrons in the outer electronic orbitals. If this atom forms one or more bonds with other molecules the outer electrons may form sp, sp^2 or sp^3 orbitals. sp^2 has one unhybridized p_z orbital. If the neighbor atom is a C-atom with the same hybridization, these orbitals may form a molecular bonding π and an anti-bonding π^*. In combination with the σ-bond between the two C-atoms, created by two hybridized sp^2 orbitals, this results in a double bond between the two C-atoms[1]. It is possible to form a chain of C-atoms with a single-bond double-bond structure as drawn in figure 2.1. The positions of the single and the double bond may be exchanged without changing the energy of the molecule. This is called a conjugated structure. A simple and well-known example is the benzene molecule with a delocalized electron cloud around the carbon ring structure. The π-electrons dominate the electronic properties of these molecules and thus of systems made up by these molecules. Because the σ-bonds remain stable on introduction of electrons and holes and during the transition of electrons from the π to the π^* orbital, from the highest occupied molecular orbital (HOMO) to the lowest unoccupied molecular orbital (LUMO), the molecular structure remains stable[2].

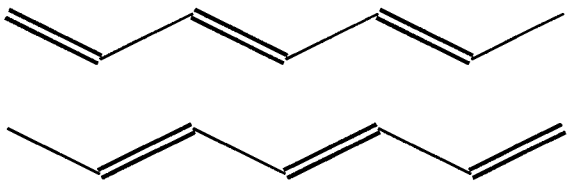

Figure 2.1: *the chemical structure of polyacetylene in the twofold degenerate ground state*

If an electron is removed from the conjugated polymer, the remaining hole can easily move from one location to another as shown in figure 2.2. This delocalization results in a (semi-) conducting polymer: the charge can easily be transported within the molecule.

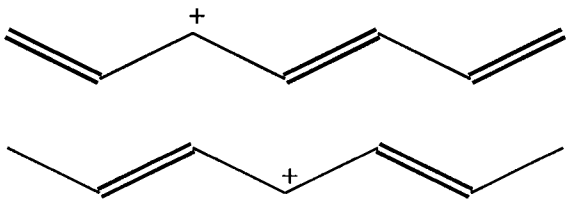

Figure 2.2: *the chemical structure of excited polyacetylene in the twofold degenerate ground state; the charge is transported within the molecule*

In macroscopic structures, the conductivity however is not dominated by the conductivity within the polymer molecule. Depending on the system, the molecules may be organized in a disordered way. Within the disordered polymer groups of polymers may form relatively well-ordered structures or domains. Charge transport within such a domain is easier than from one domain to another. The transport takes place by activated tunneling of charges from one site to another and is called hopping. This transport dominates the electrical properties and is influenced by a macroscopic disorder-term. The disorder-term includes many phenomena. For example the dispersion in the molecular structure, the length of the conjugated materials, the morphology, defects and impurities are such phenomena[3]. However, if the investigated samples are big enough, similarly prepared samples will behave similarly on a macroscopic scale[4].

2.2: Polymer Light Emitting Diode

Conjugated polymers can act as photonic devices; amongst others as light-emitting diodes, photo detectors and solar cells[5]. The pLED, the photo detectors and the solar cells consist of an active layer between two electrodes. The pLED is the simplest photoactive device and will be discussed here. If the electrodes are different, the diode has a built-in potential: below this potential only a small leakage-current is possible. This built-in potential will be discussed first.

Every material has a number of discrete energy levels. At 0K these energy levels are filled with electrons up to the Fermi-energy E_F. The energy up to which the energy bands are filled is called the work function. The Fermi-energy can correspond with one of the energy levels; this

occurs as one of the levels is only partly filled. This is the case in a metal. If at 0K all levels are completely filled or completely empty, the material is an isolator or semi-conductor. In isolators and semiconductors the HOMO and LUMO levels are respectively several and a few eV apart.

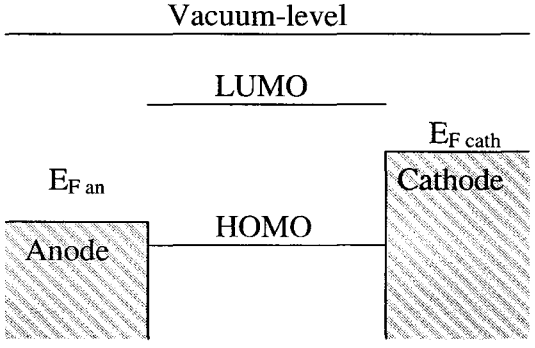

Figure 2.3a: *the active layer between two not-connected electrodes (i.e. at the built-in potential)*

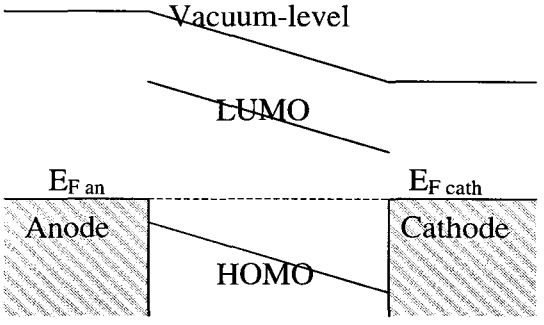

Figure 2.3b: *the active layer between two connected electrodes at V=0*

Figure 2.3 shows the idea of the term built-in potential. It shows the active energy-bands. When the electrodes are not connected all materials have their own specific work functions in relation to the vacuum level, as can be observed in figure 2.3a. The Fermi-level is between the HOMO and the LUMO and not close to either one of them. When the electrodes are connected, and no voltage is applied, there should be no current. So, the electrodes must have the same E_F. The E_F of the cathode drops in comparison to that of the anode, as can be observed in figure 2.3b. If a voltage is applied the energy levels of the electrodes will change in comparison to each other. The built-in potential is defined thus that at V_{bi} the level of the active layer is again a flat band. Figure 2.3a shows both the not-connected situation as the connected situation with a voltage applied of V_{bi}. Above this V_{bi} injected electrons can drift from the cathode to the anode and holes from the anode to the cathode contact because of the created electrical field. Below this voltage only a leakage current will flow because the effective field is in the wrong direction[6]. This is the explanation of the built-in voltage, though the situation sketched here is simplified. A more detailed description will be given in paragraph 2.5.

The behavior as a pLED is schematically drawn in figure 2.4. The pLED is a photoactive layer and two electrodes. Above the built-in potential the electrodes inject carriers because of a voltage, and these carriers recombine creating a photon.

The electrodes are chosen to minimize the barrier for charge-injection, for these barriers should be overcome to inject charges. If for an optimal performance the injection barriers are minimized the current will become bulk-limited instead of injection limited. Though the work function of a great deal of materials is known, it is difficult to predict the quantitative barrier. To determine the properties of a diode, the work functions can only be used as a rule of thumb. Photoemission spectroscopy has however proved that vacuum-level alignment is not generally valid. Moreover, for several materials, the precise work function is debated within a range of 0.2eV[7,8,9] or more.

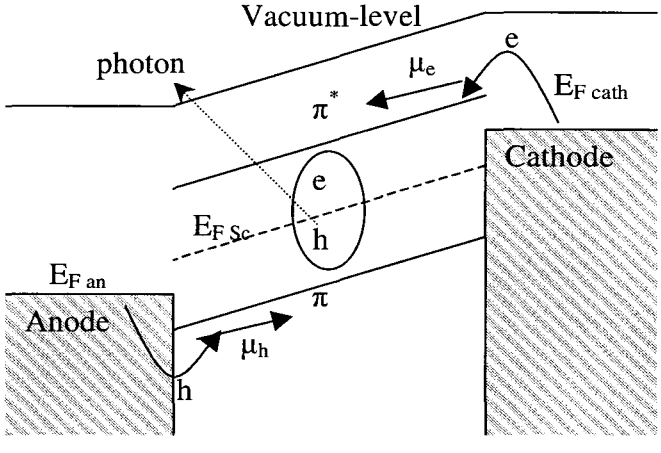

Figure 2.4: *schematic representation of the transport phenomena in a pLED: injection, transport and recombination; V is above V_{bi}*

2.3 Polymer solar cell

The solar cell also consists of an active layer between two electrodes. Instead of creating a photon with charge-recombination, accepting a photon for charge-separation is the driving force. One of the properties of an ideal solar cell is that it should absorb all photons and every photon should create an electron-hole pair. As a result of the created charges, there will be a current at V=0V. This situation is described in figure 2.5[10].

The photo-absorbent polymer that is used in this research is poly[2-methoxy-5-(3',7'-dimethyloctyloxy)-1,4-phenylene vinylene] (MDMO-PPV). The structure of this molecule can be observed in figure 2.6. The typical mobility for electron and hole transport in PPV has been determined to be 3×10^{-9} and 3×10^{-7} cm^2/V s at zero electric field and room temperature[11].

To improve the performance as a solar cell the possibility of decay must be reduced. Therefore PPV is mixed with another material that easily accepts one of the carriers. When the electrons are separated from the holes because they are in different molecules, their recombination will decrease. This situation is shown in figure 2.8. In this research, an electron acceptor material is added: 1-(3-methoxycarbonyl)propyl-1-phenyl-[6,6]-methanofullerene (PCBM). The structure of this molecule can be observed in figure 2.7. The energy difference between the LUMO of MDMO-PPV and PCBM is about 1 eV[7,8,10]. The optimum in donor-acceptor ratio for this charge transfer process depends on the phase separation of the materials and the exciton size and diffusion length in MDMO-PPV[12]. The film-thickness is also very important because it influences the absorption and the charge transport. Such a cell consisting of a blend of various materials is named bulk heterojunction solar cell. The cell consisting PPV and PCBM with all energy levels is shown in figure 2.9[7,8,9].

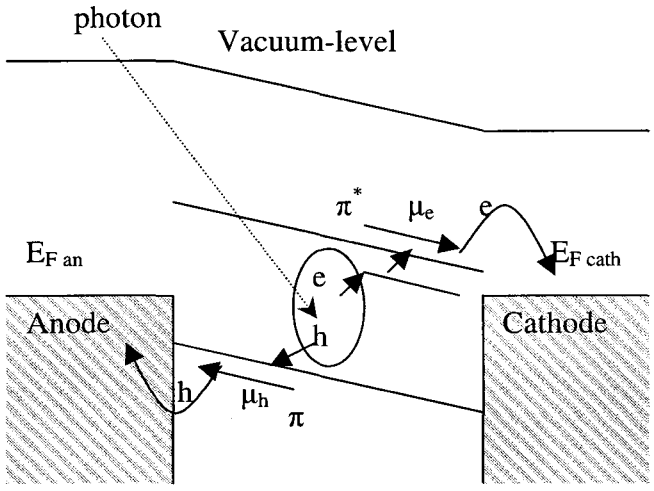

Figure 2.5: *the solar cell, V=0V. An incoming photon creates an electron-hole pair. The electron goes to the excited state, and then to the LUMO where it drifts towards the cathode; the hole vice versa*

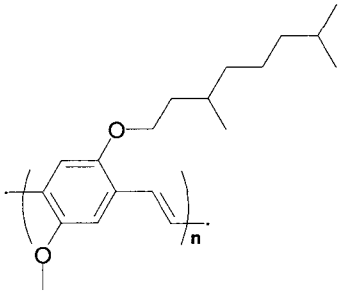

Figure 2.6: *Chemical structure of MDMO-PPV*

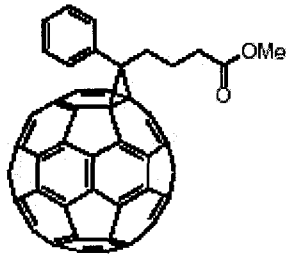

Figure 2.7: *Chemical structure of PCBM*

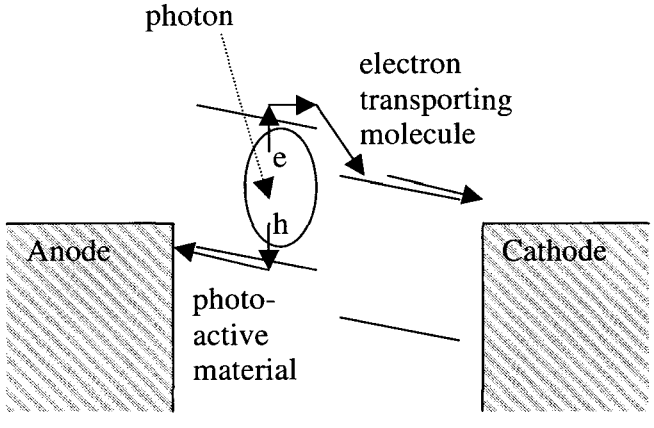

Figure 2.8: *the effect of mixing with an electron transporting material; the electrons and holes are transported by different materials and therefore cannot recombine*

The photoactive layer should be chosen to match the solar spectrum. Because this spectrum is fairly broad, the efficiency can be increased combining more materials with a variety of bandgaps in order to cover as much of the spectrum as possible. The choosing of the bandgap has a great effect on the efficiency: a small bandgap will only absorb photons with low-energy and therefore produce little energy; a bandgap that is too big will absorb almost no photons[13]. In this research MDMO-PPV is the active polymer that makes the photon-absorption. PPV has a bandgap of 2.2 to 2.5eV[7,8].

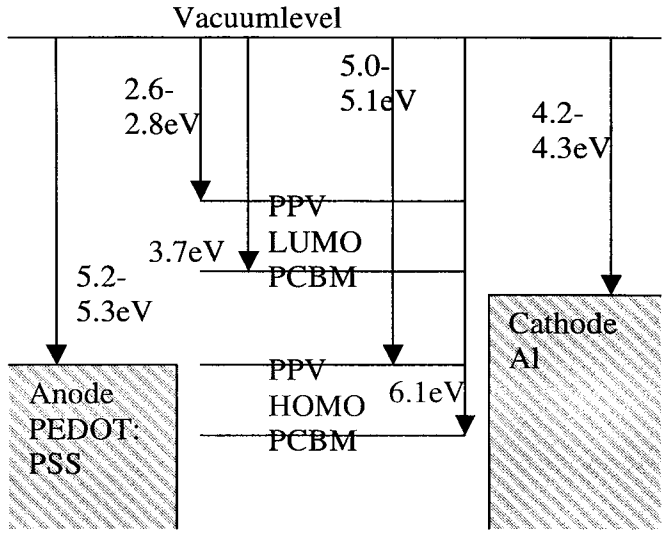

Figure 2.9: *the polymer solar cell consisting of PPV and PCBM in band diagram; the anode and the cathode are not connected*[7,8,9]

After the creation of the electron-hole pair the electron and the hole should escape their coulomb potential and be transported to the electrodes. This migration leads to an electric field opposing the "original" open circuit field. This will reduce the "original" field up to a certain distance from the electrodes. This effect is drawn in figure 2.10. As both charge carriers will reach the opposing electrodes a continuous current flow is created. The resulting electric field in the polymer layer depends thus the free electron and hole concentration, their drift and diffusion mobility. In the description so far charge transfer has been represented as an irreversible process. In reality there is a finite probability that free charge carriers again form an exciton. In fact, this does limit the efficiency at low bias[14]. Only charges that reach the electrodes and do not recombine in the active layer give a contribution to the actual current. This means that we should take the recombination into account.

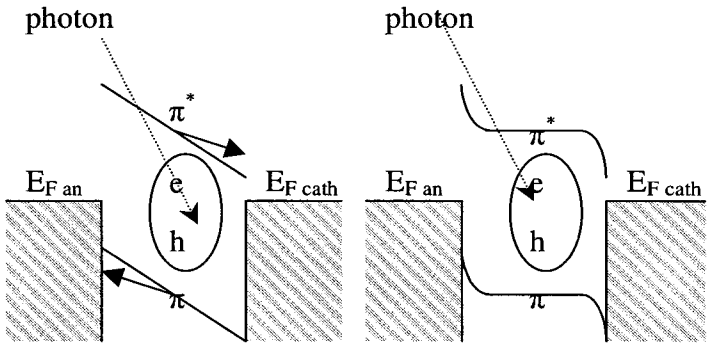

Figure 2.10: *the change in band alignment because of charge transport*

2.4: Transport

In a LED the electrons and holes should be transported through the active layer to combine and form a photon. In a solar cell the created electrons and holes should be transported to the electrodes. The transport processes are described qualitatively in the previous sections. Here, a more quantitative approach will be made.

Charge transport is due to drift, which is caused by the electric field, and diffusion because of density gradients[15]. For one carrier, the dependence of the current can be described with:

$$J = e\mu nE - eD\frac{\partial n}{\partial x} \qquad (2.1)$$

J: current density (A/m^2)
e: proton charge, $1.602*10^{-9}C$
μ: mobility (m^2/Vs)
n: charge-density (m^{-3})
E: Electric field (N/C or V/m)

D: diffusion constant (m^2/s)
x: position (m)

The electric field and the charge density are related by Poisson's equation:

$$\frac{dE}{dx} = \frac{1}{\varepsilon_0 \varepsilon_r} en(x) \tag{2.2}$$

ε_0: permittivity in vacuum, $10^7/4\pi c^2$ (C^2/Nm^2)
ε_r: relative permittivity of the material

If the material is bulk limited and not injection limited, and diffusion is ignored, a common approximation for an ohmic contact is E(x=0)=0. If the mobility is constant the current because of a single carrier can be described with[16]:

$$J = \frac{9}{8} \varepsilon_0 \varepsilon_r \mu_{n,p} \frac{V^2}{L^3} \tag{2.3}$$

n,p: electrons, holes
V: voltage (V)
L: distance between the electrodes (m)

This is the space-charge limited current. The width of the energy bands at finite temperatures determine the mobility according[17]:

$$\mu = C * \exp\left(-\left(\frac{3\sigma}{5kT}\right)\right) \tag{2.4}$$

C: material constant (m^2/Vs)
σ: band-widening constant (J)
k: Boltzmann constant, $1.380*10^{-23}$J/K
T: temperature (K)

In the formulas 2.3 and 2.4 no build-in potential is assumed. If there is a build-in potential, this should be taken as V=0, so V should be replaced with $V-V_{bi}$.

The Einstein relation, which is valid under Boltzmann statistics, relates the mobility and the diffusion constant:

$$\mu = \frac{eD}{kT} \tag{2.5}$$

For two carriers the drift-diffusion equation becomes:

$$J = \mu_n neE + \mu_p peE - eD_n \frac{\partial n}{\partial x} + eD_p \frac{\partial p}{\partial x} \tag{2.6}$$

$D_{n,p}$: diffusion constant for electrons and holes (m^2/s)
n,p: charge density of electrons and holes (m^{-3})

Taking into account the generation and recombination the charge density can be described with the continuity equation:

$$q\frac{\partial n}{\partial t} = -\nabla J + qG - qR \tag{2.7}$$

q: charge of a carrier, here -e for an electron, e for a hole (C)
n: charge density, both electrons and holes (m^{-3})
t: time (s)
G: generation ($m^{-3}s^{-1}$)
R: recombination ($m^{-3}s^{-1}$)

Where the generation can be described in a simplified way:

$$G = FP \tag{2.8}$$

F: flux of light ($m^{-2}s^{-1}$)
P: probability that a photon will be absorbed (m^{-1})

The simplest form for bimolecular recombination scales with the mobilities and the densities as stated in formulas 2.9 and 2.10[18].

$$R = \gamma pn \tag{2.9}$$

γ: recombination rate constant (m^3/s)

Where according to Langevin γ can be approximated by[19]:

$$\gamma = \frac{e}{\varepsilon_0 \varepsilon_r}(\mu_p + \mu_n) \tag{2.10}$$

2.5: Interface band-bending

As stated the description of the built-in potential in paragraph 2.2 is simplified: only drift is taken into account, where diffusion can be important as well. The situation is explained with figure 2.11. For the electron-injecting material, the cathode, electrons will diffuse from the metal to the polymer because of the large density gradient at the interface. This will create a charged interface: negative charges at the polymer part, positive at the metal part. At the hole-injection part the same process occurs, but with holes to the polymer and electrons to the anode. This will cause a change in the band at the "original" V_{bi}. This is called band bending[20]. This is shown in figure 2.11a. To reach flat-band conditions again, the "new" V_{bi}, the potential must be lowered. This is shown in figure 2.11b.

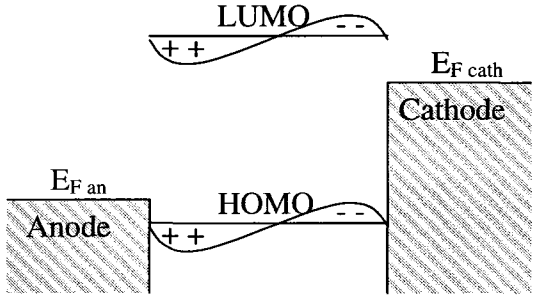

Figure 2.11a: *the change of band alignment because of diffusion. Electrons diffuse from the cathode, holes from the anode*

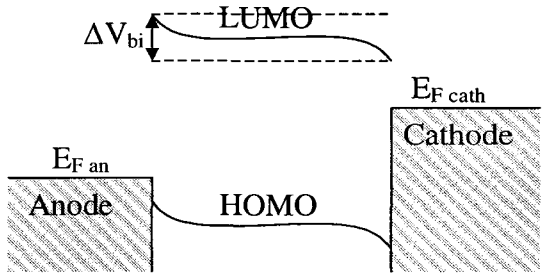

Figure 2.11b: *lowering the potential with ΔV_{bi} makes the bands flat again.*

Because diffusion is temperature dependent, the change in the built-in potential is also temperature dependent. This temperature dependence can be calculated if Boltzmann statistics are assumed. These calculations were done as a part of the research about the characterization of polymer solar cells.

We have the drift-diffusion equation (2.1), Poisson's equation (2.2) and the Einstein relation (2.5). We need one more equation, detailed balance. That states the relation of the density on both sides of the interface.

$$n_0 = n_m e^{\frac{-\phi}{kT}} \tag{2.11}$$

n_0: charge density at the polymer side of the interface (m^{-3})
n_m: charge density at the metal side of the interface (m^{-3})
φ: barrier for injection (J)

Combining the drift-diffusion equation (2.1), Poisson's equation (2.2) and the Einstein relation (2.5) we find when J=0:

$$J = e\mu \frac{dE}{dx}\frac{\varepsilon_0\varepsilon_r}{e}E - e\frac{\mu kT}{e}\frac{\varepsilon_0\varepsilon_r}{e}\frac{d^2E}{dx^2} = 0 \Rightarrow \frac{dE}{dx}E = \frac{kT}{e}\frac{d^2E}{dx^2} \tag{2.12}$$

J: current density (A/m^2)
e: proton charge, $1.602*10^{-9}C$
μ: mobility (m^2/Vs)
E: Electric field (N/C or V/m)
x: place (m)
ε_0: permittivity in vacuum, $10^7/4\pi c^2$ (C^2/Nm^2)
ε_r: permittivity of the material
k: Boltzmann constant, $1.380*10^{-23}J/K$
T: temperature (K)

Solving 2.12 gives:

$$E = -\frac{2kT}{e}\frac{1}{x - x_0} \tag{2.13}$$

x_0: integration constant (m)

Constant E is also a solution of 2.12 but implies zero charge injection what is in contradiction with the boundary condition 2.11. Combining 2.13 with Poisson (2.2) gives us for n:

$$n = \frac{2kT\varepsilon_0\varepsilon_r}{e^2}\frac{1}{(x - x_0)^2} \tag{2.14}$$

Knowing n(x=0) from 2.11 we can determine for x_0:

$$n(x=0) = n_m e^{\frac{-\phi}{kT}} = \frac{2kT\varepsilon_0\varepsilon_r}{e^2}\frac{1}{x_0^2} \Rightarrow x_0 = \pm\sqrt{\frac{2kT\varepsilon_0\varepsilon_r}{e^2 n_m}}e^{\frac{\phi}{2kT}} \tag{2.15}$$

With 2.15 we have a complete description of the electrical field E, which is dependent on the temperature, the amount of charges in the contact-material, the permittivity of the material and the injection barrier. This is for one polymer/contact-surface only. To get an impression of the character of the charge density, an example-graph is shown in figure 2.12. Here, x_0 is taken negative, as will be explained.

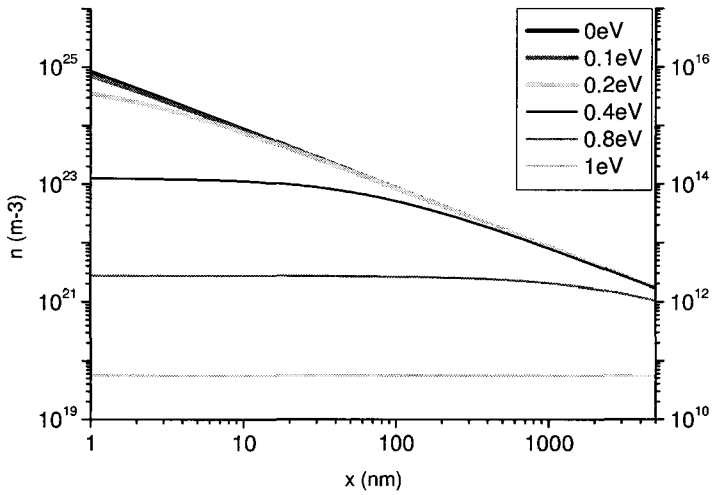

Figure 2.12: *example of the charge density field as a function of the distance. T=300K, ε_r=3, n_m=10^{28}. At low φ there is a change in the density in the distance.*

Integration of the electrical field, 2.13, gives us for the difference in built-in potential:

$$\Delta V_{bi} = \int_0^L E dx = \int_0^L -\frac{2kT}{e}\frac{1}{x - x_0} dx = -\frac{2kT}{e}\left[\ln(L - x_0) - \ln(-x_0)\right] \tag{2.16}$$

ΔV_{bi}: difference in built-in potential (V)
L: thickness of the layer (m)

This means that $x_0 < 0$, that is the minus sign in equation 2.15.

So far, we only considered one contact. Considering Boltzmann statistics and assuming that the surfaces are independent we can sum the contributions to the change in the built-in voltage. So, for two contacts, we must integrate twice over half the distance between the electrodes, with different n_m for different contacts. Altogether this gives us a formula for ΔV_{bi} for two contacts with contact materials A and B and layer C:

$$\Delta V_{bi} = -\frac{2kT}{e}\left[\begin{array}{l} \ln\left(\frac{L}{2} + \sqrt{\frac{2kT\varepsilon_0\varepsilon_{rC}}{e^2 n_{mA}}} e^{\frac{\phi_{AC}}{2kT}}\right) - \ln\left(\sqrt{\frac{2kT\varepsilon_0\varepsilon_{rC}}{e^2 n_{mA}}} e^{\frac{\phi_{AC}}{2kT}}\right) + \\ \ln\left(\frac{L}{2} + \sqrt{\frac{2kT\varepsilon_0\varepsilon_{rC}}{e^2 n_{mB}}} e^{\frac{\phi_{BC}}{2kT}}\right) - \ln\left(\sqrt{\frac{2kT\varepsilon_0\varepsilon_{rC}}{e^2 n_{mB}}} e^{\frac{\phi_{BC}}{2kT}}\right) \end{array}\right] \tag{2.17}$$

2.6: Impedance Spectroscopy

The study of the charge transport in polymer photonic devices is done in steady state (I-V curves) and frequency resolved. Frequency resolved measurements are done with impedance spectroscopy. Impedance spectroscopy is performed by applying a bias (dc)-voltage and adding an ac-voltage of a given frequency. The admittance (one over the impedance) is defined as[21]:

$$Y(\omega) \equiv \frac{I_{ac}}{V_{ac}} \equiv G(\omega) + i\omega C(\omega) \tag{2.18}$$

Y: admittance (Ω^{-1})
ω: angular frequency (s^{-1})
I_{ac}: alternating current (A)
V_{ac}: alternating voltage (V)
G: conductance (S); real part admittance
C: capacitance (F), C=Q/V; imaginary part admittance
Q: charge (C)

The relation between different contributions to the current is explained in paragraph 2.4. It is not possible to solve the given set of time dependent equations analytically. To be able to make quantitative conclusions simulations are done to understand the conducting processes and to extract information about the mobilities from the admittance spectra. However, it is possible to evaluate the dependence of the admittance (conductance and capacitance) on parameters qualitatively. The dependence on parameters of the admittance is:

$$G, C(\mu_n, \mu_p, n, p, G_{en}, R) \tag{2.19}$$

$\mu_{n,p}$: mobility of electrons and holes (m^2/Vs); temperature dependant (formula 2.5)
n,p: charge density of electrons and holes (m^{-3}); temperature dependant (formula 2.11)
G_{en}: Generation ($m^{-3}s^{-1}$); G in 2.7 and 2.8 but G_{en} here not to confuse with the conductance
R: Recombination ($m^{-3}s^{-1}$)

With the mobility and the charge density temperature dependent, the admittance is also temperature dependent.

The capacitance is the ability to store charges. When there is no active layer between the electrodes, there is a short circuit with no capacitance, C=0. (ohmic behavior) In absence of charge injection the capacitance equals the geometric capacitance:

$$C = \varepsilon_0 \varepsilon_r \frac{A}{L} \tag{2.20}$$

ε_0: permittivity in vacuum (F m^{-1}=C^2/Nm^2)
ε_r: relative permittivity in materials
A: device area (m^2)
L: layer thickness (m)

Formula 2.20 shows that the capacitance is dependent on the material and the geometrical shape. The capacitance is expected to be the geometric capacitance at 0V bias and beyond 0V bias as long as the voltage remains below V_{bi}. This is only true in a certain frequency-regime, $1/\tau_r << \omega << 1/\tau_D$. τ_r is the transit-time; τ_D is the Debye relaxation- or dipole-relaxation time that describes the relaxation of permanent dipoles present in the polymer. The Debye-effect can be modeled with formula 2.21[22].

$$\varepsilon_0 \varepsilon_r(\omega) = \varepsilon_0 + \frac{\varepsilon_0 \varepsilon_r - \varepsilon_0}{1 + (i\omega\tau_D)} \tag{2.21}$$

The value of τ_D is low. This leads to an effect at high frequencies only, above 1MHz, where in this research only up to 1MHz measurements are done. This effect is therefore negligible.

The transit time is the time a carrier needs to travel from one electrode to another. Under space charge limited current conditions the transit-time can be calculated with formula 2.22[21]:

$$\tau_r = \frac{4}{3} \frac{l^2}{\mu |V - V_{bi}|} \tag{2.22}$$

The transit time for a layer of 100nm PPV between PEDOT-PSS and Aluminum ($V_{bi} \approx 0.75$V) is in the order of 10^{-5}s for V=0V. For a single carrier device, for frequencies much lower than $1/\tau_r$ C=3/4 of $C_{geometric}$ because of density and velocity effects[21]. The effects of the transit- and relaxation-time are shown in figure 2.13.

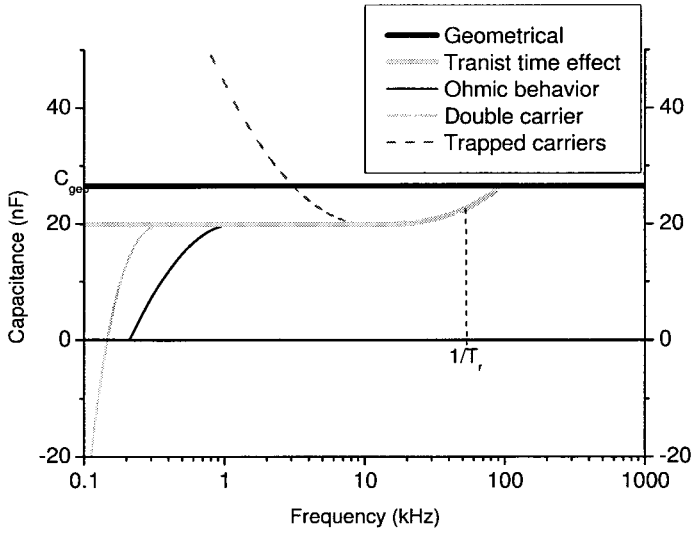

Figure 2.13: *the course of the capacitance. Values are typically for the used cells, 100nm thickness, ε_r=3, A=1cm^2. The capacitances with only a transit time effect and with only a Debye relaxation are added.*

At voltages that do not equal zero, and under illumination, the capacitance can differ from the geometrical capacitance[23]. To understand this, one should remind that the capacitance is the stored charge per bias. If the capacitance is higher than the geometrical capacitance, this can be

explained with trap-states: charges get trapped what makes it possible to store more charges. This will only work up to a certain frequency. Beyond that frequency the traps cannot follow the field modulation and therefore can no longer contribute to the capacitance.

If the capacitance is lower than the geometrical capacitance or even becomes negative, there is a contribution from a double carrier. As written before, the capacitance is the stored charge per bias. The presence of space charge will thus give a different capacitance. Because space charge lags behind the field that created this charge, its contribution is negative. For bipolar currents the positive and negative charges compensate each other. Therefore, the amount of space charge can be larger than in the unipolar situation[24]. This will make it possible that the negative change in the capacitance is larger than the geometrical capacitance and therefore the capacitance will become negative.

The relevant time scales can be understood by the response to a step potential[25]. For high frequencies, only the displacement current contributes to the capacitance, which will become the geometrical capacitance. For low frequencies, both carriers will contribute to the capacitance. As the injection barriers at both sides of the active layer are set ohmic, the fastest carriers will determine the field in the following time interval. This field remains stable until the second carrier responds, changing the field. This is followed by a response on the fastest carrier, and this will go on till the field and thus the currents have converged towards the equilibrium. This equilibrium is determined by the mobilities of both carriers and the recombination rate[26].

The capacitances with traps and with double carriers are also plotted in figure 2.13.

Chapter 3: Experimental Set-up

3.1: Sample preparation

Figure 3.1 describes the structure of the samples that are made. Glass with an ITO structure is commercially available. The glass with ITO is cleaned using acetone, soap and iso-propanol. Then the sample is placed under UV-ozone for 30 minutes. Polyethylenedioxythiophene:polystyrenesulfonate (PEDOT:PSS) is filtered and then spin coated on top of the ITO. The sample is annealed by 180^{0}C for two minutes to remove water from the PEDOT:PSS layer. The active layer, solved in chlorobenzene and stirred overnight, is spin coated on top of the PEDOT:PSS. The blend and the sample are kept out of the light as much as possible. After spin coating the active layer, the sample is brought into a glove box filled with nitrogen and from there brought in an evaporation chamber under a shadow-mask. In the evaporation chamber 1 nm of LiF (optional) and 100nm of Al are evaporated on the sample while the maximum temperature was kept below 40^{0}C.[1]

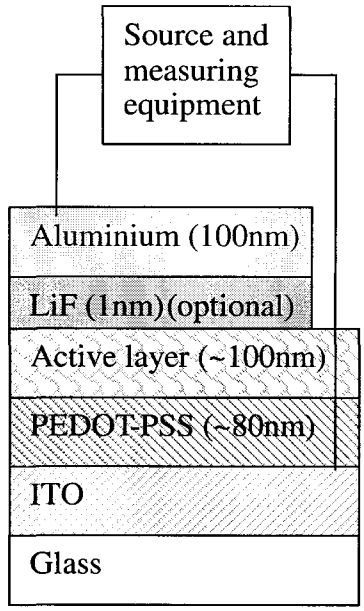

Figure 3.1: *the structure of the solar cell. The active layer can be PPV, PCBM or a blend of PPV and PCBM.*

Screwing gold contacts to the sample can make a circuit: one to the Al, the other on a place where there was no Al evaporated because of the shadow-mask to the ITO. To screw to and not through the Al, what would give a short circuit, is a problem tackled by inserting a spring in the screw. Other experimentalists locally remove ITO by etching from the part where the aluminum-contact would be set before spin-coating the PEDOT:PSS.

The described procedure gives working devices and is reproducible, as will be further discussed in paragraphs 4.2 and 4.3.

3.2: Electrical measuring set-up

As described in 1.2 and 2.6, I-V measurements and impedance spectroscopy-measurements are done on the devices. To measure IV-curves and impedance-spectroscopy with different temperatures, a set-up is built. The set up is described in figure 3.2.

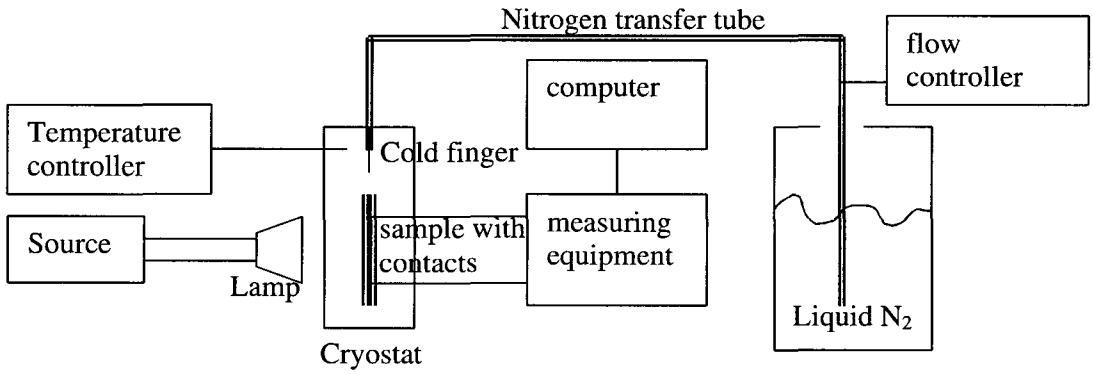

Figure 3.2: *the set-up for electrical measurements. The sample is situated in a cryostat with contacts to an external device. This can be a Keithley for IV characterization or an HP impedance-measurer. The temperature is regulated with a flow of liquid nitrogen cooling and an intelligent temperature controller heating. A white-light halogen lamp can illuminate the sample.*

The set-up is designed to reach each temperature between 80K and 300K and remain stable at that temperature. In the dark, this is extremely stable, in an hour the temperature changes less

than 0.2K. Under illumination, the accuracy of the temperature is about 0.2K. The sample can be set in the dark as well as set under illumination. In the glove box IV-measurements are done with a halogen lamp with a power of 150mW/cm^2. In the cryostat, illumination was done with a halogen lamp. The short-circuit current was comparable with the measurements in the glove box if the lamp was set on its maximum value of 4A. Most measurements were done with the current through the lamp set on 2.5A instead of the maximum 4A, for the maximum value would cause too much degradation to the sample. The set value is also under the value where the short-circuit-current has its maximum.

I-V-measurements can be done as well as impedance measurements. They cannot be done at the same time. I-V measurements are done with a Keithley 2410 and have no big uncertainties in I or V, they are reliable within 1% and 0.001V respectively. Impedance spectroscopy is done with an HP 4192A. Impedance spectroscopy gives some problems: there is a serial resistance in the apparatus. The resistance changes when one changes from one regime to another, typically around the resistance and capacitance of the used solar cells, that is ~1kΩ and ~10nF. Therefore every set bias-voltage is measured with a multi-meter before the measurements begin. Even with this correction the accuracy of the applied bias-voltage is disputable within 0.05V.

Considering all these qualities, the set-up functions very well in controlling the temperature, the illumination and measuring I-V characteristics. The impedance, mostly the applied voltage, must be taken with a relatively high uncertainty of 0.05V. The given frequency is reliable within 0.1%.

Chapter 4: Preliminary Measurements

4.1:Thickness measurements

Thickness-measurements are carried out on dummy-samples to learn the thickness of the different layers. The dummy-samples were made in the same procedure as the corresponding samples but without the evaporation of the top-electrode. Then, a scratch was made on these dummies. With an alpha-stepper, that uses a needle taken over a surface, the depth of the scratch and thus the thickness of the layer were measured. This gives different thicknesses for different series of samples. Different measurements on the same dummy can make a difference up to 13nm for the standard samples and the pure PCBM samples. The pure PPV dummy had a spread of 18nm.

For the standard-samples the thickness including PEDOT-PSS changes from 160 to 190nm over all samples. The PCBM samples were made on difficult circumstances because of the low viscosity of PCBM in benzene solvent. The set made on November 4th had a thickness of only 99nm including PEDOT. The sets made on November 18th and December 3d had thicknesses of 125 and 136nm including PEDOT. Pure PPV gives a thickness of 218nm including PEDOT. Dummy samples with only PEDOT-PSS had thicknesses of ~80nm. A thickness of 80nm is assumed in the further report.

All results of the thickness-measurements are presented in appendix I.

4.2: Comparable samples from different days: I-V measurements

It is important to know the reproducibility of the measurements. Therefore measurements have been done on a group of samples. These samples were made according the same procedure but on different days. At room temperature I-V and impedance spectroscopy measurements were done.

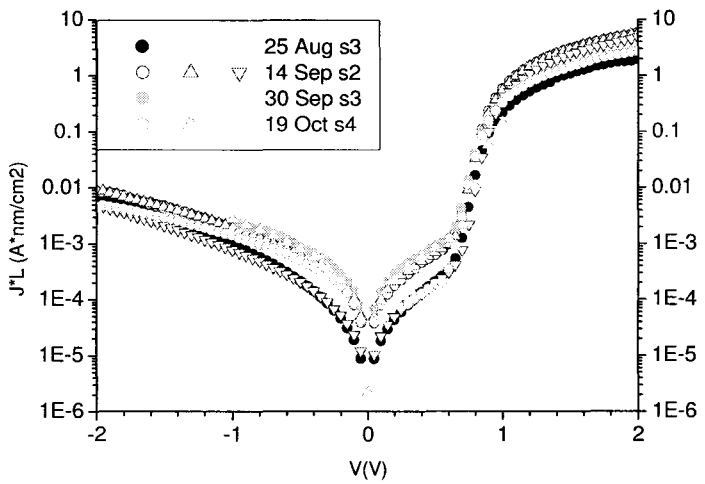

Figure 4.1: *Current, normalized for thickness and length (L), as a function of voltage. The samples used consist of an ITO-layer, a PEDOT-PSS layer of ~80nm, a blend-layer of MDMO-PPV and PCBM in the ratio of 1:4 with a thickness between 80 and 110nm, different for different samples, a LiF-layer of 1nm and an Al-layer of 100 nm. All measurements were taken at room temperature. Different symbols of the same color are different measurements on the same sample.*

Figure 4.1 shows the current as a function of the applied voltage for similar samples. It gives an impression of the reproducibility of the measurements. The forward current can differ from different samples, up to a factor of 3 at 2V. The leakage current can also differ within one sample, up to an order. The forward current differs less than a factor of 2 within one sample. The built-in potential, at about 0.8V, does reproduce within 0.1V. The built-in potential is determined by extrapolating the line above V_{bi} down to zero. Where the line crosses the x-axis is Vbi.

Comparable samples of which the results are not shown here had much higher leakage-currents, orders, than the results shown. Samples where a too high voltage was applied, that is above 3V, or that were illuminated too long, that is for several hours, also had a much higher leakage current. These measurements are not shown because of their small accuracy. So we can conclude that the difference in leakage-current strongly depends on the fabrication and the history of the sample.

For the given voltages, between -2V and 2V, we can state that the uncertainty only depends on the equipment that gives the voltage and is accurate within 0.01V. The given temperature is accurate within 0.1K. The measurement of the current depends only on the measuring equipment. This equipment is accurate. The uncertainty in the values of the current is given by the sample preparation and the history.

4.3: Comparable samples from different days: impedance spectroscopy

Figure 4.2 shows the capacitance as a function of frequency for two similar samples made on different days at a bias-voltage of 0V. The used samples are the same as in figure 4.1. The capacitance at low frequencies, 10Hz to 10kHz, is the geometrical capacitance. As can be observed in figure 4.2, these geometrical capacitances are the same for the two samples within 1nF. At high frequencies, f>10kHz, the capacitance drops to zero. This occurs at different frequencies for the two samples. The contact materials cause this effect, as will be analyzed in paragraph 4.5.

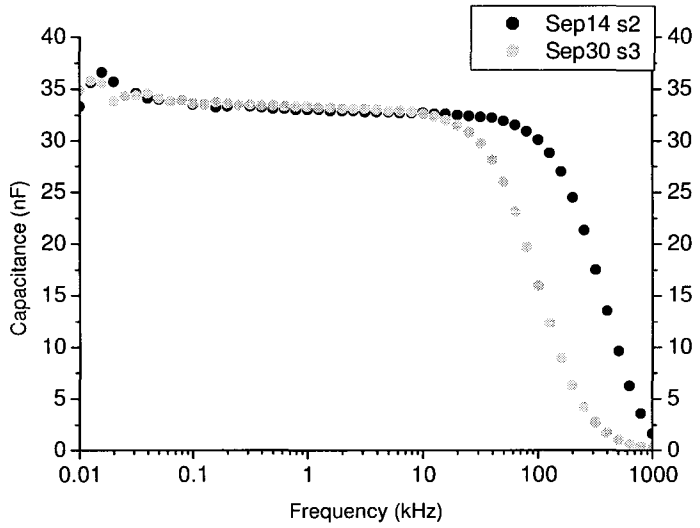

Figure 4.2: *Capacitance as a function of frequency at 300K and 0V in the dark. The geometrical capacitances are the same.*

Figure 4.3 shows the conductance of the two samples at room temperature with different positive bias-voltages. First, we focus on the low-frequency behavior. At 0V bias, the conductance results from the leakage-current only and is about 2 to $3*10^{-5}$S. Increasing the voltage to 0.5V does make a small increase of the conductance, as it does with the leakage current as can be seen in figure 4.1. Then, both samples have a large increase of the conductance between 0.5V and 0.75V. At higher bias the conductance increases to a maximum, which is different. The maximum conductance at high biases is the same as the conductance at high frequencies.

The conductance reproduces within a factor 2. Only the difference in leakage-current is observed again. The differences at 0.75V partly are because of the set-up of the impedance-spectroscopy where the given voltage is not necessary the applied voltages. These voltages are checked with a multi-meter. Still, there is an uncertainty of 0.05V, which is also frequency dependent. For 1.25V the difference is a factor 3 what is consistent with figure 4.1. At higher

frequencies, above 1kHz, the conductance raises to a maximum that is the same within one sample for all voltages. This effect will be further discussed in paragraph 4.5.

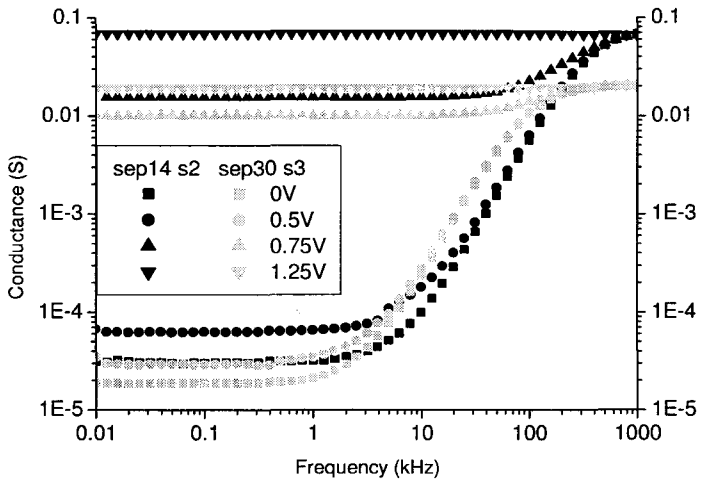

Figure 4.3: *Conductance as a function of frequency at 300K in the dark. For low frequencies, the samples have the same leakage-conductance at low bias and a maximum conductance at high bias. This maximum conductance is the same as the maximum conductance at high frequencies.*

Figure 4.4 shows the capacitance as a function of the frequency with several bias-voltages. At low frequencies, the capacitances of the samples are the same for small voltages, below 0.75V. At 0.75V bias for both samples the capacitance decreases - that is, for frequencies above 50Hz. At higher voltages, for both samples the capacitances become negative.

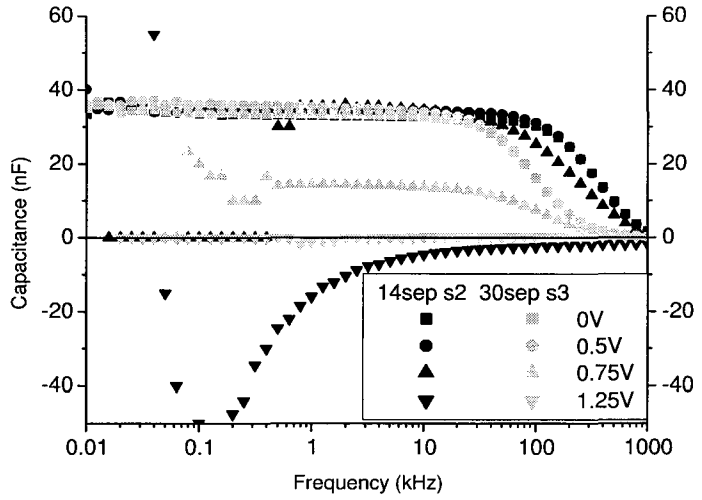

Figure 4.4: *Capacitance as a function of frequency at 300K in the dark. For low frequency and low bias, the capacitances are the same. At high biases the capacitance decreases to zero and to negative values, which differ for the two samples.*

At 0.75V and 1.25V bias, the values seem of little accuracy. This is because of the described problems of setting the bias-voltage with the HP that has an uncertainty of 0.05V. Around and above the built-in potential little changes in the voltage can have a relatively large effect on the admittance and thus on the capacitance. Another problem is that the HP cannot measure the

capacitance when the impedance is too low, below 100Ω. The signs however, both absolute as in reference to the geometrical capacitance, seem to have qualitative meaning.

We can conclude from the presented data that quantitative impedance measurements can only be done in a limited parameter space. The uncertainty for the impedance-spectroscopy measurements is because of the preparation and history, and because of the uncertainty of the given voltage. Contact effects also do play an important role at frequencies above 10kHz, as will be discussed in paragraph 4.5.

At V=0V the capacitance is reliable and depends on the preparation only. At $V=V_{bi}$ the uncertainty in the capacitance is large because of the uncertainty in voltage. Above V_{bi} the uncertainty increases because the capacitance is highly voltage-sensitive. Trends, as an increase of an order of magnitude in the conductance, or the capacitance becoming negative for example, do reproduce. So we can conclude we have reproducible samples within the limits indicated above and can make reproducible measurements.

4.4: Electrical wear

Not every measurement on one sample is exactly the same: the history of the sample can play an important role, as stated in paragraph 4.2. Therefore some measurements have been done to compare the performance of a sample at its first measurement, after cooling, after illuminating and after waiting. All measurements were done at room temperature at 0V bias. Figure 4.5 shows the results.

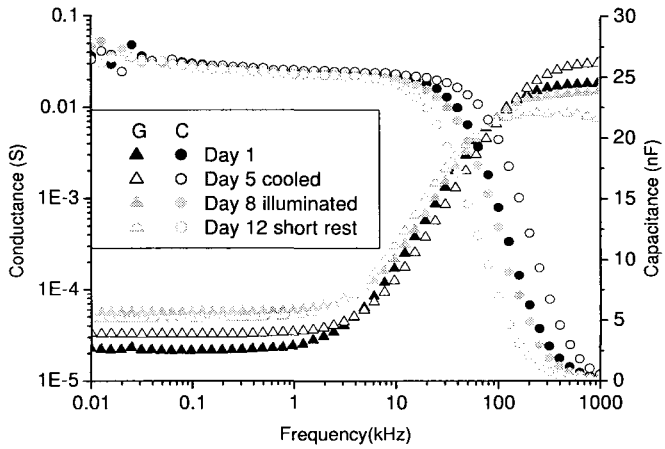

Figure 4.5: *Conductance and capacitance as a function of frequency at 0V bias for different sample-history at 300K in the dark. The sample consist of an ITO-layer, a PEDOT-PSS-layer of 80nm, a 20%PPV/80%PCBM layer of 110nm and an Al layer of 100nm. The history seems to have little influence on the sample.*

As can be observed, the geometrical capacitance does only change within 1nF. The frequency where the capacitance decreases does decrease after illumination over almost an order. The conductance increases after series of measurements of the sample, up to a factor of 2 to 3. This increase of the leakage-conductance however is small. We can conclude that the performance of the sample for low frequencies, below 10kHz, does change but within a factor 3 for the conductance and 1nF for the capacitance, so that we can compare measurements made on different days. The increase of the conductance and the decrease of the capacitance at high frequencies are explained in paragraph 4.5.

4.5: High frequency effects

As can be observed in figures 4.2, 4.4 and 4.5, the capacitance drops to zero at high frequencies. This is in contradiction with the description in 2.6. A consistent explanation is assuming that the contact-electrodes have a resistance that cannot be neglected. In the original model[1] the set-up is described as a parallel resistance and capacitance, both dominated by the behavior of the photoactive layer. In the new model, also recently used by others[2], there is a resistance in series with this layer, which is caused by the PEDOT:PSS and possibly other resistances. To compare the two models, figure 4.6 shows both.

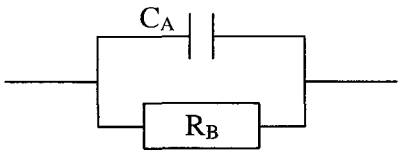

Figure 4.6a: *the classic model describing the set-up; this is highly dominated by the photoactive layer*

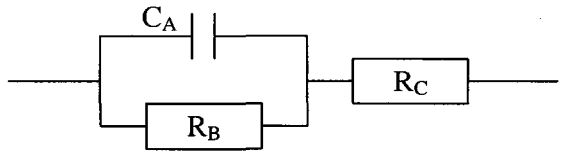

Figure 4.6b: *the new model, where the resistance of the PEDOT-PSS and the wires cannot be neglected*

In the situation where the total resistance is highly dominated by the photoactive layer, the admittance Y is:

$$Y = \frac{1}{Z} = G + i\omega C = \frac{1}{R_B} + i\omega C_A \tag{4.5}$$

With Z the impedance. When $\omega \downarrow 0$, $G \rightarrow 1/R_B$ and $C \rightarrow C_A$. Measurements with a multi-meter on the samples used in 4.2 and 4.4 give $R_B \approx 10^4 \Omega$, what does seem to fit with the conductance at low frequencies at 0V bias. C_A is simply the geometrical capacitance. When $\omega \rightarrow \infty$, the same conditions for G and C are still valid, when the Debye relaxation is not taken into account.

In the situation that the resistance of the other parts also plays a role of importance, as described in figure 4.6b, the total impedance is:

$$Z_{total} = \frac{R_B}{1 + i\omega C_A R_B} + R_C \tag{4.6}$$

Which gives an admittance Y of:

$$Y = G + i\omega C = \frac{\left(\omega^2 C_A^2 R_B^2 R_C + R_B + R_C\right) + i\omega\left(C_A R_B^2\right)}{\omega^2 C_A^2 R_B^2 R_C^2 + \left(R_B + R_C\right)^2} \tag{4.7}$$

Assuming $R_B >> R_C$ this gives us for the limits of ω: $\omega \downarrow 0$: $G \rightarrow 1/R_B$ and $C \rightarrow C_A$, the same when the resistance of the photoactive layer is taken as highly dominant. But for $\omega \rightarrow \infty$: $G \rightarrow 1/R_C$ and $C \rightarrow 0$. This is consistent with the measurements shown in figures 4.2 and 4.3 if $R_C \approx 10\text{-}100\Omega$. The resistance may be different for different samples but should lie within this range.

Measurements are carried out to find out the resistance R_C[3]. These measurements were done on a sample consisting of an ITO-contact, PEDOT-PSS, a gold contact and the normal used wires with a multi-meter. The measured value is 60Ω, what is in the given area. With this value, the typical frequency where the resistance of the PEDOT-PSS becomes dominant is between 10^4 and 10^5 Hz. This is also consistent with the data shown in figures 4.2 and 4.3.

We can conclude that the measurements are well described with the model that takes the resistance of the PEDOT-PSS and other elements in account.

Chapter 5: Results PPV

In this chapter the results of the electrical characterization of the sample with PPV are shown and are shortly discussed. The PPV sample consists of ITO/PEDOT:PSS/PPV/LiF/Al. A picture of the structure can be viewed in figure 3.1. The PEDOT:PSS is ~80nm thick, the PPV-layer 138±9nm, the LiF 1nm and the Al 100nm. First, the characterization with IV measurements is done, in the dark and under illumination, at different temperatures. Then the impedance measurements are shown. We hope to find what carriers there are, some clues of the mobilities and their behavior in dark and under illumination. The results shown here are only the most important; the sample is measured at five temperatures with different bias-voltages. The other results are in appendix II.

5.1: IV-measurements in dark and light

IV-measurements were done on the sample with PPV under different temperatures. To fully observe the electrical phenomena a comprehensive treat of this sample is necessary. From the temperature measurements we can expect a rise in the mobility with rising temperatures, and therefore a rise in the current and the conductance. The results of the IV-measurements are shown in figure 5.1.

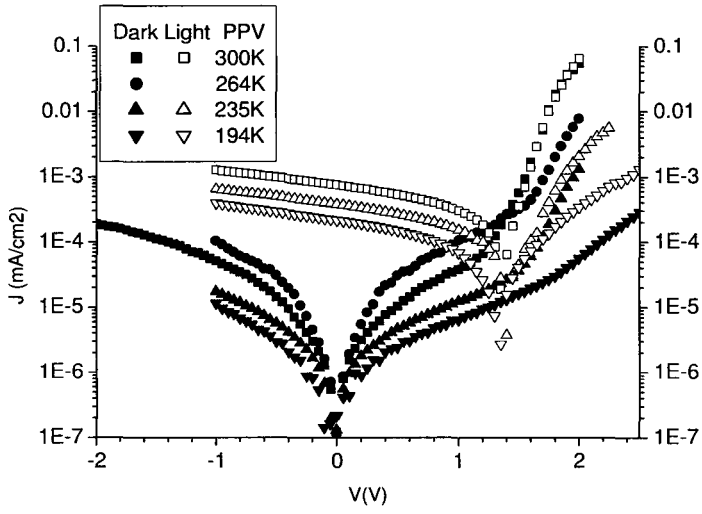

Figure 5.1: *IV-curve of the PPV sample at different temperatures under illumination and in the dark. The build-in potential is about 1.3V increasing with decreasing temperatures. The sample behaves like a solar cell.*

Figure 5.1 shows the IV-measurements done on the sample. In the dark, we see a small current below the built-in potential, the leakage current. There is a drop of the leakage current when decreasing the temperature, except for the measurement at 264K. This exception at 264K is because of wear; this measurement is done after cooling to 194K and illumination. At 1V the leakage current drops an order when the temperature drops from 300K to 194K.

At V_{bi}, 1.3V, the current rises fast due to the onset of the space charge limited current. The built-in potential is determined by extrapolating the line above V_{bi} down to zero. Where the line crosses the x-axis is V_{bi}. Decreasing temperature leads to a small increase in the built-in potential, about 0.05V, and a large decrease in the current. At 2V the current decreases an order decreasing the temperature from 300K to 264K. Below 194K, there is almost no current that can be discriminated from the leakage-current. This temperature dependence is expected, for a higher mobility is expected for higher temperatures.

With formula 2.3 we can calculate the mobilities for the different temperatures. The results are shown in table 5.1. With these mobilities we can determine the band widening σ by plotting according formula 2.4, what gives 0.094±0.02eV. The graph can be observed in paragraph 8.1, figure 8.4. The value of 0.094eV is near the value of 0.11eV from literature[1].

Table 5.1: *Mobility as a function of temperature; σ is 0.094±0.02eV*

T(K)	μ(cm^2/Vs)
300	$2.5\pm0.2*10^{-6}$
264	$4\pm0.6*10^{-7}$
235	$1.3\pm0.4*10^{-7}$
194	$4\pm2*10^{-9}$

Under illumination, there is a huge increase in the current below V_{OC}, the open-circuit voltage where the current is zero. At -1V, this is more than an order. At 0V, there is a significant current, in contrast to the current in the dark. Therefore we can conclude that this sample behaves like a solar cell, even without PCBM. Increasing the temperature from 194K to 300K gives an increase of the current below V_{bi} of almost an order. Above V_{OC} the current in the dark and under illumination are almost the same, within the uncertainty. Only at 194K the current is much higher under illumination in comparison to the dark, a factor of 3.

The difference in increasing V_{OC} and V_{bi} with decreasing temperatures is because different effects determine the specific voltages. V_{OC} is determined by the parameters that determine V_{bi}, the dissociation probability of a bound electron–hole pair into free charge carriers, the generation rate of bound electron-hole pairs G and the Langevin recombination rate of free electrons and holes R^2.

We can conclude that this cell is a solar cell with a temperature-sensitive mobility: the current is temperature sensitive and below 194K the current is not significant different from the leakage-current.

5.2: Impedance in the dark

Impedance spectroscopy is done on the PPV sample. Figure 5.2 shows the conductance at room temperature for different bias-voltages.

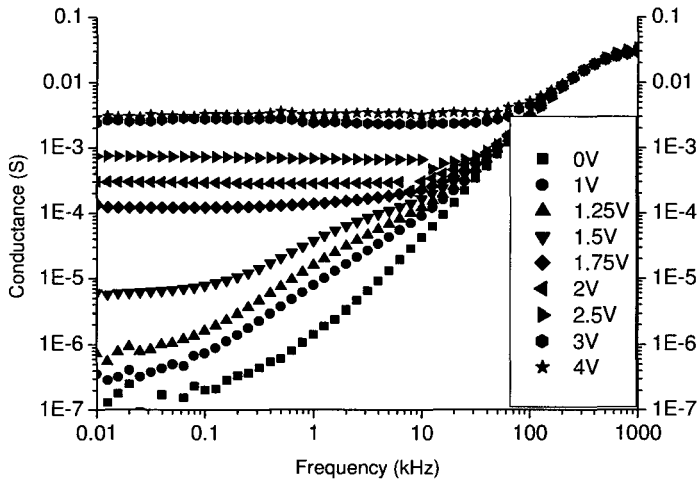

Figure 5.2: *Conductance at 300K at different bias in the dark. There is a significant rise at 1.5V*

At low frequencies, 10-100Hz, the conductance is the leakage conductance below V_{bi} of 10^{-6} ~10^{-7}S. With a bias higher than 1.25V the conductance rises up to 0.03S at 3V and remains at this value. Above 3V the conductance remains the same. This is consistent with the I-V measurements where the values of the current rise fast above V_{bi} but seem to reach a maximum above 2V. In figure 5.1, the curve only goes to 2V, but a change in the slope is visible. I-V measurements are

done up to 4V, where the change in the current between 2V and 4V is only an order, what is consistent with figure 5.2.

The capacitance is shown in figure 5.3. At 0V, the capacitance is the geometrical capacitance. This geometrical capacitance is only 80% of the expected capacitance from formula 2.20, possible because of the PEDOT:PSS that could partly contribute to the thickness. Increasing the voltage above 1V the capacitance rises for frequencies below 1kHz. This indicates the filling of traps. This continues beyond the built in potential to 1.5V. Then, there is a drop, leading to negative capacitances for high voltages, above 2V, indicating double carrier injection.

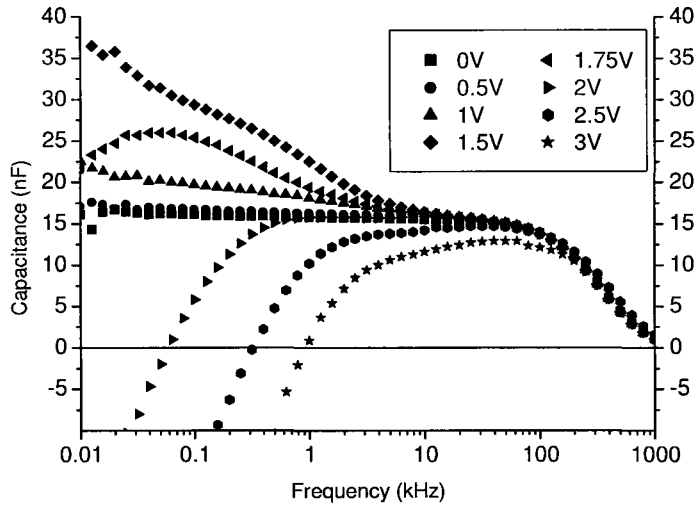

Figure 5.3: *Capacitance at 300K at different bias in the dark. There is a serious rise to 1.75V followed by a drop to negative values.*

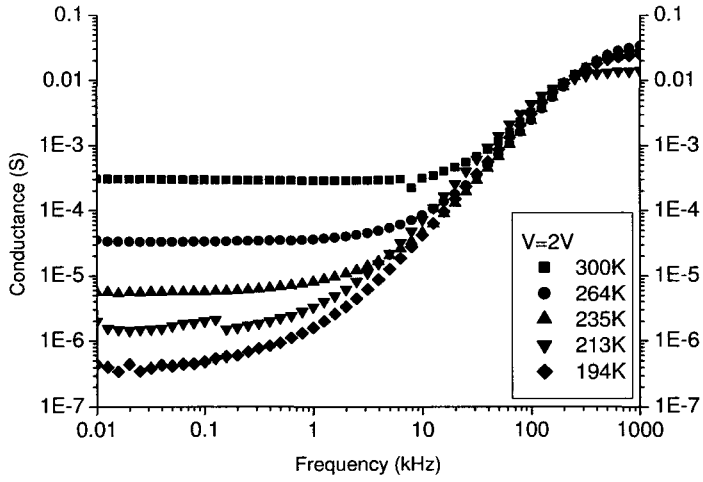

Figure 5.4: *Conductance at 2V at different temperatures in the dark. There is a significant decrease with temperature*

Figure 5.4 shows the conductance at 2V as a function of temperature. At low frequencies, there is a decrease with decreasing temperature, from $2*10^{-4}$S at 300K to $3*10^{-6}$S at 194K. This is consistent for the behavior of currents in figure 5.1. At 194K the conductance is in the same order as the leakage conductance, the conductance at 0V.

At 0V, the temperature has almost no effect on the capacitance, which stays the same within a nF. At 1V at low temperatures, 213K, there is no trapping of charges. Above V_{bi} the temperature has effect on the capacitance. As can be seen in figure 5.5, the filling of traps is temperature dependent and occurs only above 235K.

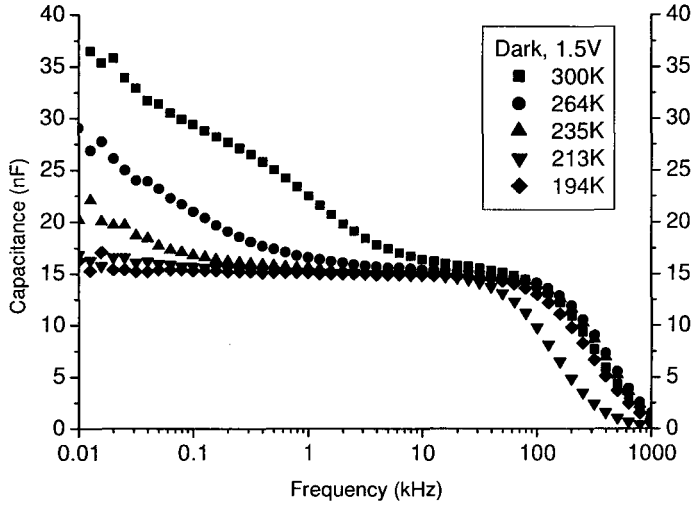

Figure 5.5: *Capacitance at 1.5V at different temperatures. There is a significant decrease of the capacitance with decreasing temperatures.*

As can be seen in figure 5.6, at 2.5V above 235K the capacitance becomes negative at higher frequencies with increasing temperature, indicating double carrier injection. At 3V, the capacitance crosses the x-axis at higher frequencies than at 2.5V. Also trapping occurs.

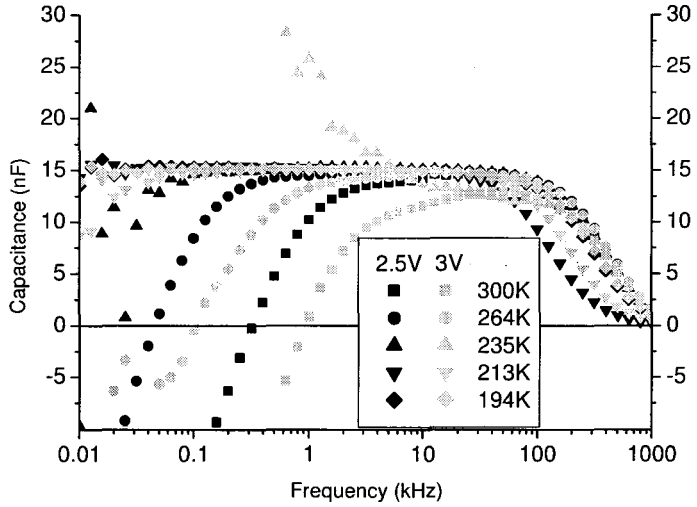

Figure 5.6: *Capacitance at 2.5 and 3V at different temperatures in the dark. There is a significant change in crossing the X-axis with temperature*

5.3: Impedance under illumination

Under illumination, charges are created. An increase of the conductance is expected, especially at 0V. Because charges are generated in pairs, one expects two carriers.

In figure 5.7 one can see that illumination has only a small effect on the conductance, an increase of less than an order at 0V. At higher bias there is also a small increase of the conductance.

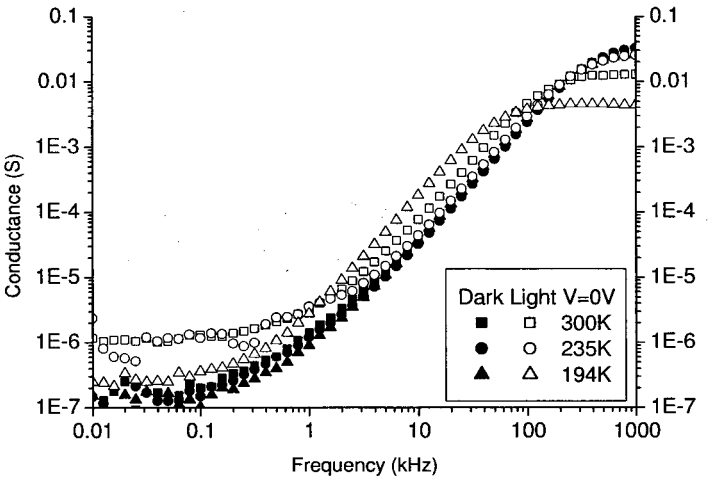

Figure 5.7: *Conductance at 0V at different temperatures under illumination and in the dark. There is only a small increase under illumination*

For the capacitance, at 0V illumination has little effect, the capacitance remains the geometrical capacitance within 1nF. Though there are two carriers, there is no negative capacitance. Because the change in the conductance is also small, the effect of the illumination seems to be small. For higher voltages, the frequencies where the capacitance is negative decreases under illumination in comparison of the frequencies in the dark, but less then an order, as can be observed in figure 5.8. The filling of traps remains the same under illumination as in the dark.

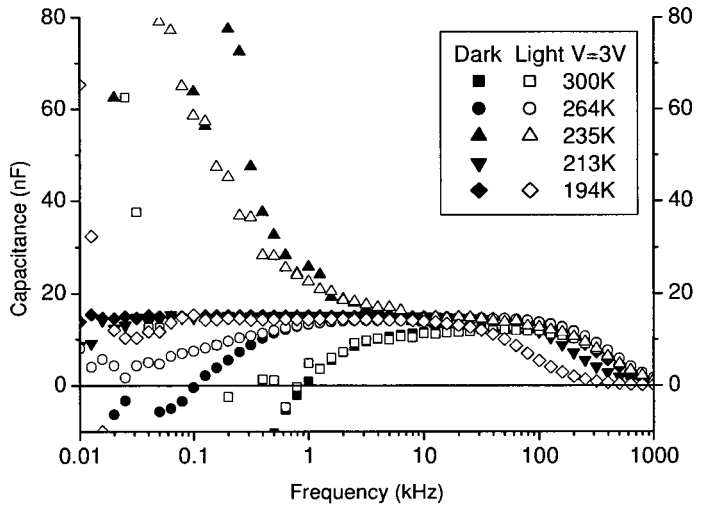

Figure 5.8: *Capacitance at 3V at different temperatures in the dark and under illumination. There is a decrease in the frequency where the capacitance is zero*

5.4: Conclusions

The most important features about this characterization of the PPV sample are shortly presented here. At bias voltages above the built-in potential trapping becomes important, and at higher voltages, 2V, there is double carrier injection. This means that the Al electrode does inject electrons.

At low temperatures, below 235K, there is almost no current, a very low conductance and a geometrical capacitance. While, as we will see in chapters 6 and 7, PCBM and the blend of PPV and PCBM do conduct well, discriminative from the leakage conductance, at even lower temperatures. Any temperature effect in the blend below 235K therefore must be because of the PCBM.

The band-widening σ is 0.094±0.02eV, which is in agreement with literature.

Without PCBM, PPV does behave like a solar cell; there is a current at 0V under illumination. This performance is however three orders less then in the blend as will be shown in figure 7.2. The effect of light on the conductance and the capacitance is small, indicating that charge separation is weak, which is in agreement of the performance as a solar cell that is much less than the performance of the blend.

Chapter 6: Results PCBM

As discussed in the theory, adding PCBM to PPV improves the separation of photo-generated charges. To understand this blend better, also an electrical characterization of PCBM is made. The sample now consists of ITO/PEDOT:PSS/PCBM/LiF/Al. The PEDOT is about 80nm thick, the PCBM varies in thickness, the LiF 1nm and the Al 100nm. Because of the variation of the different samples, the results are either normalized for the thickness or the thickness is mentioned. First, the characterization with IV measurements is done, without and with light, at different temperatures. Then the impedance measurements are shown. The complete set of measurements is in appendix III.

6.1: IV-measurements in dark and light

IV-measurements were done on the sample with PCBM under different temperatures. From the temperature dependent measurements we can expect a rise in the mobility with rising temperatures, and therefore a rise in the current and the conductance. The results of the IV-measurements are shown in figure 6.1.

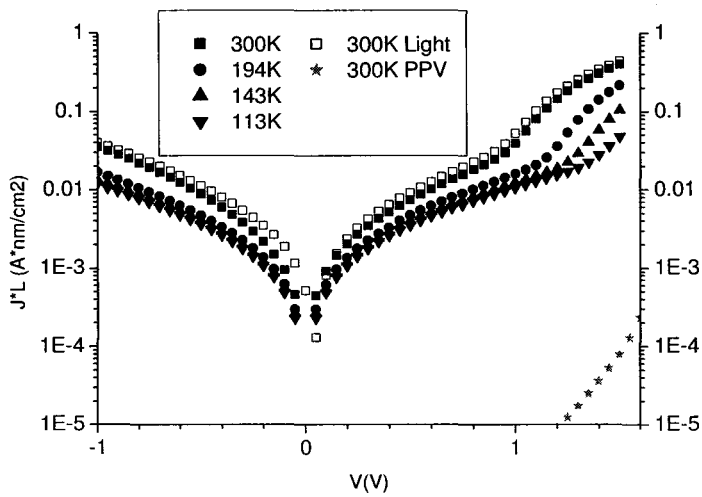

Figure 6.1: *I-V curve of the PCBM cell. The current is multiplied by the thickness for comparison reasons: the PPV layer was 7 times as thick as the PCBM layer. Illumination has no effect. For comparison, the current in the PPV sample is shown. The current is several orders higher for PCBM than for PPV. The leakage current is relative high, but this can be because of the small thickness of the sample, that is only 19nm.*

As can be seen in figure 6.1, the current is several orders higher in PCBM than in PPV: 3 orders at 1.5V. The leakage current is relatively large because of the small thickness; this is just thick enough to make it a proper sample. Illumination has clearly no effect at all, as is expected because PCBM does not absorb photons in the visual range.

The temperature dependence is not that dominating as with the PPV sample: at 113K there still is a difference visible between the leakage current and the current above V_{bi}, where for PPV there was no difference below 194K. At 1.5V for example, the current is a factor 2 of the leakage current at 113K. V_{bi} is about 1V, increasing up to 1.2V with decreasing temperatures up to 113K.

The mobilities are presented in table 6.1. With these mobilities we can determine the band widening σ by plotting according formula 2.4, what gives 0.015±0.006eV. The graph can be observed in paragraph 8.1, figure 8.4. The value of 0.015±0.006eV is within an order consistent with literature, which give 0.073eV[1]. The difference is because of the LiF, as will be shown in paragraph 8.1.

Table 6.1: *Mobility as a function of temperature; σ is 0.015±0.006eV*

T(K)	μ(cm^2/Vs)
300	$1\pm0.2*10^{-6}$
194	$8\pm2*10^{-7}$
143	$6\pm2*10^{-7}$
113	$5\pm2*10^{-7}$

6.2: Impedance

The geometrical capacitance of the PCBM-sample is about 1.2 to 1.3 times the geometrical capacitance of the PPV sample. This can be explained with the higher relative permittivity of PCBM; 3.9 for PCBM and 3.0 for PPV[1,2]. Both capacitances are however 20% lower than the capacitance calculated with formula 2.20. This could be because of the PEDOT:PSS that could partly contribute to the thickness.

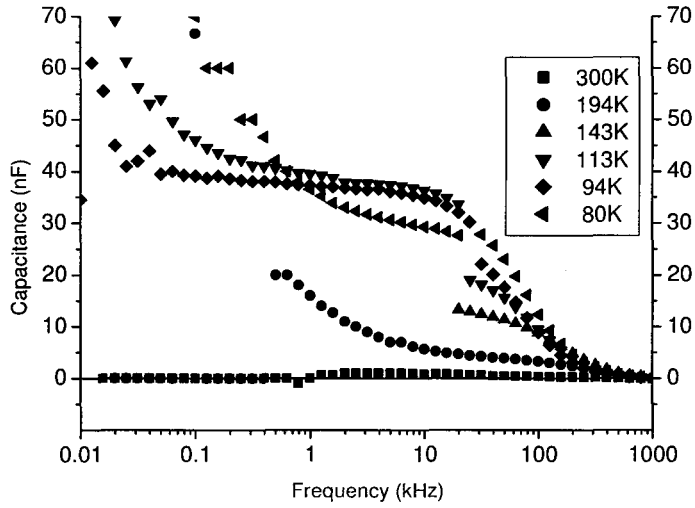

Figure 6.2: *the capacitance at 1.5V bias at different temperatures in the dark. There is a negative capacitance at 300K.The thickness of the sample here is 56nm*

As can be observed in figure 6.2, at lower temperatures, 113K and lower, trap-states occur. At room temperature the capacitance becomes negative at a frequency just below 1kHz. This indicates a bipolar current. This is in contradiction with ref [3], where it is claimed that PCBM in this configuration is a unipolar electron conductor. The negative capacitance here is only slightly negative, one nF, and is within the uncertainty of the HP analyzer. At other measurements, the negative capacitance is much more clear, as can be observed in figure 6.3.

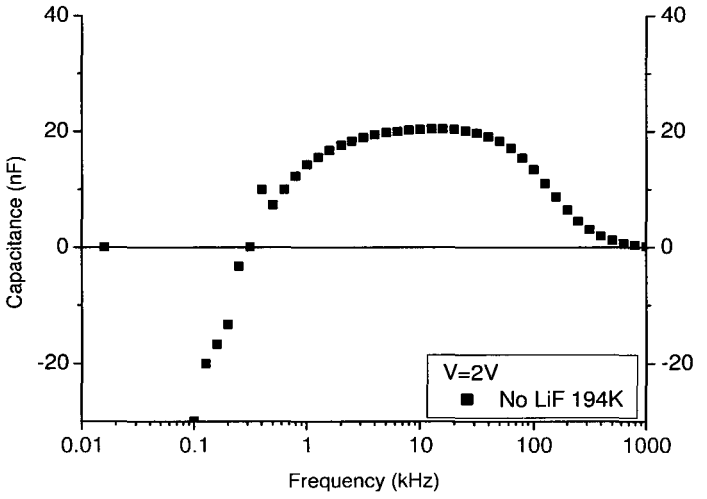

Figure 6.3: *the capacitance at 2V bias at 194K for a sample without LiF in the dark. The capacitance clearly becomes negative at frequencies below 0.1kHz. The thickness of the sample here is 45nm*

6.3: Conclusions

From the sample with only PCBM, two major conclusions can be made from the impedance spectroscopy. First, it does not behave like a solar cell, as expected. Second, it can conduct both types of carriers.

The mobility is less temperature sensitive and $\sigma=0.015\pm0.006$eV.

Chapter 7: Results Blend

In this chapter the results of the electrical characterization of the PPV/PCBM blend are shown and are shortly discussed. The blend sample consists of ITO/PEDOT-PSS/PPV-PCBM/LiF/Al, with about 80nm PEDOT, 97nm active layer, 1nm LiF and 100nm Al. The blend consists of 20%(wt) of PPV and 80%(wt) of PCBM. A picture of this sample can be observed in figure 3.1. Comparing the results with the results of the pure PPV and the pure PCBM sample will help to understand the behaviour of the blend. The fact that PPV does hardly conduct at temperatures below 194K helps discriminate the different contributions of the materials.

7.1: IV-measurements in dark and light

Measurements were done on the standard sample. For comparison reasons, also the results of the pure materials are shown. The IV-characterization in the dark can be observed in figure 7.1.

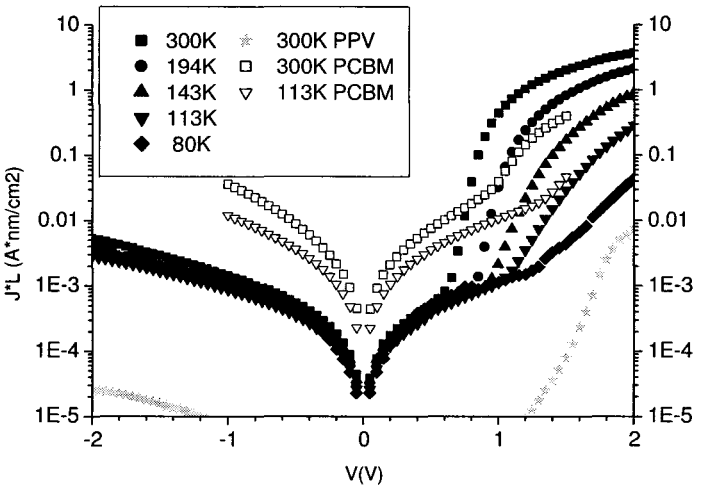

Figure 7.1: *IV-curve of the blend at different temperatures in the dark; the built-in potential is around 0.75V, increasing with decreasing temperatures. The leakage current is about 10^{-3} times the current at 1V. The thickness is 97nm here. The current is normalized for the thickness, because the thickness varies a factor 7 between the samples with PCBM and PPV.*

Figure 7.1 shows the I-V curves of the sample. We can observe a leakage current at negative voltage and small positive voltage. Then we can observe a huge increase of the current of three orders around V_{bi}, 0.75V. Decreasing the temperature from 300K to 113K leads to an increase of V_{bi} from 0.7V to 1.1V and a decrease of the current of an order at 2V. The temperature has little effect on the leakage current, a factor of two from increasing from 80K to 300K at -2V.

Comparing with the pure materials, the currents are much higher, more than two orders at 2V, than for the PPV sample. This could be expected because of the higher mobility for the PCBM sample. The leakage current is an order higher for the PCBM-sample than for the blend. This is probably because of the thickness: this sample is only 19nm thick, almost not thick enough to be a proper cell, what will lead to a relatively large leakage current. The current at high temperatures, 300K, above V_{bi}, is also higher for the blend in comparison to PCBM, a factor 5 at 1.5V. This is more than the sum of the currents for PCBM and PPV. This is because PCBM conducts electrons very well, but is a poor hole-conductor and PPV conducts holes very well. Together, they can conduct both carriers very well. This is called bipolar conduction. PPV is also suspected to conduct better if blended with PCBM.

At low temperatures, 113K, the currents for PCBM and the blend are almost the same, PCBM a little higher than the blend, possibly because the mobility in the PPV decreases fast with decreasing temperature.

Under illumination, the blend cell behaves like a solar cell, as can be observed in figure 7.2. Below V_{OC}, the open-circuit voltage where the current is zero, there is an almost constant current, decreasing with decreasing temperatures, a factor 3 between 300K and 113K at -2V. At 113K there is still a photocurrent, while there was no current in the PPV. This means that there is still charge separation because of light at these temperatures. The reason this doesn't show up in PPV is the high recombination rate without PCBM.

The photocurrent is more than an order higher than the leakage current at -2V. At room temperature the open circuit voltage V_{OC} is comparable with the built-in potential. The difference is less than 0.1V, as expected. The current above V_{OC} is only a factor 2 bigger under illumination than in the dark. With decreasing temperature the V_{OC} increases not as fast as V_{bi}. This makes a huge difference in the current just above V_{OC}, up to an order at 143K. The difference in increasing V_{OC} and V_{bi} with decreasing temperatures is because different effects determine the specific voltages. V_{OC} is determined by the parameters that determine V_{bi}, the dissociation probability of a bound electron–hole pair into free charge carriers, the generation rate of bound electron-hole pairs G and the Langevin recombination rate of free electrons and holes R. The generated electrons influence the electric field and thus the voltage where a positive current is possible[1].

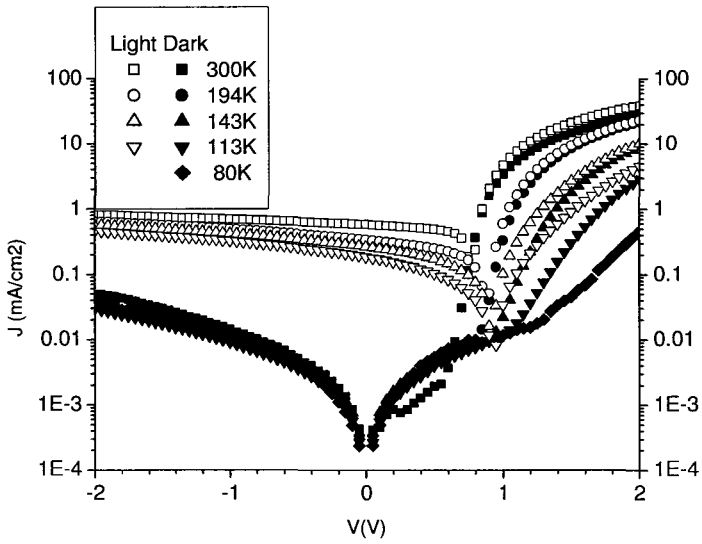

Figure 7.2: *IV-curve of the blend at different temperatures under illumination; the cell behaves like a solar cell. The thickness is 97nm here.*

7.2: Impedance in the dark

The geometrical capacitance of the blend is 1.15 times the capacitance of the PCBM sample and 1.5 times the capacitance of the PPV sample, as can be observed in figure 7.3. The blend has more charge storage then the components. In the samples shown here there is LiF. In paragraph 8.2 it will show up that this higher capacitance is due to the LiF. Where the measured capacitances from the PPV and PCBM were less then the capacitances calculated with formula 2.20, for the blend, the measured en calculated capacitances are comparable.

Changing the temperature has little effect on the geometrical capacitance; it changes less than one nF or 3%.

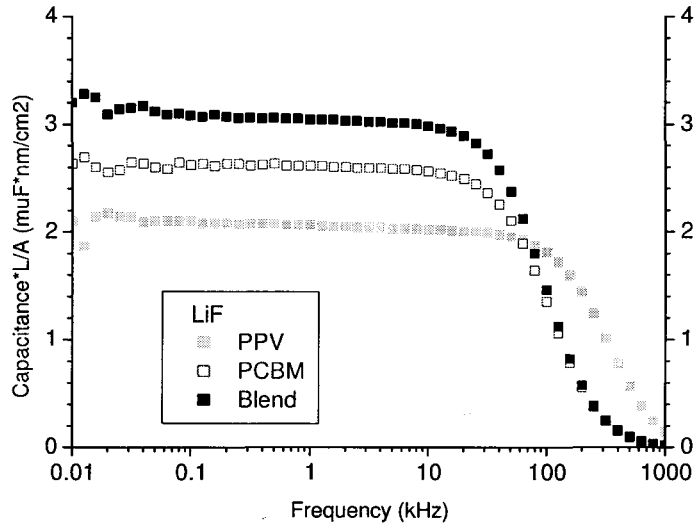

Figure 7.3: *Geometrical capacitance for the blend in comparison to PPV and PCBM at V=0V in the dark*

For a bias of 0.75V, there is an effect: at lower temperatures, 194K, 0.75V is far, >0.1V, from the built-in potential. Thus, the conductance and the capacitance behave like at a bias of 0V. For higher voltages, the potential is above V_{bi} and there is a change in conductance and capacitance; therefore only these higher voltages are discussed in more detail. At 1.25V, the conductance increases with increasing temperatures analog with the rising current in figure 7.1.

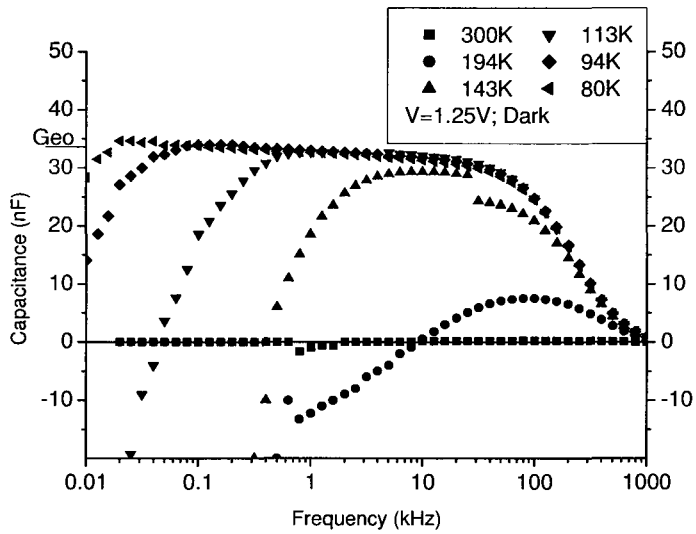

Figure 7.4: *Capacitance as a function of frequency at different temperatures for a blend sample at 1.25V bias in the dark. The capacitance decreases with increasing temperature for increasing frequencies. Geo is the geometrical capacitance from measurements at 0V bias.*

As can be observed in figure 7.4, for all temperatures above 80K at low frequencies the capacitance differs from the geometrical capacitance at 1.25V bias. The capacitance between -2V and 0.5V changes only 1nF between the different temperatures.

Between 113K and 194K the capacitance for low frequencies becomes negative indicating double carrier injection. The frequency where the capacitance crosses the x-axis increases with the temperature, from 50Hz at 113K to 7kHz at 194K. A double carrier below a temperature of 194K suggests that PCBM conducts both charges, for the mobility of PPV is very low there;

however, PPV is claimed to conduct better in the blend what can also be an explanation of the double carrier at 194K.

The frequency where the capacitance becomes negative is the highest for the blend, then for PCBM, as can be observed in figure 7.5. This indicates that the double carrier injection for the higher frequencies is possible in the blend where this is not possible for any of the components, what is expected, for the blend conducts both carriers. In figure 7.5 the capacitance is only -1nF for the PCBM and the blend sample. There were no other measurements on all three samples at one temperature and voltage. Other measurements were consistent with the trend.

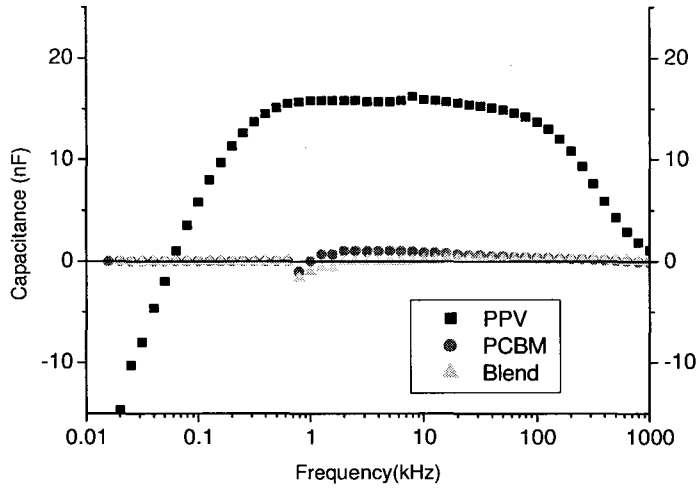

Figure 7.5: *Capacitance as a function of frequency at 300K for different samples. The voltage is 0.4V above V_{bi}. The thicknesses are 138nm for PPV, 56nm for PCBM and 97nm for the blend.*

7.3: Impedance under illumination

A series of impedance measurements are done on this blend sample under illumination. Figure 7.6 shows the conductance and the capacitance as a function of frequency at different temperatures at 0V bias. As can be observed, at room temperature illumination seems to have an effect on the conductance only. The conductance increases an order, because the amount of charges increases. There is no effect on the capacitance because the created charges compensate each other.

The capacitance at 0V seems to be highly dependent on the temperature, where the conductance is temperature independent. For low frequencies, 50Hz, the capacitance increases and the capacitance becomes frequency dependent. This effect increases up to 5nF as the temperature decreases. At ~5kHz the capacitance under illumination and in dark are the same. A possible explanation is that dissociation/association between electrons and immobile holes can behave like trapping. At low temperatures this will lead to a behavior comparable with trapping.

Under illumination, there are two carriers, but at 0V there is no double carrier injection from the contact electrodes, for there is no negative capacitance.

The conductance at 0V increases an order under illumination, what is consistent with the increase in leakage current as shown in figure 7.2. The conductance at 0V is temperature independent, what is different from the expectations from 7.2.

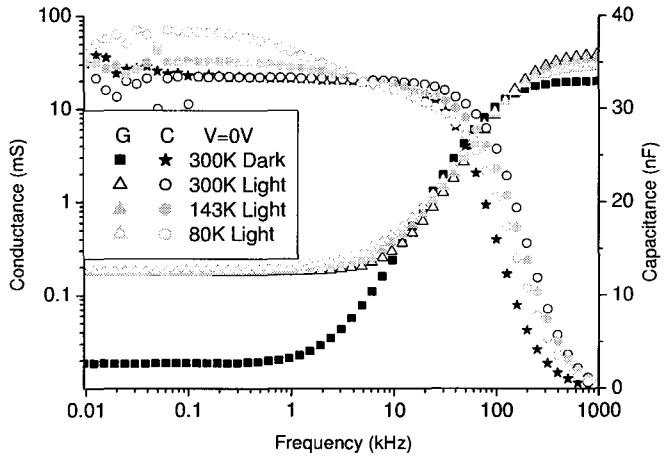

Figure 7.6: *Conductance and capacitance as a function of frequency at different temperatures under illumination at 0V bias for the blend sample. For comparison, the capacitance and the conductance in the dark are plotted, which are temperature independent. G seems temperature independent.*

Applying a negative bias at room temperature in the dark does not change the capacitance; neither does it at room temperature under illumination. Under illumination at low temperatures, the capacitance increases at V=0V. As can be seen in figure 7.7, the capacitance approaches the geometrical capacitance as the negative bias increases. This is probably because the electrical field makes it possible to transport the holes and thus to eliminate the effect.

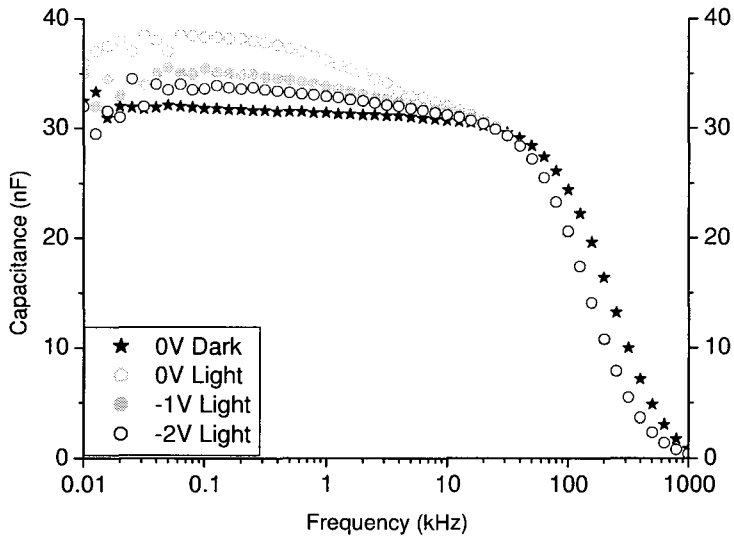

Figure 7.7: *Capacitance as a function of frequency at different bias voltages at 80K for a standard sample. The capacitance decreases as the bias becomes more negative.*

Figure 7.8 shows the capacitance at 1.25V under illumination. For comparison, the capacitance in the dark is plotted as well. The capacitance at high bias-voltages, here 1.25V, changes under illumination. At high temperatures, above 194K, the capacitance does not change qualitatively.

When the temperature is decreased to 143K the capacitance under illumination is high, μF, and positive at low frequencies, 50Hz, indicating traps, where there were no traps in the dark; in

the dark, the capacitance is highly negative. The illumination creates electron-hole pairs. Probably these created charges fill traps.

Decrease of the temperature from 194K to 94K makes the capacitance in the dark less negative, the capacitance under illumination more positive. Under illumination, more charges are trapped, where in the dark the minority carrier injection stops at lower frequencies. This stops below 94K where both with and without illumination approach the geometrical capacitance. The capacitance becoming less negative with decreasing temperature is consistent with the decreasing mobility in PPV with decreasing temperatures; with a low mobility in PPV double carrier injection is more difficult.

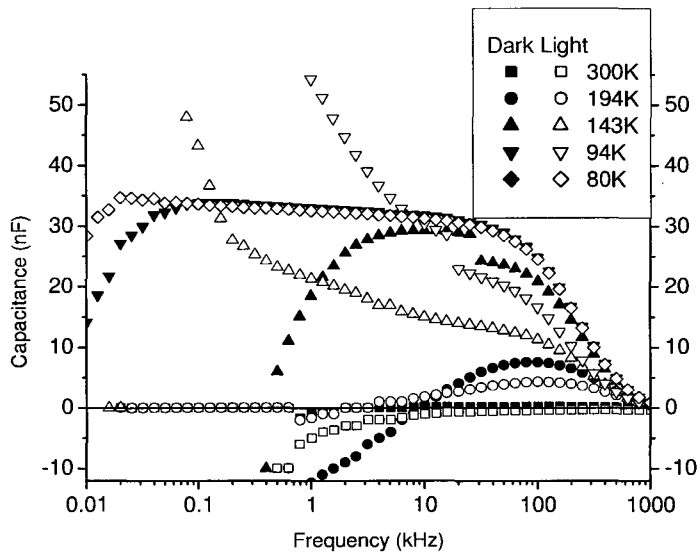

Figure 7.8: *Capacitance as a function of frequency at different temperatures with 1.25V bias for a standard sample under illumination. At low temperatures the capacitance differs a lot.*

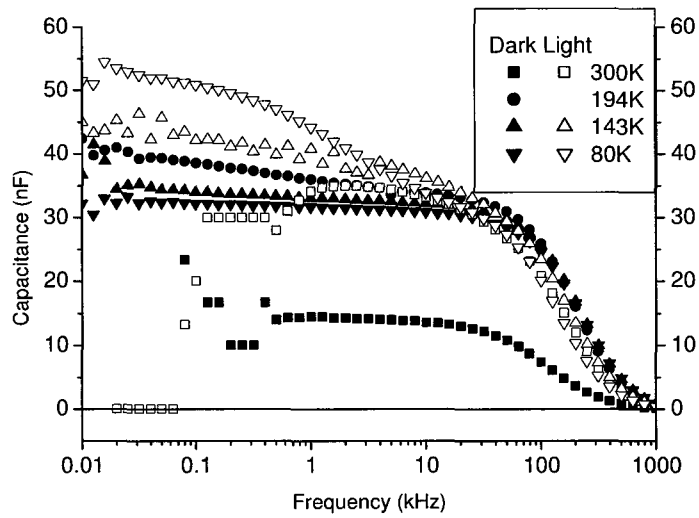

Figure 7.9: *Capacitance as a function of frequency at different temperatures with 0.75V bias for a blend sample under illumination. At low temperatures the capacitance differs more than 10nF*

At 0.75V bias, much closer to V_{OC} and V_{bi}, there is a different trend in the capacitance as can be observed in figure 7.9. Under illumination the capacitance at low frequencies increases as a

function of temperature and keeps on increasing. In the dark the capacitance increases to a maximum at 194K. Further decrease of the temperature makes the capacitance in the dark decrease and go to the geometrical capacitance. The trend in the dark can be explained by the increasing of V_{bi} with decreasing temperature, as can be observed in figure 7.1. From 80K to 194K the voltage approaches V_{bi}. At higher temperatures, $V>V_{bi}$ and the same trends occur as with 1.25V. Under illumination however there seems to be another trend: at 143K trapping seem to occur, which is consistent with figure 7.8 where traps also play an important role. These traps do thus get filled at voltages below the built-in voltage. This can be explained with dissociation/association of electrons with immobile holes that can behave like trapping, as discussed after figure 7.6.

7.4: Conclusions

From the characterization of the blend we can draw some conclusions. Most important is that there is a double carrier in the blend, as expected. This is also the case for temperatures where the mobility in the PPV approaches zero. No traps occur in the dark. Under illumination, traps occur. Above V_{bi}, at low temperatures, 94K-143K, and at 0V.

The conductance under illumination at 0V is an order higher than in the dark. Under illumination, there are two carriers, but at 0V there is no double carrier injection from the contact electrodes.

Chapter 8: Results Without LiF

In the previous chapters, all samples had a thin, 1nm, LiF layer. Adding this material helps the efficiency of the solar cell, though there are several possible explanations[1]. It is expected to contribute to the dipole layer at the surface and thus to higher the work function, to protect the active layer against the Al bombardment during evaporating and to dissociate and form doping. To learn more about this layer, also measurements without LiF are done for the pure materials and the blend. The samples now consist of ITO/PEDOT:PSS/active layer/Al. Here, PEDOT is about 80nm thick, Al 100nm. Only the most important results are discussed here. All results are shown in appendices V (PPV), VI (PCBM) and VII (blend).

8.1: I-V measurements in dark and light

In figure 8.1 we can observe a large difference in V_{bi} between the samples with and without LiF, 0.3V. The current seems higher here but this is because of this change in built-in potential. The mobilities are determined and can be observed in table 8.1. The mobilities are comparable. So there is no significant effect in the bulk as expected. The increase of V_{bi} with decreasing temperature is small, only 0.1V between 300K and 235K.

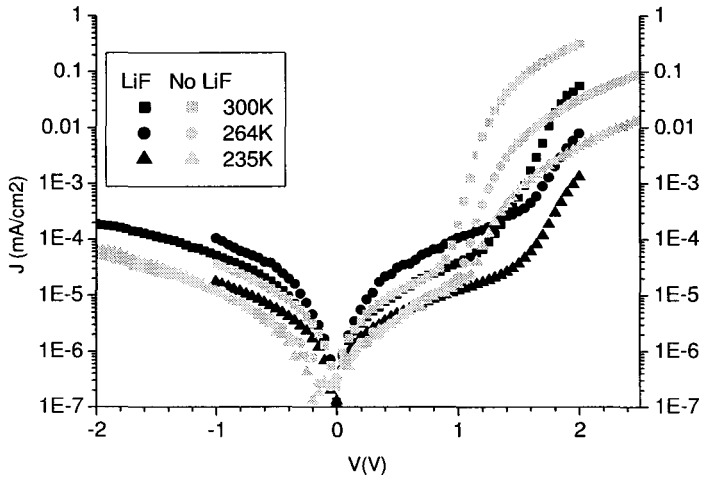

Figure 8.1: *IV-measurements on PPV with and without LiF in the dark. There is a difference of 0.3V in built-in potential*

Table 8.1: *Mobility as a function of temperature for PPV with and without LiF; σ is 0.094±0.02eV with and without LiF*

T(K)	μ(cm^2/V s) LiF	μ(cm^2/V s) without LiF
300	$2.5\pm0.2*10^{-6}$	$3.5\pm0.4*10^{-6}$
264	$4\pm0.6*10^{-7}$	$4\pm0.5*10^{-7}$
235	$1.3\pm0.4*10^{-7}$	$8\pm1*10^{-8}$
194	$4\pm2*10^{-9}$	

For PCBM, there is a difference in V_{bi} of about 0.1V as can be observed in figure 8.2. This indicates that the LiF indeed has an effect on the work function: a higher work function would make a difference in the built-in potential for PPV, where it would make no or just a small difference for PCBM. This is explained in figure 8.3.

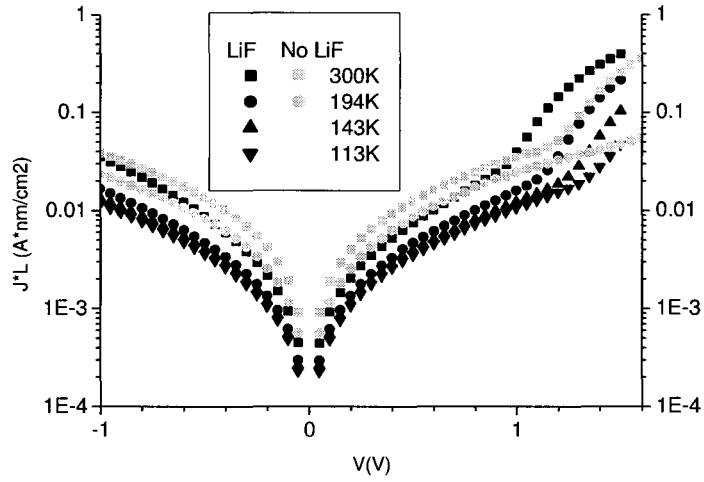

Figure 8.2: *IV-measurements on PCBM with and without LiF in the dark. The current is normalized for the thickness because the thickness of the two different samples differs a factor of two. There is a difference in the current above V_{bi}*

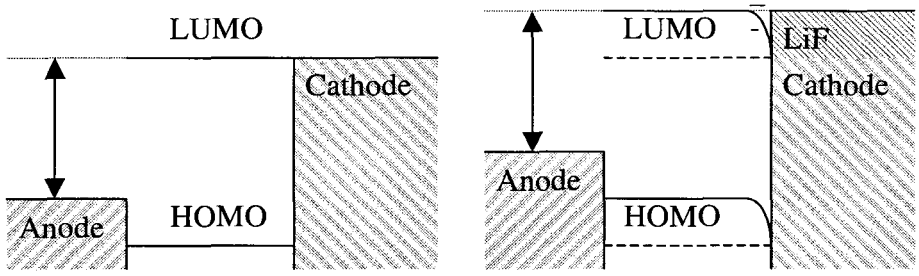

Figure 8.3: *changing of work function because of LiF. In the left picture is the situation without LiF, in the right with LiF. Electrons would flow until the charges would create a field that makes the LUMO higher.*

The small difference in V_{bi} in PCBM is because the work function of the cathode with LiF would be lower than the LUMO (the gap would be smaller), what is not possible and therefore leads to band-bending. Therefore the built-in potential does not change if the cathode in higher. See also figure 2.9. As analyzed in paragraph 2.5, this number is only a rule of thumb, but it does explain the qualitative effect. The same effect is expected for the blend: a small or no change in the built-in potential. For PPV, with LiF the LUMO remains the same because the work function of the cathode remains higher then the LUMO, but the V_{bi} does decrease because of lower cathode.

For PCBM, the current is lower without LiF than with LiF, especially at lower temperatures. The mobilities are determined and presented in table 8.2; the difference is significant.

Table 8.2: *Mobility as a function of temperature for PCBM with and without LiF; σ is 0.015±0.006eV with and 0.053±0.015eVwithout LiF*

T(K)	μ(cm^2/V s) LiF	μ(cm^2/V s) without LiF
300	$1\pm0.2*10^{-6}$	$3\pm0.5*10^{-7}$
235		$8\pm3*10^{-8}$
194	$8\pm2*10^{-7}$	$4\pm2*10^{-8}$
143	$6\pm2*10^{-7}$	
113	$5\pm2*10^{-7}$	

With these mobilities we can determine the band widening σ by plotting according formula 2.4, as can be observed in figure 8.4. σ is 0.094±0.02eV for PPV, both with and without LiF, 0.015±0.006eV for PCBM with LiF and 0.053±0.015eV for PCBM without LiF. The value of 0.053eV approaches the value from literature of 0.073eV. The resemblance for σ in PPV and the

difference in PCBM with and without LiF is clearly visible in figure 8.4. The change in the bend widening with LiF is remarkable.

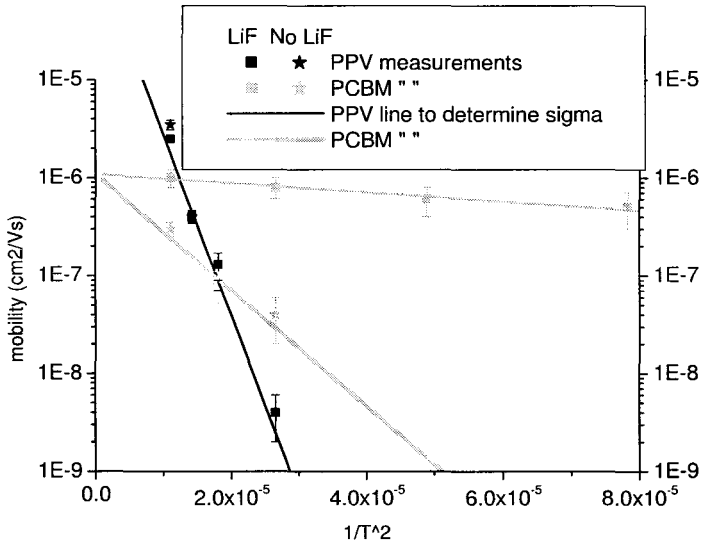

Figure 8.4: *mobility as function of one over the temperature squared for PPV and PCBM with and without LiF. The mobilities for PPV are on a single line, where for PCBM the mobilities with and without LiF are on different lines.*

For the blend, at room temperature there is no difference in the current with and without LiF, as can be observed in figure 8.5. This is consistent with the previous graphs, where the difference in mobility in PPV and PCBM hardly changed at room temperature if LiF was added. For PPV the change in the current is because of the change in the built-in potential, and so is the change in the current for PCBM at room temperature. With an equal built-in potential, the currents should be the same. At lower temperatures, 113K, there is a large difference, an order at 2V. This is consistent with the lower mobility at lower temperatures in PCBM without LiF. The difference in the built-in potential is small, less than 0.1V.

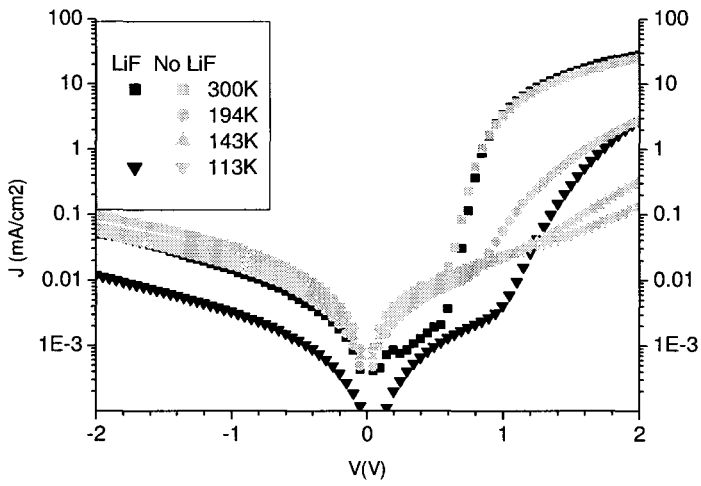

Figure 8.5: *IV measurements on the blend with and without LiF in the dark. At low temperatures there is a difference in the current above* V_{bi}

The performance as a solar cell with LiF in comparison to without LiF is especially increasing at low temperatures. In the light, the currents behave in the same trend: comparable at room

temperature, and without LiF lower at lower temperatures. The performance as a solar cell is however also better at room temperature with LiF. With LiF, the fill factor is 0.50±0.05 for the blend with LiF, and 0.48±0.02 for the blend without LiF; the efficiency 1.11±0.14% and 0.92±10 respectively. The uncertainties are 68% interval.

8.2: Impedance

The geometrical capacitance of PPV remains the same within 5%. The capacitance for PCBM without LiF drops to the level of the PPV, as can be observed in figure 8.6. The capacitance for the blend without LiF drops to the capacitance of PCBM with LiF. The higher capacitance with LiF for PCBM and the blend can be explained with the higher work function. When the work function of the cathode would be higher than the LUMO, the LUMO will bend till the flat part of the band is in level with the cathode; else, electrons would keep on flowing to the LUMO. See also figure 8.3. This leads to a high concentration of charges within the LUMO at the interface with the cathode, so the active layer is quasi-metallic here, what leads to a higher permittivity and thus to a higher capacitance. However, apart from the capacitance of the blend with LiF, all measured capacitances are only 80% of the calculated capacitances. This is possibly because of the PEDOT:PSS that could partly contribute to the thickness.

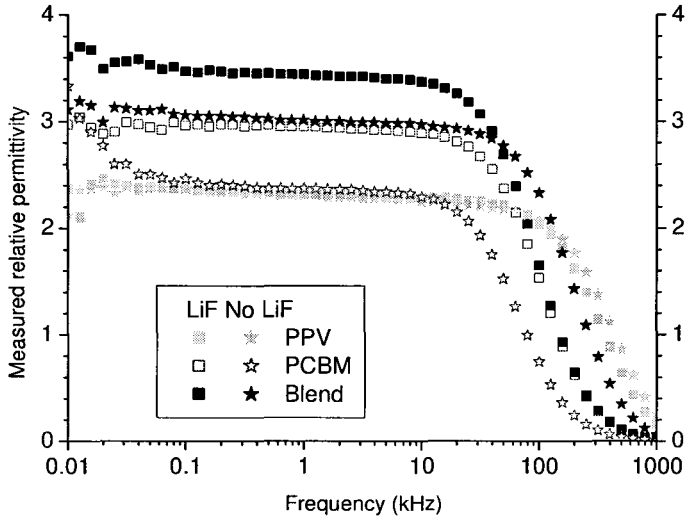

Figure 8.6: *measured geometrical capacitance of PPV, PCBM and the blend, with and without LiF; V=0V in the dark*

At high voltages, the character of the capacitance of the PPV changes: without LiF, there are no double carriers anymore, only traps instead, and the traps start at higher voltages, as can be observed in figure 8.7. LiF thus lowers the injection barrier for the minority carriers, so double carrier injection is possible. Protection by the LiF of the PPV against the bombardment of Al-atoms probably prevented some trapping at voltages below V_{bi}.

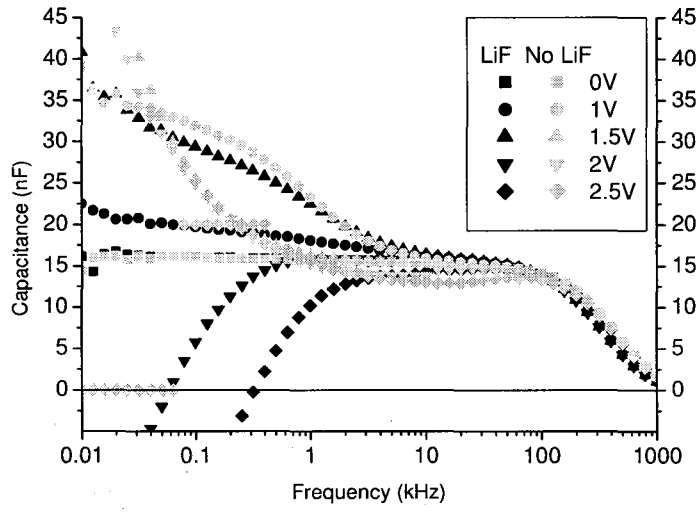

Figure 8.7: *capacitance of PPV at 300K with and without LiF in the dark, there are no double carriers without LiF*

For the PCBM sample, without LiF there are no traps, as can be observed in figure 8.8. Did the LiF protect so trapping of holes could decrease in PPV, the trapping of electrons increase with LiF on PCBM. The geometrical capacitances seem the same but are not normalized for surface and thickness, which are different, 1.06cm^2 and 56nm with LiF and 0.90cm^2 and 45nm without LiF respectively.

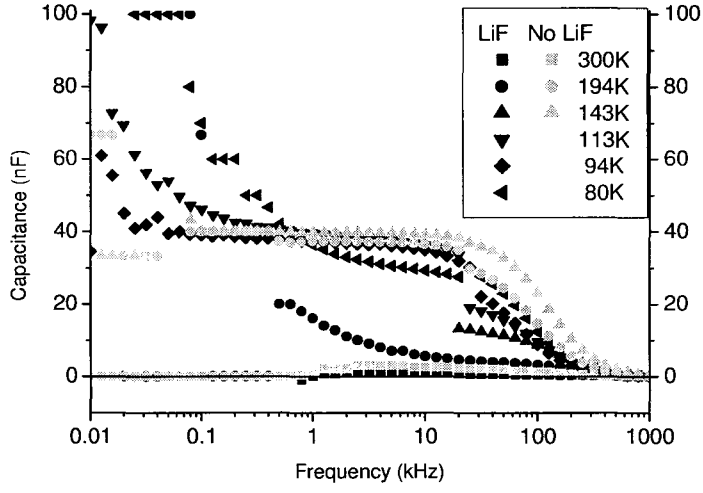

Figure 8.8: *capacitance at 1.5V for PCBM with and without LiF in the dark. Without LiF there are no traps.*

For the blend, without LiF there are less traps, as can be observed in figure 8.9. This is consistent with the decrease of traps in PCBM, considering the holes as the minority carriers and thus as the minor traps. LiF probably lowers the injection barrier for electrons a little bit, as in the PPV, and prevents trap-formation for holes and helps trap formation for electrons. Double carrier injection stops at lower frequencies, but this effect is small and within the uncertainty.

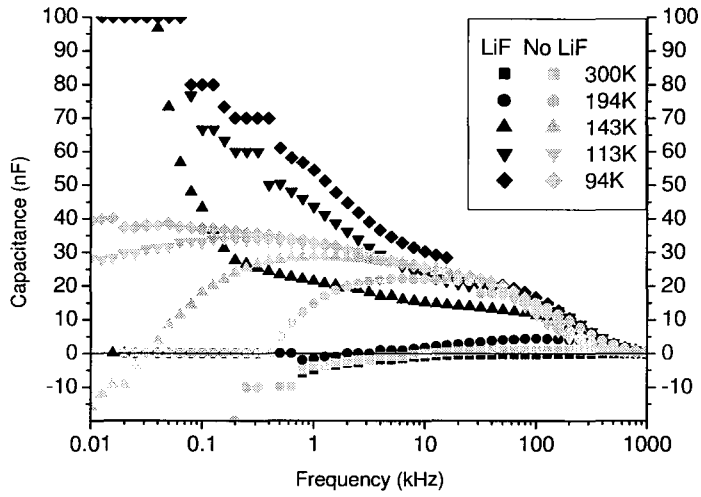

Figure 8.9: *capacitance at 1.25V for the blend with and without LiF in the dark. Without LiF, there are less traps and double carrier injection stops at lower frequencies.*

8.3: Conclusions

From the characterization of the samples without LiF we can draw some conclusions. The LiF seems to decrease the work function of the cathode, which leads to a lower built-in potential for PPV and a higher capacitance for PCBM and the blend. LiF also seems to increase the mobility at low temperatures in PCBM, what leads to a decrease of the band-widening σ.

With LiF the fill-factor and the efficiency increase with 4 and 21% respectively.

LiF lowers the injection barrier for electrons, helps filling traps for electrons and prevents filling traps for holes.

Chapter 9: Interface Band-Bending

In paragraph 2.5, a model for the interface band-bending is distracted from the Poisson and drift-diffusion equations and the Einstein-relation. In this chapter this formula will be compared with the experimental data from the IV-measurements from the different samples.

9.1: Comparison of model with measurements

A great number of built-in voltages are determined from IV-measurements. The built-in potentials are determined by exceeding the lines above V_{bi} down to zero. Where the line crosses the x-axis is Vbi. In figure 9.1 the measured built-in voltages are shown (symbols). They are compared with the model (lines). Here, the fit-parameters of the model are chosen to fit the measurements, with the constraints mentioned in paragraph 2.5. As can be observed, the difference between the model-fit and the measured values is within the spread of those values.

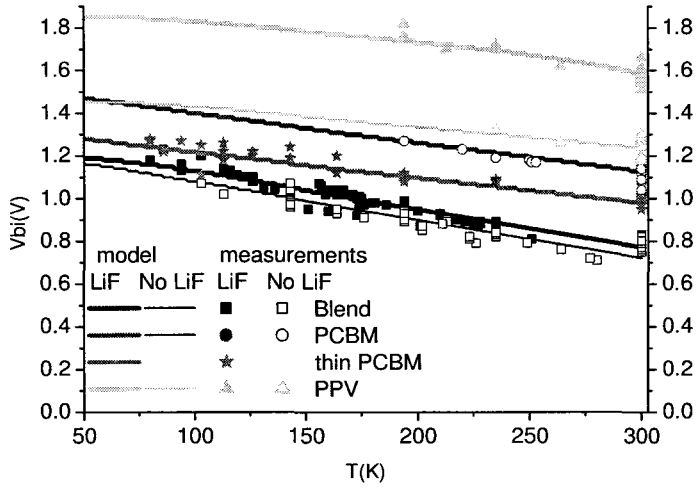

Figure 9.1: *the measured built-in voltages as a function of temperature, the scatter, compared with the model, the lines. The spread of the scatter is bigger than the difference between the lines and the scatter. The lines for PCBM with and without LiF are the same.*

A thin PCBM sample, only 20nm thick, is shown in figure 9.1 by stars. This sample has values of V_{bi} lower than should be expected from the model. For the fit, it is assumed that the bandgap is smaller. The used parameters for all the lines in figure 9.1 are listed in table 9.1.

Table 9.1: *Parameters in the model; some are measured (1) dependent on other parameters (2) or taken from literature*

	PPV	PCBM	Blend	Thin PCBM
thickness (nm)[1]	140	56	100	20
effective thickness (nm)[1]	70	28	50	10
ε_r[3]	3	3.9	3.72	3.9
n_{mAl} (m^{-3})[3]	$1.81*10^{29}$	$1.81*10^{29}$	$1.81*10^{29}$	$1.81*10^{29}$
n_{mPEDOT} (m^{-3})[3]	$3*10^{26}$	$3*10^{26}$	$3*10^{26}$	$3*10^{26}$
n_0 (m^{-3})[3]	$3*10^{26}$	$3*10^{26}$	$3*10^{26}$	$3*10^{26}$
E_{gap} (eV)	2.4[3]	2.4[3]	1.35	2.2
φ_{Al} (eV)	0.85	0.05	0.05	0.05
φ_{LiF} (eV)	0.45	0[3]	0	0
φ_{PEDOT} (eV)	0.1[3]	0.85	0.1	0.85
V_{bi0} (V)[2]	1.45	1.5	1.2	1.3
$V_{bi0,LiF}$ (V)[2]	1.85	1.55	1.25	1.35

The parameters for the model are chosen to match the measurements. The actual number of free parameters however is small: only five, not mentioning the thin PCBM sample. The thicknesses are measured. The permittivity of PPV[1] and PCBM[2,3] is known in literature. The permittivity of the blend is taken as a weighted average. The charge density of aluminum is the same as in literature, the density of PEDOT taken equal to n_0 in PPV[3], which is an order above literature[4], which is $1.8*10^{25}m^{-3}$. The gaps of PPV and PCBM do match literature[5,6,7], and so does the injection barrier of LiF in PCBM[3] and PEDOT in PPV[8]. Since Al is an electron injector, PEDOT a hole injector, PCBM an electron conductor and PPV a hole conductor we can state that the electron injection barrier of Al and LiF into the blend are the same as into PCBM, and the hole injection barrier of PEDOT into PPV is the same as into the Blend. The built-in potential at 0K is the energy gap minus the injection barriers. So, only the injection barriers of Al into PPV and PCBM, LiF into PPV, PEDOT into PCBM and the energy gap of the blend are chosen to match the measurements.

So only five fitting parameters are used to match the measurements, where this model describes the measurements well.

9.2: Dependence V_{bi}

Figure 9.1 gives an impression of the dependence of the built-in voltage on the temperature. The built-in voltage is however also dependent on the thickness, the injection barrier and the charge density. In the previous paragraph, the freedom of these parameters is shortly discussed. Here, the dependence on these parameters will be shown.

A sample with an ε_r of 3 is assumed. Also we assume only one contact here and a gap of 1.35eV, and V_{bi}=1.2V at 0K. An injection barrier of 0.1eV, a thickness of 100nm and a charge density of $1*10^{29}m^{-3}$ are assumed, unless stated otherwise. The results can be observed in figures 9.2, 9.3 and 9.4.

As can be observed in figure 9.2, the dependence on the thickness is small; the thickness has to change orders to make a serious difference, more than 0.1V, where the accuracy of the measurements of V_{bi} is about 0.1V.

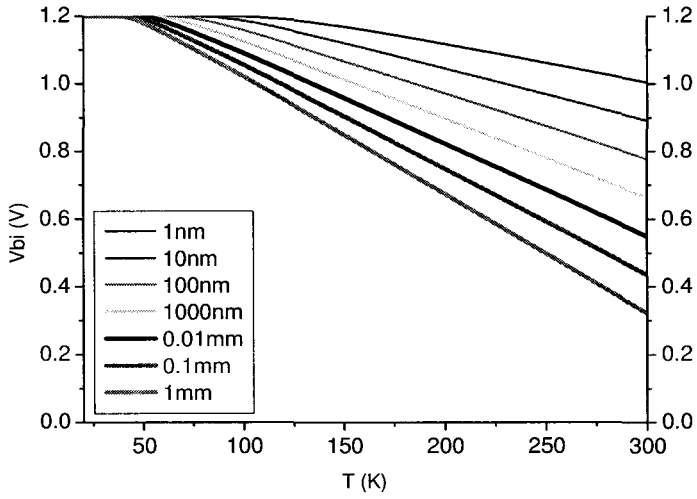

Figure 9.2: *built-in voltage for several thicknesses; only the slope changes*

As can be observed in figure 9.3, the injection barrier determines the temperature where the band bending starts. This is almost a linear process. Above 0.5eV increasing the injection has no effect up to 300K. The values of the injection barrier between Al and PPV and the injection barrier between PEDOT and PCBM, that are high, do not influence the curves. These two injection barriers are not really fitting parameters. The injection barrier has no effect on the slope of the curve as long as the density of states in the polymer does not equal its maximum. For φ=0eV this does occur what leads to a smaller density, which leads to less band-bending. For φ is 0.2eV and higher this does not happen.

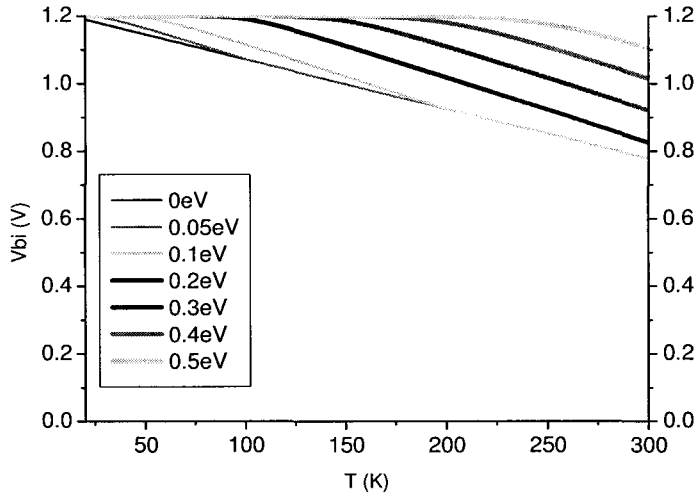

Figure 9.3: *built-in voltage for several injection barriers, the knee changes*

As can be observed in figure 9.4, the charge density of the electrode has an effect on the slope of the curve. The effect is however small, the density should increase two orders for a change of 0.1V at 300K. For charge densities above n_0 the slope changes from a certain temperature.

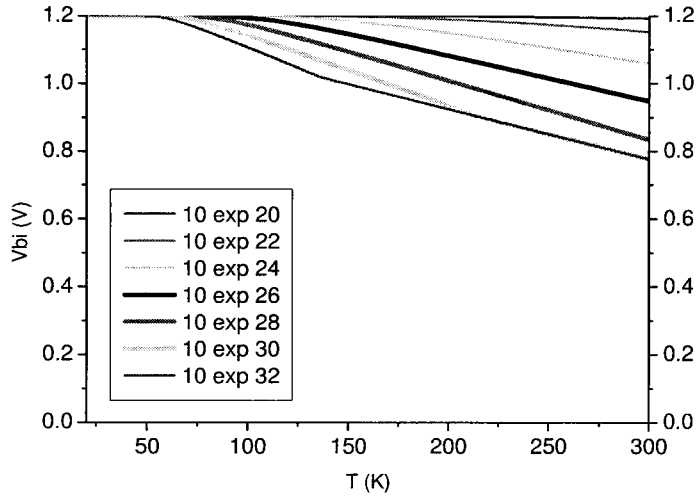

Figure 9.4: *built-in voltages for several charge densities of the contact electrode, the slope changes*

From the graphs we can conclude that the injection barrier, if small, less than 0.5eV, has the most effect on the built-in voltage. The thickness and the charge density determine the slope.

9.3: Conclusions

The measured built-in voltages do match the model described in paragraph 2.5. Only a small set of three fit parameters is used: the injection barriers of Al into PCBM, LiF into PPV and the energy gap of the blend. Therefore we can conclude that the model is promising. It is also well comparable with the model of Simmons[9] from 1971, but has the advantage of the analytical approach.

Chapter 10: Conclusions and Discussion

In the previous chapters dealing with the results, a start has been made in drawing conclusions and starting a discussion. That was mostly of the results in the particular chapter. Here, an approach will be made to discuss if the blend solar cell can be described as a combination of the PPV and PCBM samples, and what features in the blend are really new. This both for the samples with and without LiF. Here the parameters as permittivity, mobility, traps, double carrier and band alignment will be discussed.

10.1: Permittivity

With LiF, the permittivity of the blend is not a weighted average of the permittivity of PPV and PCBM, as can be observed in figure 8.6: the geometrical capacitance of the blend is bigger than the geometrical capacitances of both PPV and PCBM. This is because the bending of the LUMO what makes the sample behave quasi-metallic, and thus will lead to a higher capacitance. LiF helps the blend and the PCBM to store charges.

The relation between the geometrical capacitances of PPV and PCBM however can be explained with the ratio between the permittivities. Calculating the expected capacitances according formula 2.20, there is a difference of 20% between the measured and calculated capacitances, except for the capacitance of the blend with LiF. The measured capacitances are lower than the calculated capacitances. This is possibly because of the PEDOT:PSS that could partly contribute to the thickness.

10.2: Mobility

The current in the blend is higher than the sum of the currents of the pure materials. This is because PCBM conducts electrons very well, but is a poor hole-conductor and PPV conducts holes very well. Together, they can conduct both carriers very well. This is called bipolar conduction. PPV is also suspected to conduct better if blended with PCBM. At low temperatures, 113K, the currents for PCBM and the blend are almost the same, PCBM a little higher than the blend, because the mobility in the PPV decreases fast with decreasing temperature.

For the mobility at high temperatures the blend cannot be described as a sum of the PPV and the PCBM. At low temperatures, T<194K, the mobility in PPV decreases and the effects in PCBM and in the blend are almost the same, both with and without LiF.

10.3: Traps and double carriers

In the dark, traps occur in PPV and PCBM, but not in the blend. Under illumination, traps do occur in the blend, as in the PPV and the PCBM. For double carrier injection, the blend injects both carriers at higher frequencies, probably because the mobility of PPV is higher in the blend.

Under illumination, at 0V at low temperatures there are traps in the blend that are not in the PPV or the PCBM. Without LiF under illumination, there are less traps and more double carriers in the blend, while there are more traps and less double carriers in the PPV and the PCBM.

In these features, the blend cannot be understood as the combination of the pure materials.

10.4: Band alignment

The parameters describing the band bending are well comparable, assuming PEDOT:PSS to be the hole injector, with a low barrier for PPV and high for PCBM, and Al and LiF to be the electron injectors with low barriers to PCBM and high to PPV. Combining these materials the blend has the injection barrier of PEDOT into PPV and Al and LiF into PCBM. With the gap the built-in voltages thus are described in a correct way. LiF seems to simply increase the work function of Al; it is less negative. Here, the bend is the combination of the components.

10.5: Summary conclusions

The blend is in many ways a combination of the components. For the permittivity, the blend is bigger then both components. For the mobility the blend is the combination of the components, bipolar conduction.

For traps and double carriers, the blend cannot easily be described as a combination of the pure materials.

In terms of the injection barriers with the band alignment, the blend is the combination of the pure materials. LiF does not change the possibility in describing the blend as a sum of the PPV and the PCBM.

References and Notes

1: Introduction

1: K.Michaelian; More Options Offered for Long-Term Energy Solutions, Physics Today, http://www.physicstoday.org/vol-58/iss-4/p12.html (2005)
2: World Energy Council; Energy for Tomorrows World, Chapter 2: The 1993 Report—Energy demand analysis http://www.worldenergy.org/wec-geis/default.htm (2000)
3: R.F.Service; Organic Solar Cells Playing Catch-Up, Science, Vol 306, Issue 5704, 2034 (17 December 2004)
4: B. Rånby; Conjugated Polymers and Related Materials: The Interconnection of Chemical and Electronic Structures, Oxford University, Oxford (1993)
5: F.C.Chen, Q.Xu, Y.Yang; Applied Physical Letters, vul 84, nr 16, 3181-3183 (2004)
6: J.K.J.v.Duren; Polymer:Fullerene Bulk-Heterojunction Solar Cells (2004)

2: Theory

1: J.R.Hanson; Functional Group Chemistry, p 1-23 (2001)
2: M.Hatano, S.Kambara, S.Okamoto; Journal of Polymer Science, vol 51, S26 (1961)
3: Z.Vardeny, E.Ehrenfreund, O.Brafman, B.Horovitz; Physical Review Letters, vol 54, nr 1, p75 78 (1985)
4: J.Nelson; Physics of Solar Cells, chapter 8.1, p211-212,UK (2003)
5: Sze, Physics of Semiconductor Devices, John Wiley & Sons, Inc. New York (1981)
6: B.v.Zeghbroeck; Principles of Semiconductor Devices, chapter 3 (2004)
7: N.v.Malm, J.Steiger, H.Heil, R.Schmechel, H.v.Seggern; Electronic traps and percolation paths in electroluminescent polymers, Journal of Applied Physics vol 92, p7564-7570 (2002)
8: H.Mattoussi, L.H.Radzilowski, B.O.Dabbousi, E.L.Thomas, M.G.Bawendi, M.F.Rubner; Electroluminescence from heterostructures of poly(phenylene vinylene) and inorganic CdSe nanocrystals, Journal of Applied Physics vol 83, p7965-7974 (1998)
9: R.Friend, J.Burroughes, T.Shimoda; Lasers and Optics: Polymer Diodes, Physics World, p35-40 (june 1999)
10: C.J.Brabec, N.Serdar Sariciftci, J.C.Hummelen; Plastic Solar Cells, Advanced Functional Materials, vol 11 p15-26 (2001)
11: H.C.F.Martens; Ph.D thesis, Universiteit Leiden (2000)
12: J.K.J.v.Duren; Polymer:Fullerene Bulk-Heterojunction Solar Cells, chapter 5.3, p91-97 (2004)
13: J.Nelson; Physics of Solar Cells, chapter 2.5, p28-35, UK (2003)
14: V.D.Mihailetchi, L.J.A.Koster, J.C.Hummelen, P.W.M.Blom; Physical review Letters 93, 216601 (2004)
15: H.U.Baranger, J.W.Wilkins; Physical Review B, vol 30 nr 12, p7349-7351 (1984)
16: G.Pfister, A.I.Lakatos; Physical Review B, vol 6, nr 8, p3012-3018 (1972)
17: V.D.Mihailetchi, J.K.J.v.Duren, P.W.M.Blom, J.C.Hummelen, R.A.J.Janssen, J.M.Kroon, M.T.Rispens, W.J.Verhees, M.M.Wienk, Adv. Funct. Mat. vol 13, p43, (2003)
18: I.Chen; Effects of bimolecular recombination on photocurrent and photoinduced discharge, Journal of Applied Physics 49, p1162-1172 (1978)
19: Langevin; Ann. Chim. Phys. vol 28, p433 (1903)
20: H.Ishii, K.Sugiyama, E.Ito, K.Seki; Advanced Materials vol 11, p605 (1999)
21: R.Kassing; Calculation of the frequency dependence of the admittance of SCLS diodes, Physical static solids A vol 28, p107-117 (1975)
22: P.Debye; Polar Molecules (Chemical Catalogue Co.), p. 92. (1929)
23: J.Werner, A.F.J.Levi, R.T.Tung, M.Anzlowar, M.Pinto; Origin of the excess capacitance at intimate Schottky contacts, Physical Review Letters 60, p53-56 (1988)

24: M.A.Lampert, P.Mark; Current Injection in Solids, 1st ed. (London, Academic Press, 1970)
25: M.Ershov, H.C.Liu, L.Li, M.Buchanan, Z.R.Wasilewski, A.K.Jonscher; IEEE Trans. Electron. Devices vol 45, p2196 (1998)
26: H.Bässler; Phys. Stat. Sol. B vol 175, p15 (1993)

3: Experimental Set-Up

1: J.K.J.v.Duren; Polymer:Fullerene Bulk-Heterojunction Solar Cells, chapter 2.3, p15-19 (2004)

4: Preliminary Measurements

1: L.F.Marsal, J.Pallare`s, X.Correig, J.Calderer, R.Alcubilla; Electrical model for amorphous/crystalline heterojunction silicon diodes (n a-Si:H/p c-Si), Semiconductor Science and Technology, vol 11 p1209-1213 (1996)
2: V.Shrotriya, Y.Yanga; Capacitance–voltage characterization of polymer light-emitting diodes, Journal of Applied Physics, vol 97, p054504 (2005)
3: Measurement done by A.M.Nardes, Eindhoven University of Technology (2005)

5: Results PPV

1: V.D.Mihailetchi, J.K.v.Duren, P.W.M.Blom, J.C.Hummelen, R.A.J.Janssen, J.M.Kroon, M.T.Rispens, W.J.H.Verhees, M.M.Wienk; Electron Transport in a Methanofullerene, Advanced Functional Materials, vol 13 p43-46 (2003)
2: L.J.A.Koster, V.D.Mihailetchi, R.Ramaker, P.W.M.Blom; Light intensity dependence of open-circuit voltage of polymer:fullerene solar cells, Applied Physics Letters vol 86, p123509 (2005)

6: Results PCBM

1: V.D.Mihailetchi, J.K.v.Duren, P.W.M.Blom, J.C.Hummelen, R.A.J.Janssen, J.M.Kroon, M.T.Rispens, W.J.H.Verhees, M.M.Wienk; Electron Transport in a Methanofullerene, Advanced Functional Materials, vol 13 p43-46 (2003)
2: P.W.M.Blom, M.J.M.d.Jong, M.G.v.Munster; Electric-field and temperature dependence of the hole mobility in poly(p-phenylene vinylene), Physical Review B vol 55, nr 2, p656-659 (1997)
3: E.J.Meijer, D.M.d.Leeuw, S.Setayesh, E.v.Veenendaal, B.H.Huisman, P.W.M.Blom, J.C.Hummelen, U.Scherf, T.M.Klapwijk; Solution-processed ambipolar organic field-effect transistors and inverters, nature materials, VOL 2, p678-682 (2003)

7: Results Blend

1: L.J.A.Koster, V.D.Mihailetchi, R.Ramaker, P.W.M.Blom; Light intensity dependence of open-circuit voltage of polymer:fullerene solar cells, Applied Physics Letters vol 86, p123509 (2005)

8: Results without LiF

1: L.S.Hung, C.W.Tang, M.G.Mason; Enhanced electron injection in organic electroluminescence devices using an Al/LiF electrode, Applied Physics Letters vol 70, p152-154 (1997)

9: Interface band-bending

1: P.W.M.Blom, M.J.M.d.Jong, M.G.v.Munster; Electric-field and temperature dependence of the hole mobility in poly(p-phenylene vinylene), Physical Review B vol 55, nr 2, p656-659 (1997)

2: V.D.Mihailetchi, J.K.v.Duren, P.W.M.Blom, J.C.Hummelen, R.A.J.Janssen, J.M.Kroon, M.T.Rispens, W.J.H.Verhees, M.M.Wienk; Electron Transport in a Methanofullerene, Advanced Functional Materials, vol 13 p43-46 (2003)

3: V.D.Mihailetchi, P.W.M.Blom, J.C.Hummelen, M.T.Rispens; Cathode dependence of the open-circuit voltage of polymer:fullerene bulk heterojunction solar cells, Journal of Applied Physics vol94, nr 10, p6849-6854 (2004)

4: Private communication

5: N.v.Malm, J.Steiger, H.Heil, R.Schmechel, H.v.Seggern; Electronic traps and percolation paths in electroluminescent polymers, Journal of Applied Physics vol 92, p7564-7570 (2002)

6: H.Mattoussi, L.H.Radzilowski, B.O.Dabbousi, E.L.Thomas, M.G.Bawendi, M.F.Rubner; Electroluminescence from heterostructures of poly(phenylene vinylene) and inorganic CdSe nanocrystals, Journal of Applied Physics vol 83, p7965-7974 (1998)

7: R.Friend, J.Burroughes, T.Shimoda; Lasers and Optics: Polymer Diodes, Physics World, p35-40 (june 1999)

8: C.Melzer, E.J.Koop, V.D.Mihailetchi, P.W.M.Blom; Hole transport in Poly(phenylene vinylene)/Methanofullerene Bulk-Heterojunction Solar Cells, Advance Functional Materials vol 14 p865-870 (2004)

9: J.G.Simmons; Theory of metallic contacts on high resistivity solids - I. Shallow traps, Journal of chemical solids vol 32, p1987-1999 (1971)

Appendices

Contents:

Appendix I: Thickness

Table I.1: *Thickness measurements; all including PEDOT:PSS*

Sample	Measured thicknesses (nm)		
8 sep (blend)	169		
14 sep (blend)	163	161	
30 sep (blend)	180	174	
19 oct (blend)	203	190	
4 nov (PCBM)	105	92	
18 nov (PCBM)	120	130	
3 dec (PCBM)	134	138	138
17 dec (PPV)	225	212	218
14 jan (PEDOT)	88	86	

Appendix II: PPV with LiF

All measurements are on the same sample made on 17 December (approximately 138nm thick).

II.1: IV-measurements

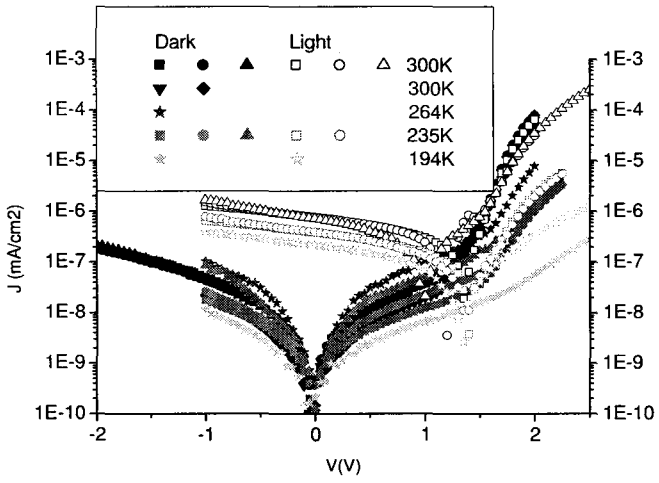

Figure II.1: *I-V measurements on PPV in light and dark for different temperatures. All measurements are on the same sample*

II.2: Capacitance

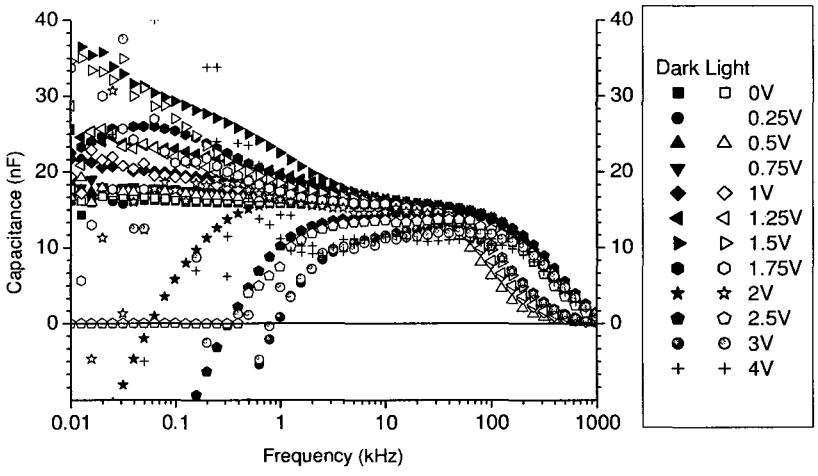

Figure II.2: *capacitance in dark and light of PPV with LiF at 300K*

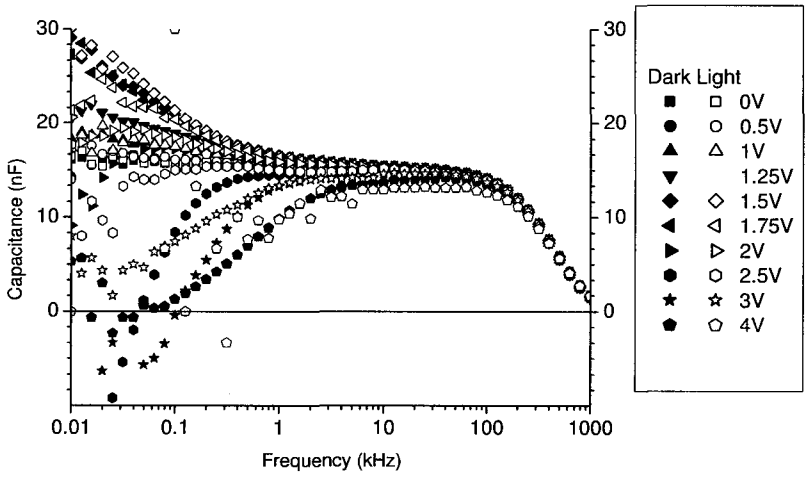

Figure II.3: *capacitance in dark and light of PPV with LiF at 264K*

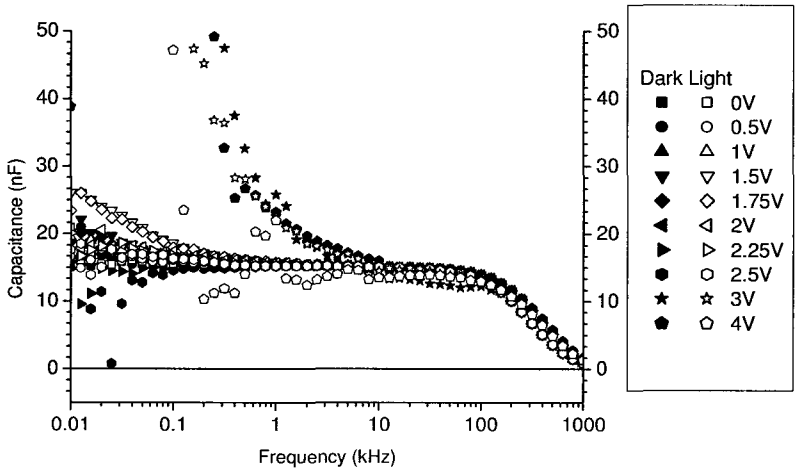

Figure II.4: *capacitance in dark and light of PPV with LiF at 235K*

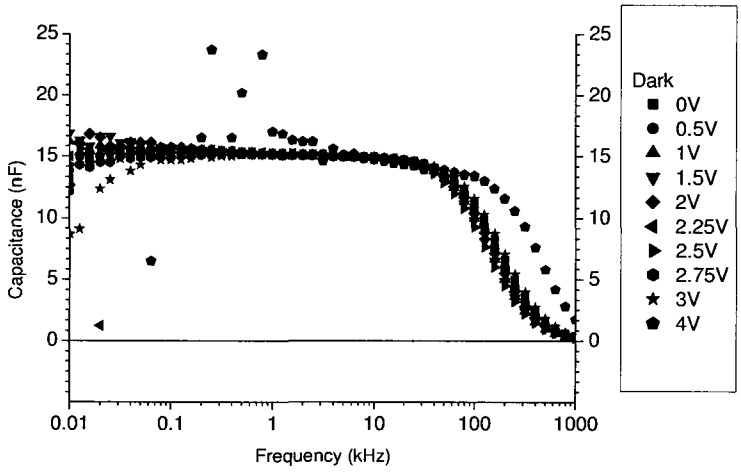

Figure II.5: *capacitance in dark of PPV with LiF at 213K*

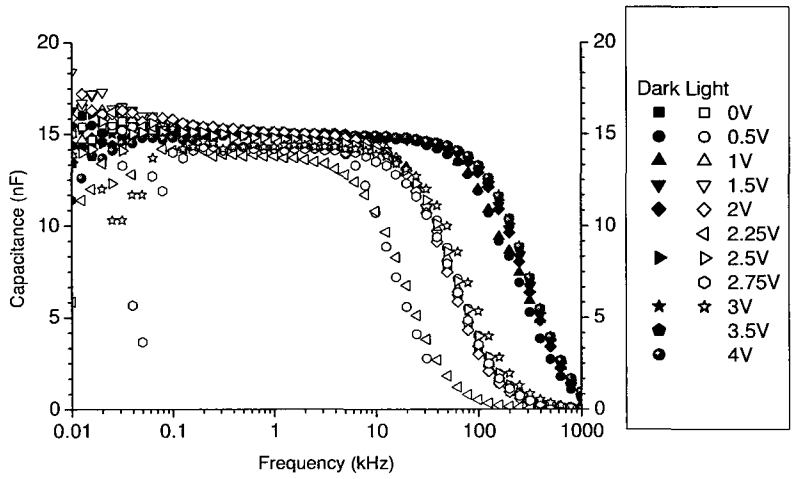

Figure II.6: *capacitance in dark and light of PPV with LiF at 194K*

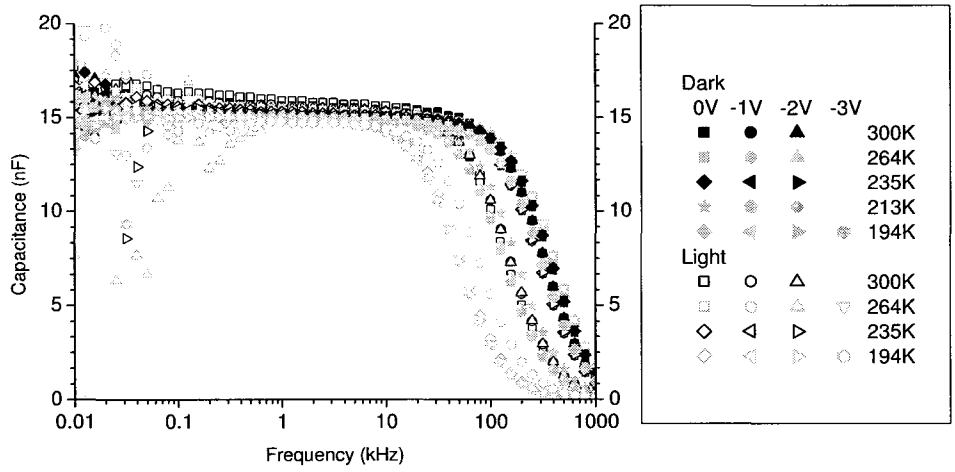

Figure II.7: *capacitance in dark and light of PPV with LiF at negative voltages*

II.3: Conductance

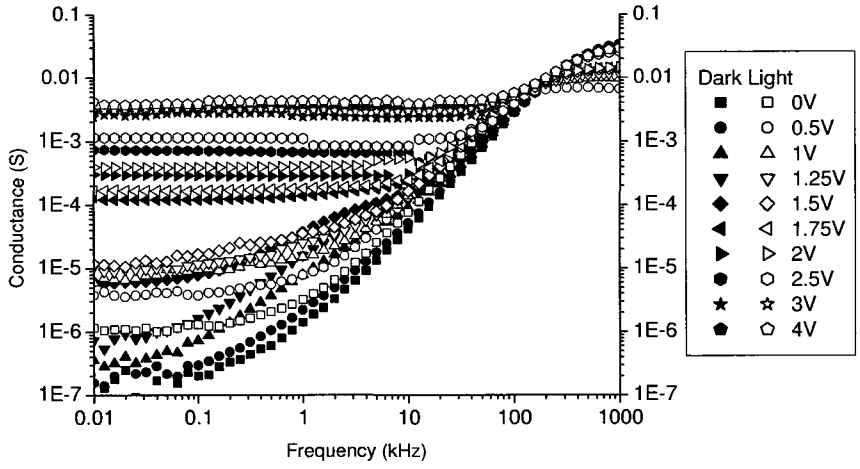

Figure II.8: *conductance in dark and light of PPV with LiF at 300K*

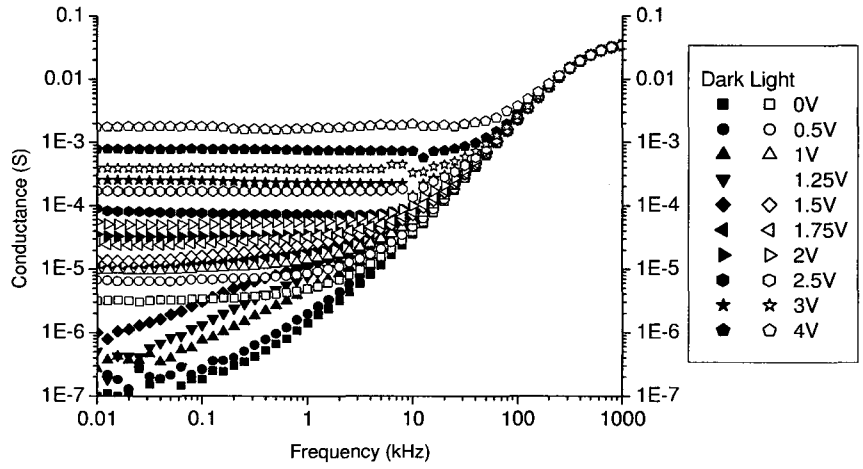

Figure II.9: *conductance in dark and light of PPV with LiF at 264K*

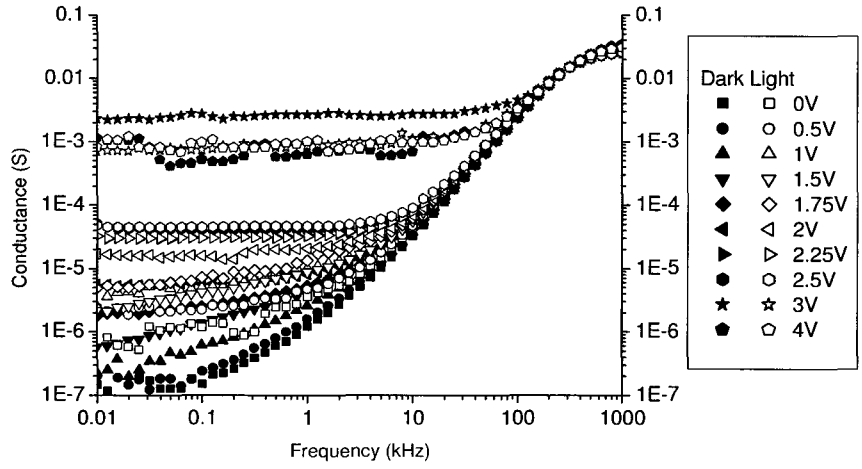

Figure II.10: *conductance in dark and light of PPV with LiF at 235K*

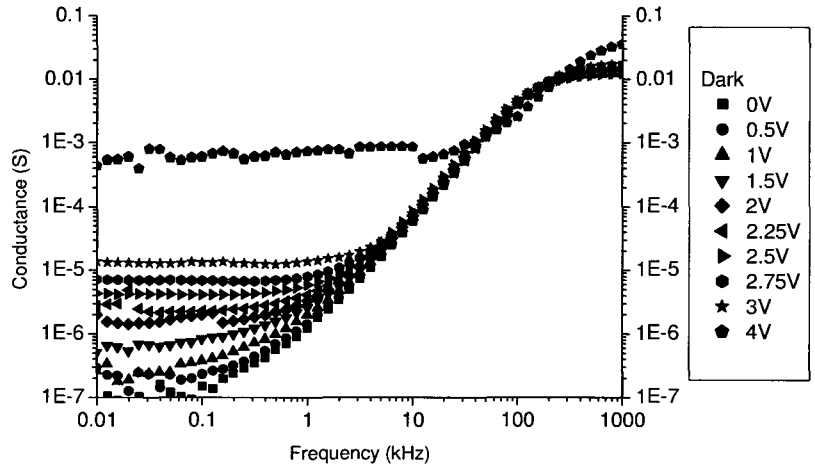

Figure II.11: *conductance in dark of PPV with LiF at 213K*

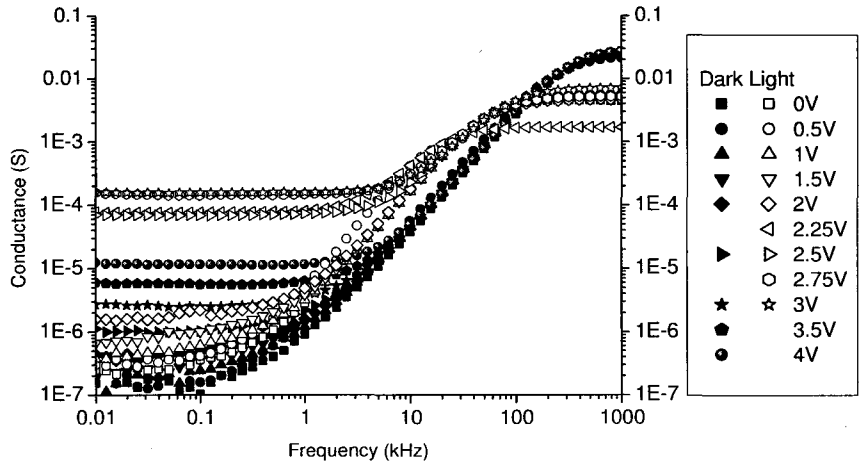

Figure II.12: *conductance in dark and light of PPV with LiF at 194K*

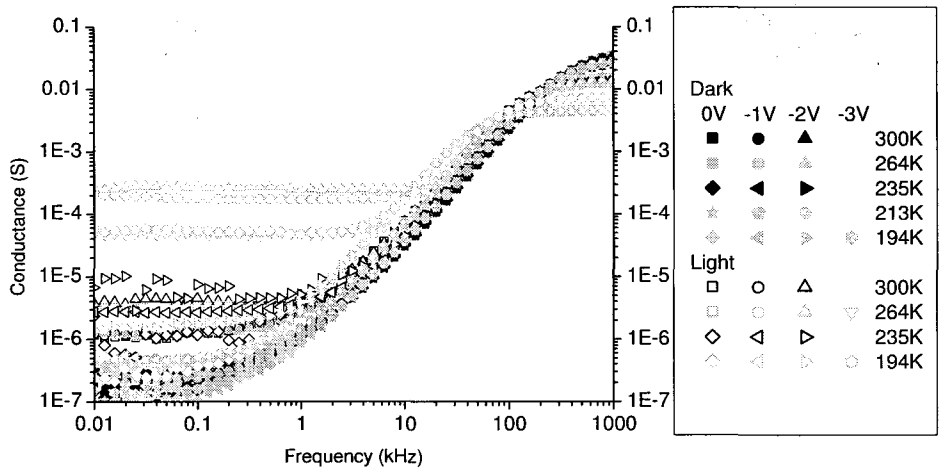

Figure II.13: *conductance in dark and light of PPV with negative voltages*

Appendix III: PCBM with LiF

For the IV measurements samples from different data are used, for the impedance measurements a sample of 3 December is used (approximately 56nm thick)

III.1: IV-measurements

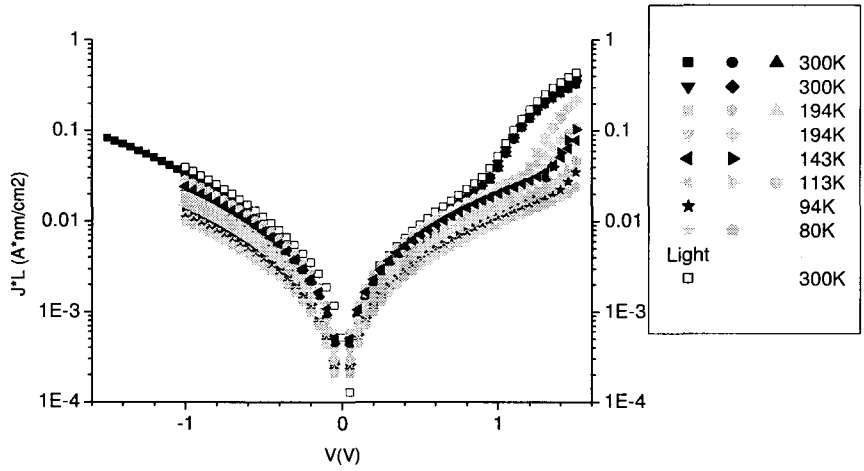

Figure III.1: *I-V measurements on PCBM in light and dark for different temperatures. All measurements are on the same sample (3) made on 4 November*

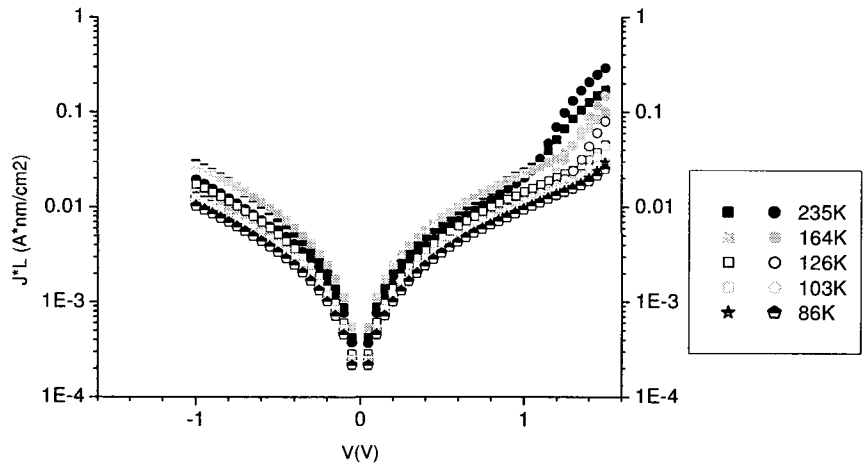

Figure III.2: *I-V measurements on PCBM in dark for different temperatures. All measurements are on the same sample (3) made on 4 November*

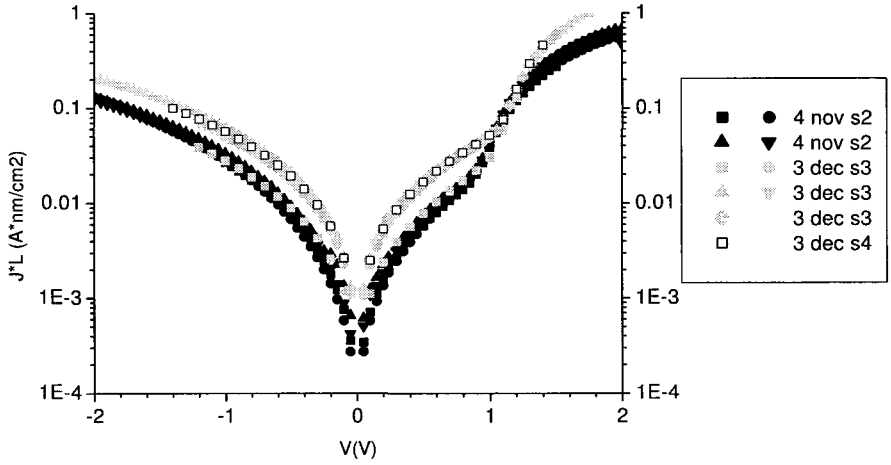

Figure III.3: *I-V measurements on PCBM in dark at 300K for different samples.*

III.2: Capacitance

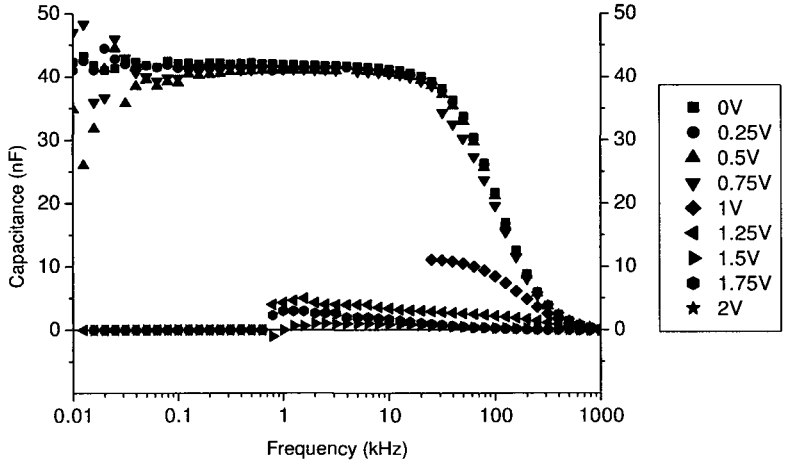

Figure III.4: *capacitance in dark of PCBM with LiF at 300K*

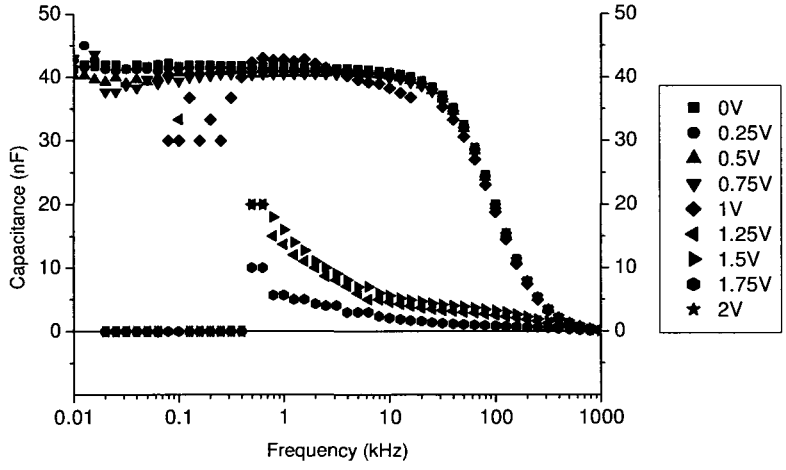

Figure III.5: *capacitance in dark of PCBM with LiF at 194K*

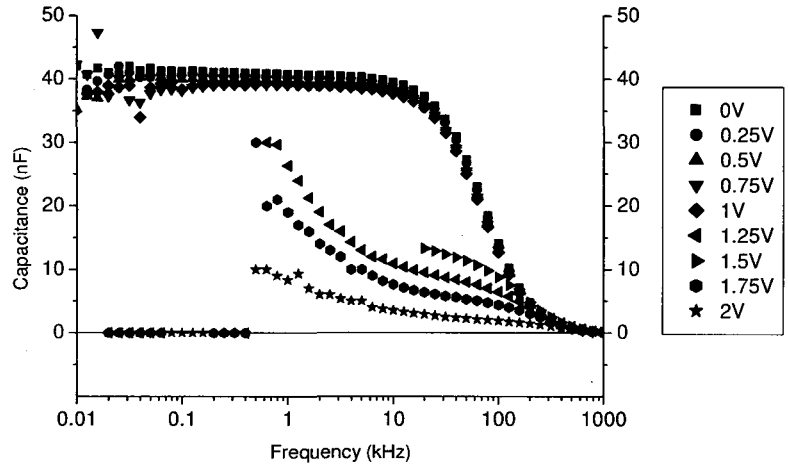

Figure III.6: *capacitance in dark of PCBM with LiF at 143K*

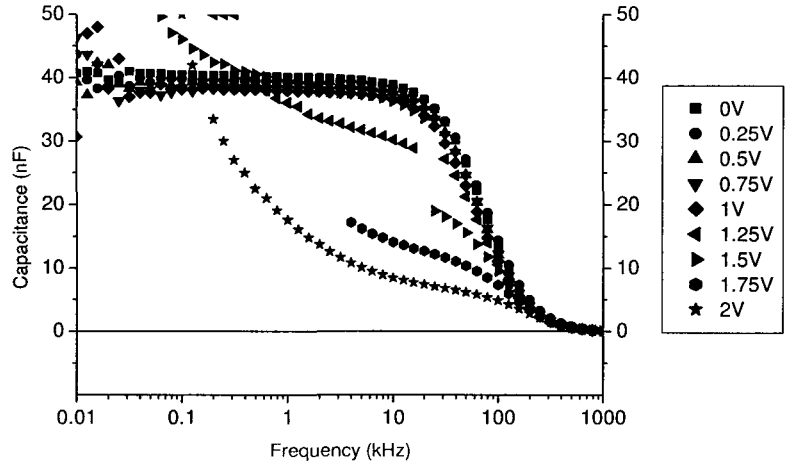

Figure III.7: *capacitance in dark of PCBM with LiF at 113K*

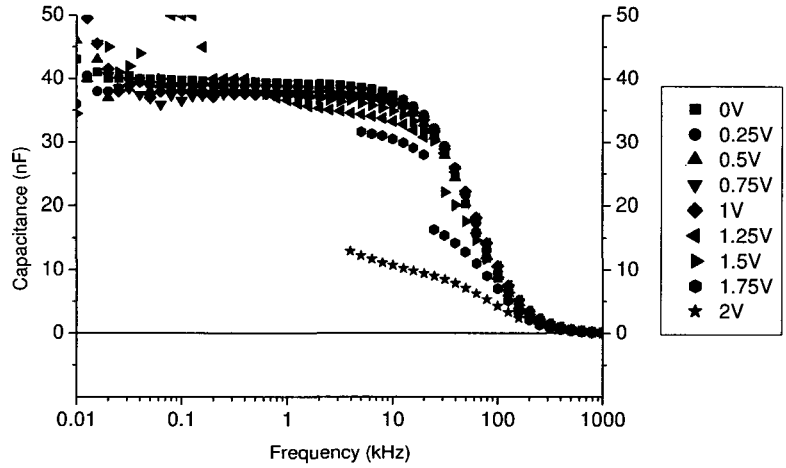

Figure III.8: *capacitance in dark of PCBM with LiF at 94K*

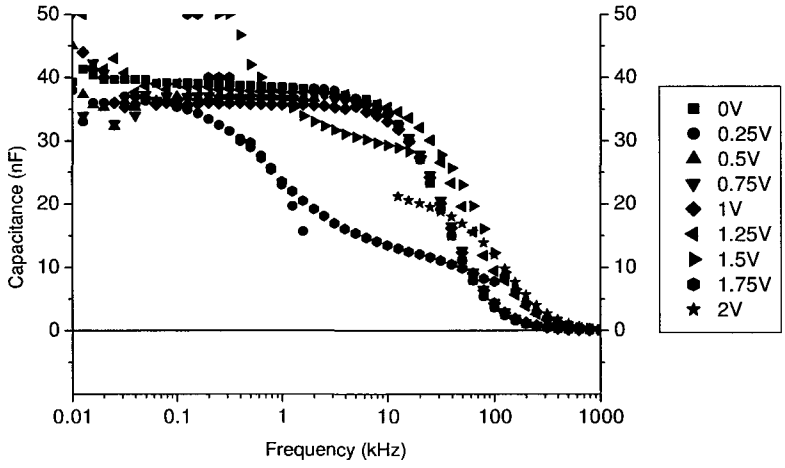

Figure III.9: *capacitance in dark of PCBM with LiF at 80K*

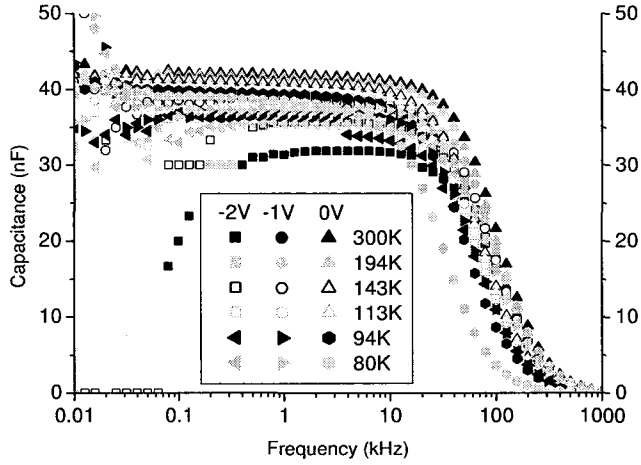

Figure III.10: *capacitance in dark of PCBM at with LiF with negative voltages*

III.3: Conductance

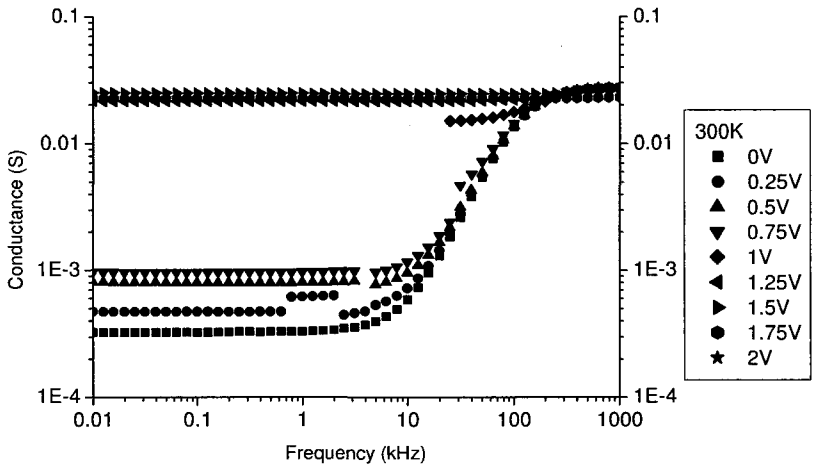

Figure III.11: *conductance in dark of PCBM with LiF at 300K*

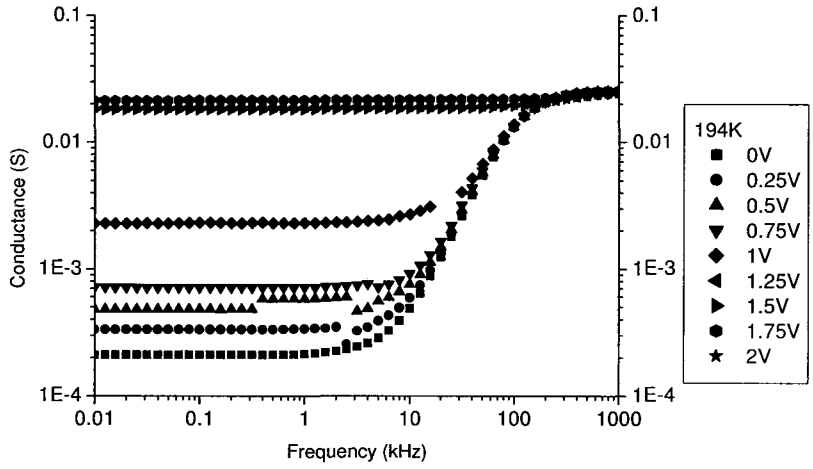

Figure III.12: *conductance in dark of PCBM with LiF at 194K*

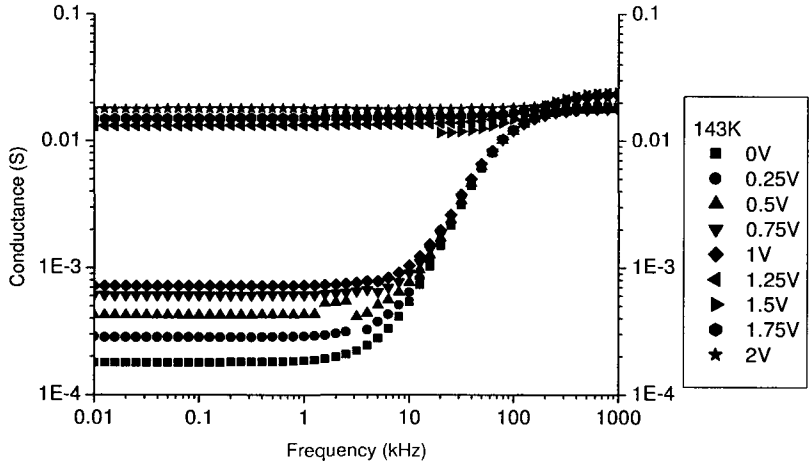

Figure III.13: *conductance in dark of PCBM with LiF at 143K*

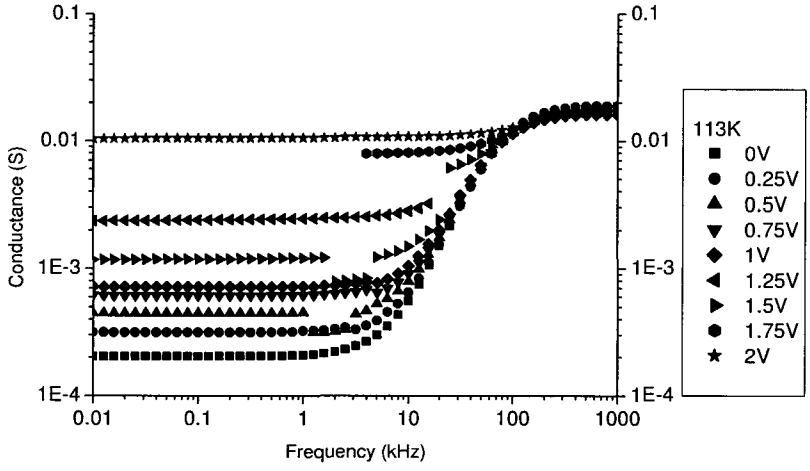

Figure III.14: *conductance in dark of PCBM with LiF at 113K*

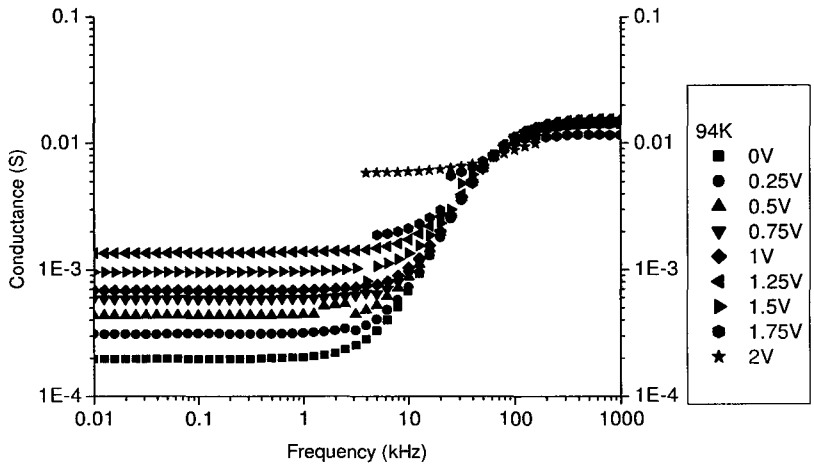

Figure III.15: *conductance in dark of PCBM with LiF at 94K*

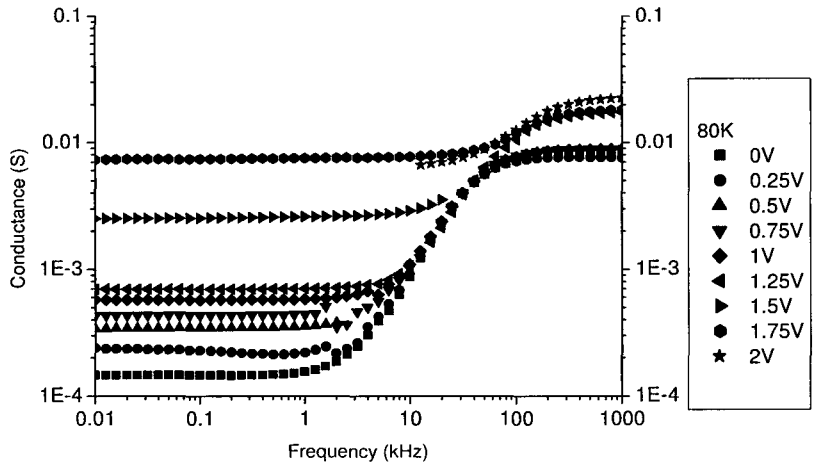

Figure III.16: *conductance in dark of PCBM with LiF at 80K*

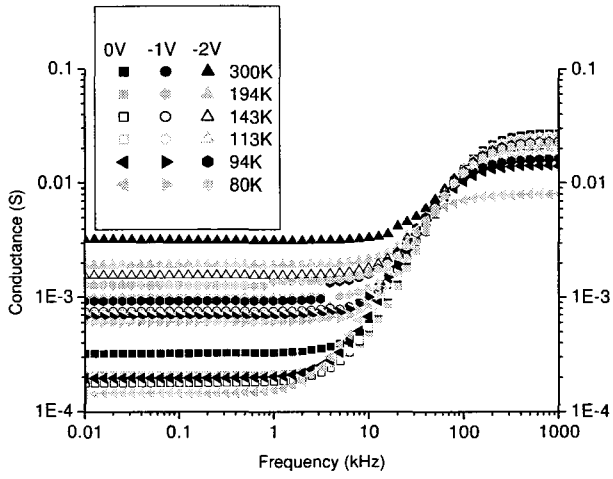

Figure III.17: *conductance in dark of PCBM with LiF with negative voltages*

Appendix IV: Blend with LiF

The sample used in the impedance measurements is of 30 September (approximately 97 nm thick).

II.1: IV-measurements

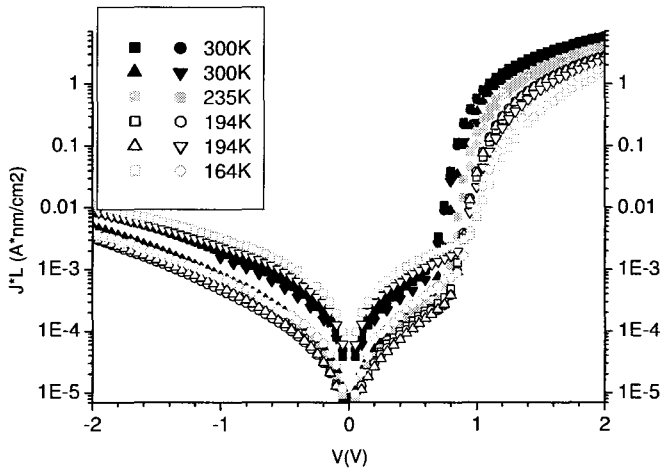

Figure IV.1: *I-V measurements on the blend in the dark for different temperatures on a sample (2) made on 14 September*

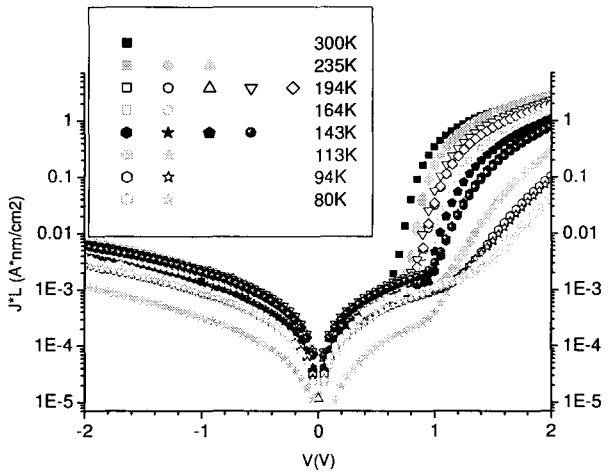

Figure IV.2: *I-V measurements on the blend in the dark for different temperatures on a sample (3) made on 30 September*

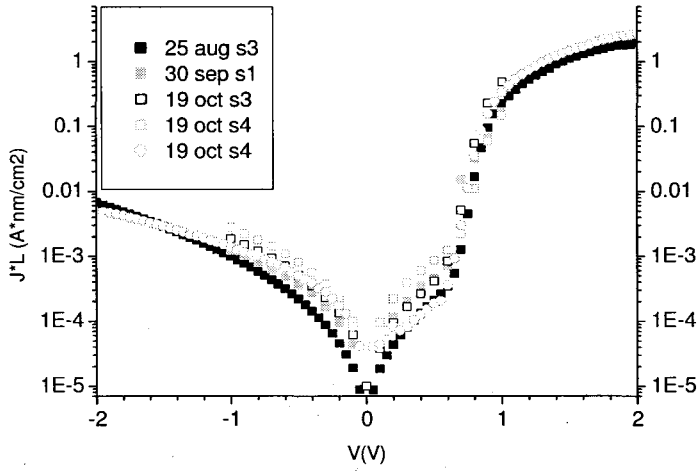

Figure IV.3: *I-V measurements on the blend in the dark for different samples at 300K; the thickness of the sample of 25 August is not measured but assumed to be 85nm*

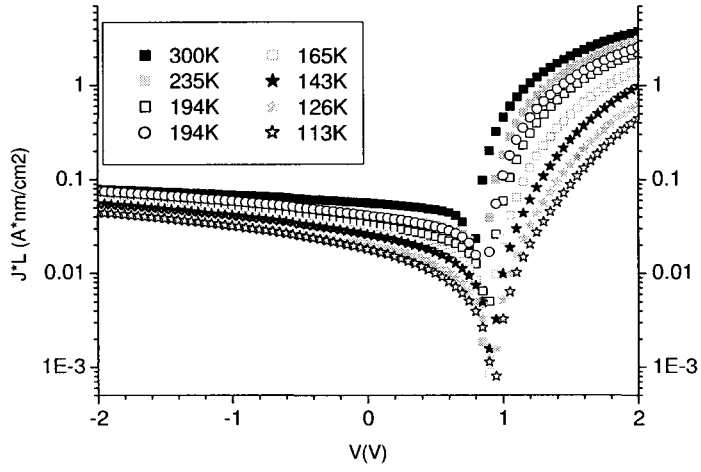

Figure IV.4: *I-V measurements on the blend in the light for different temperatures on a sample (3) made on 30 September*

IV.2: Capacitance

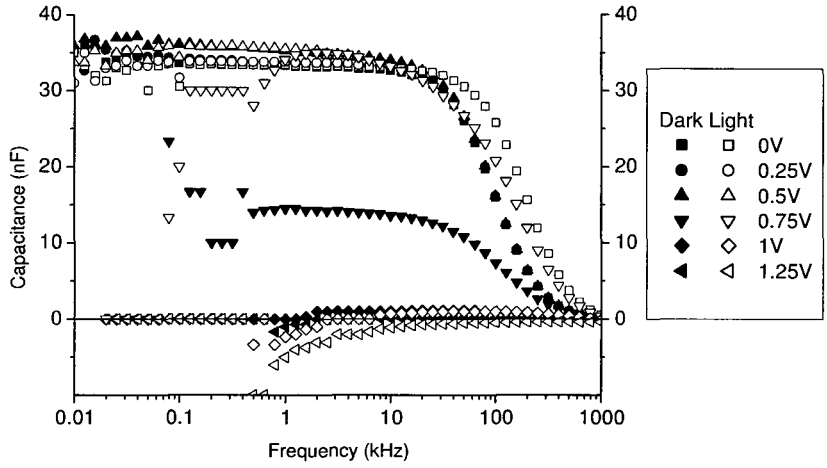

Figure IV.5: *capacitance in dark and light of the blend with LiF at 300K*

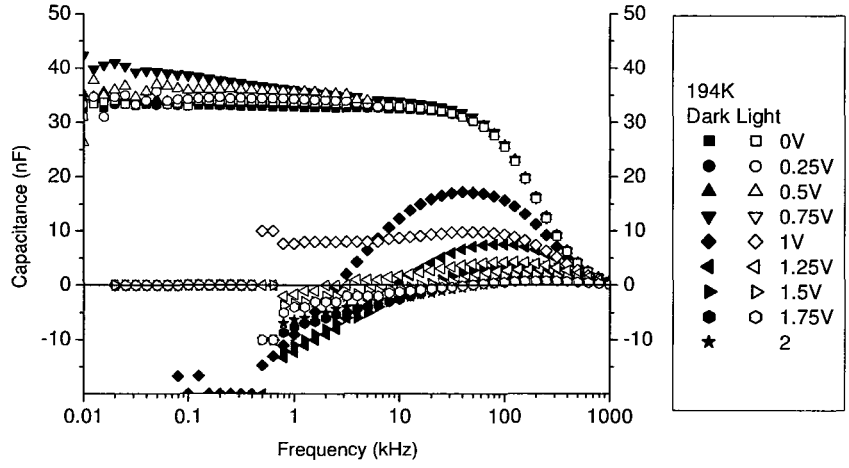

Figure IV.6: *capacitance in dark and light of the blend with LiF at 194K*

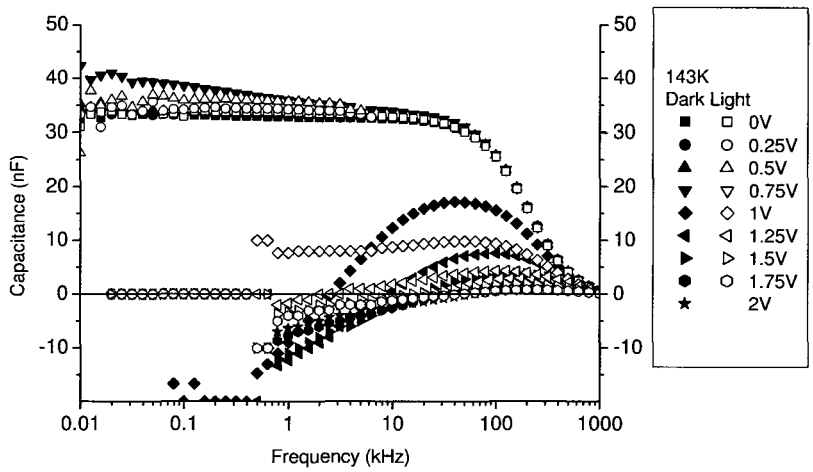

Figure IV.7: *capacitance in dark and light of the blend with LiF at 143K*

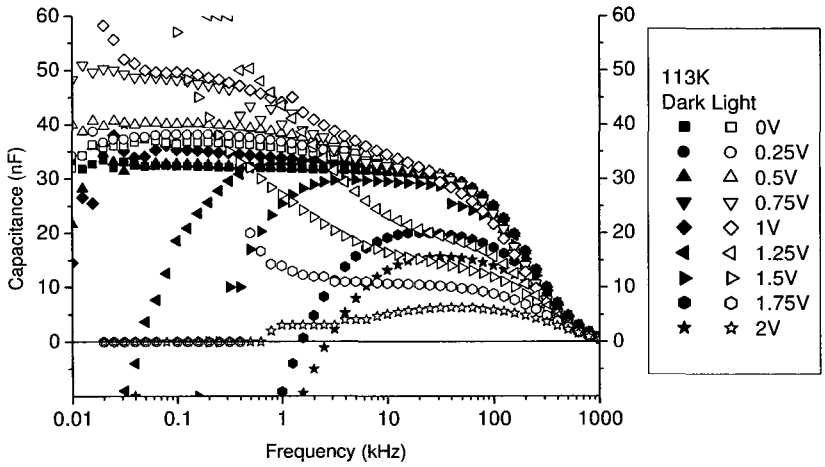

Figure IV.8: *capacitance in dark and light of the blend with LiF at 113K*

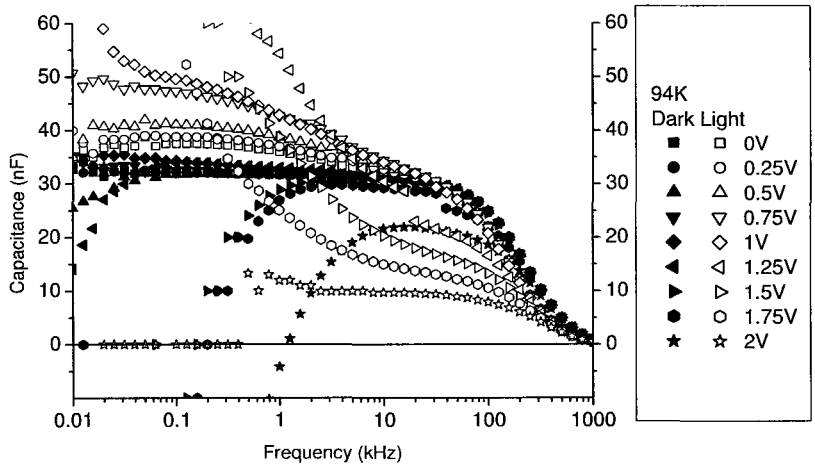

Figure IV.9: *capacitance in dark and light of the blend with LiF at 94K*

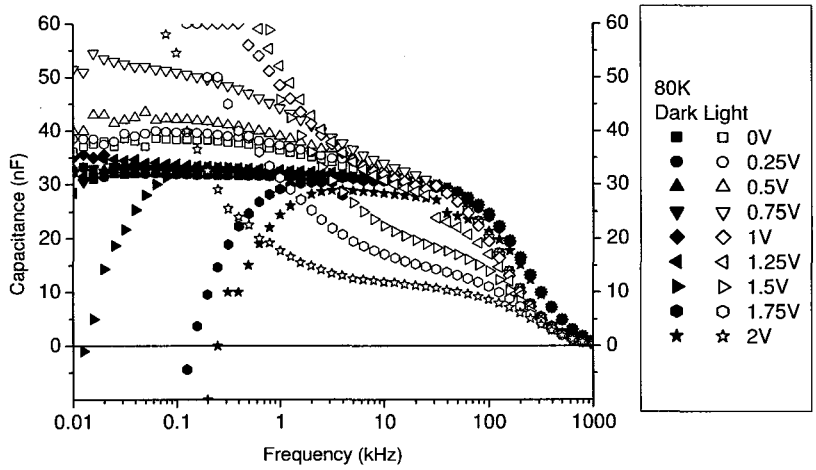

Figure IV.10: *capacitance in dark and light of the blend with LiF at 80K*

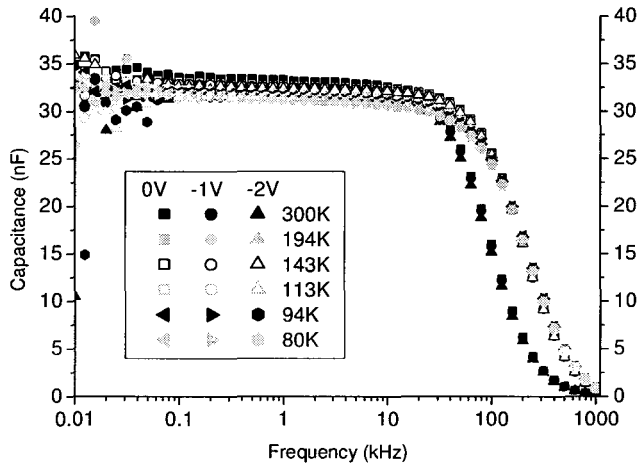

Figure IV.11: *capacitance in dark of the blend with LiF at negating voltages*

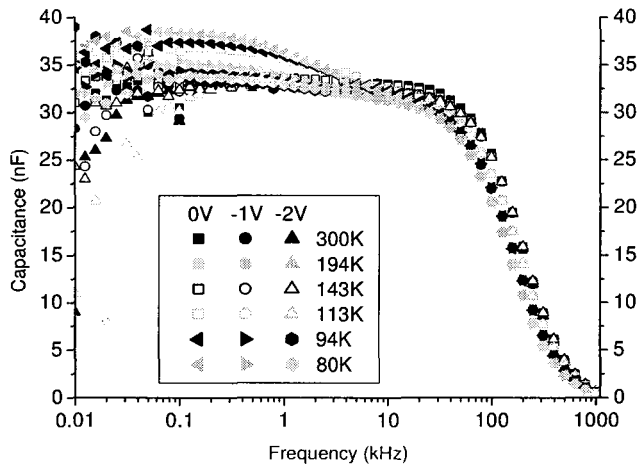

Figure IV.12: *capacitance in light of the blend with LiF at negating voltages*

IV.3: Conductance

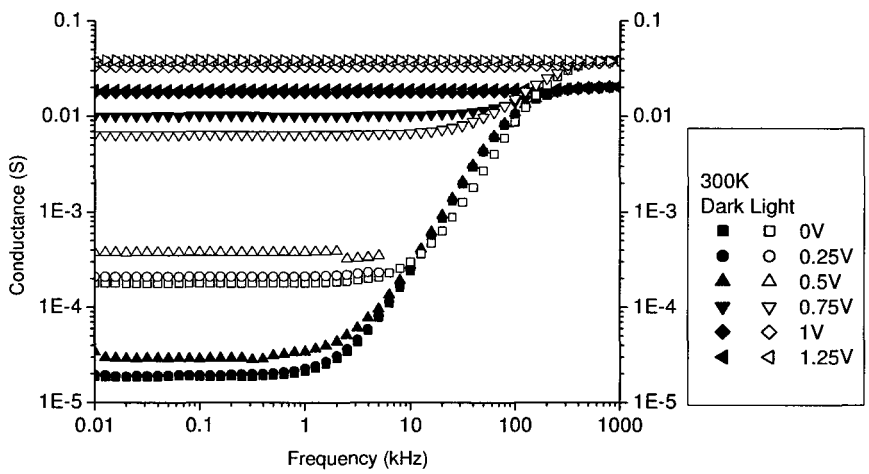

Figure IV.13: *conductance in dark and light of the blend with LiF at 300K*

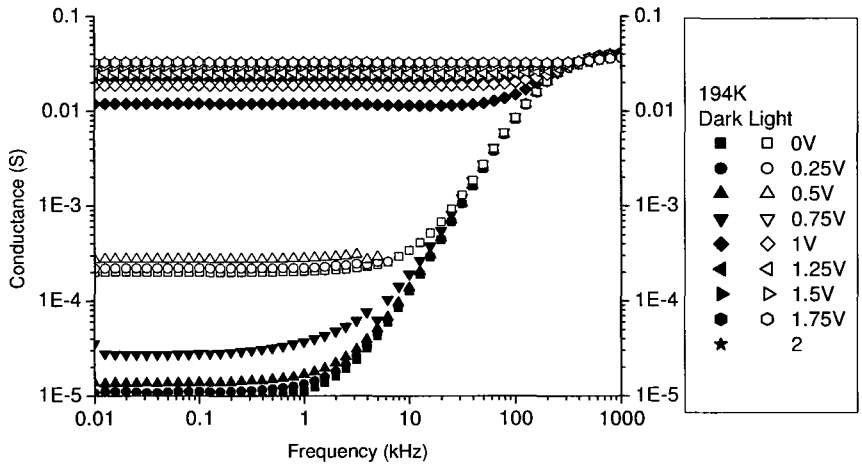

Figure IV.14: *conductance in dark and light of the blend with LiF at 194K*

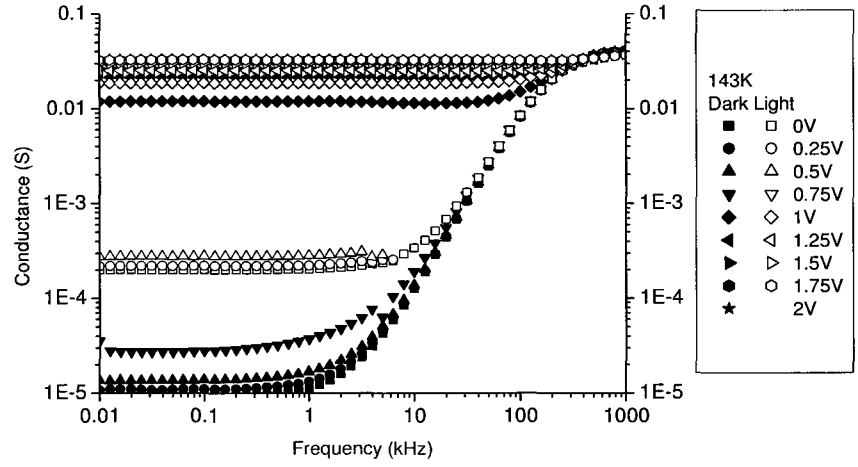

Figure IV.15: *conductance in dark and light of the blend with LiF at 143K*

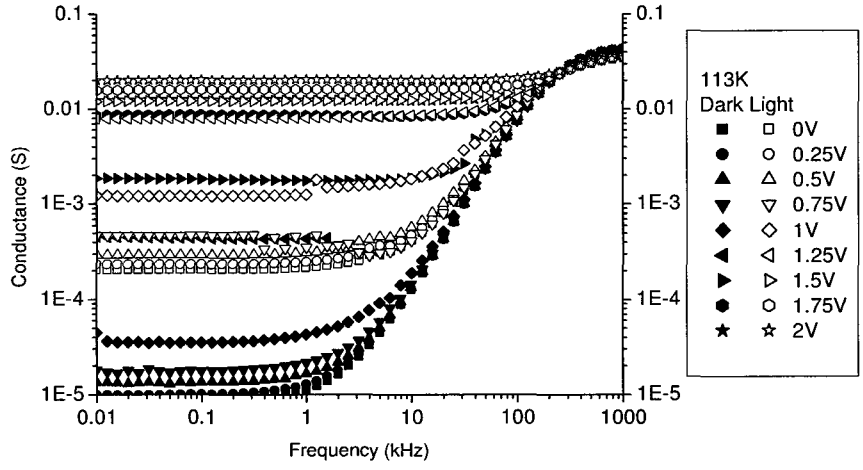

Figure IV.16: *conductance in dark and light of the blend with LiF at 113K*

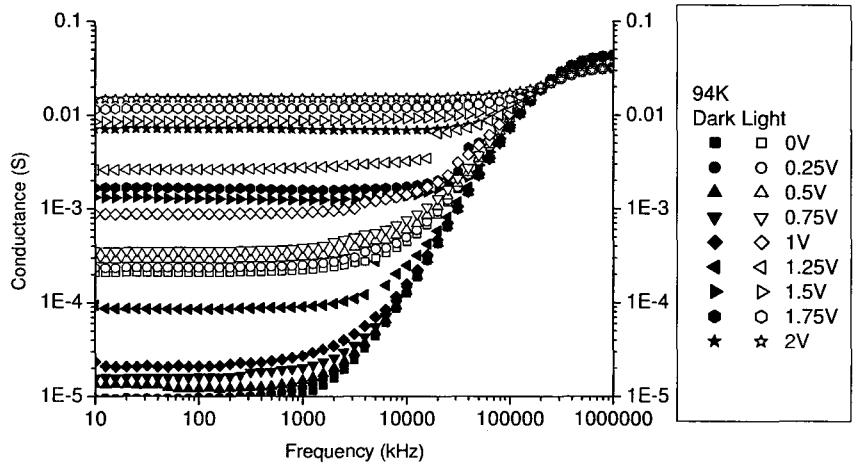

Figure IV.17: *conductance in dark and light of the blend with LiF at 94K*

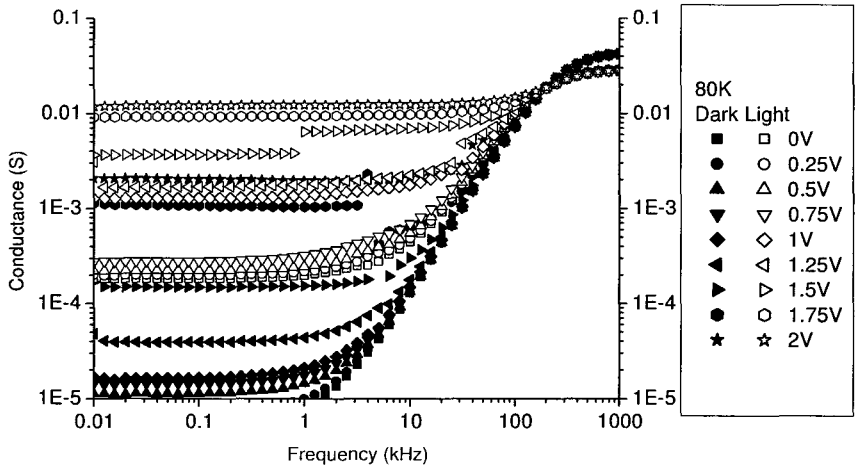

Figure IV.18: *conductance in dark and light of the blend with LiF at 80K*

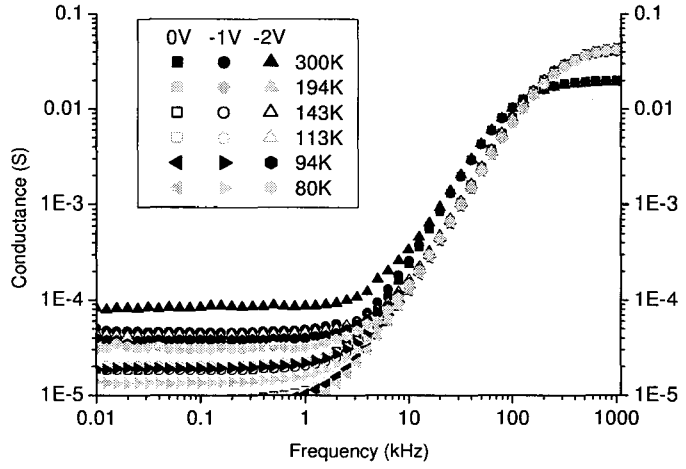

Figure IV.19: *conductance in dark of the blend with LiF at negative voltages*

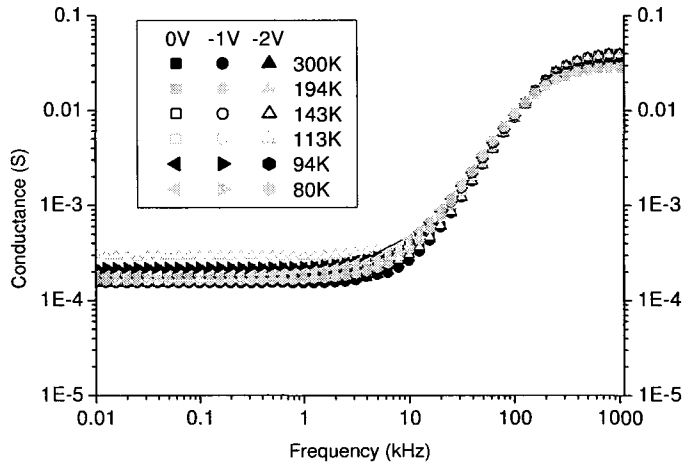

Figure IV.20: *conductance in light of the blend with LiF at negative voltages*

Appendix V: PPV without LiF

All measurements were on the same sample of 17 December

V.1: IV-measurements

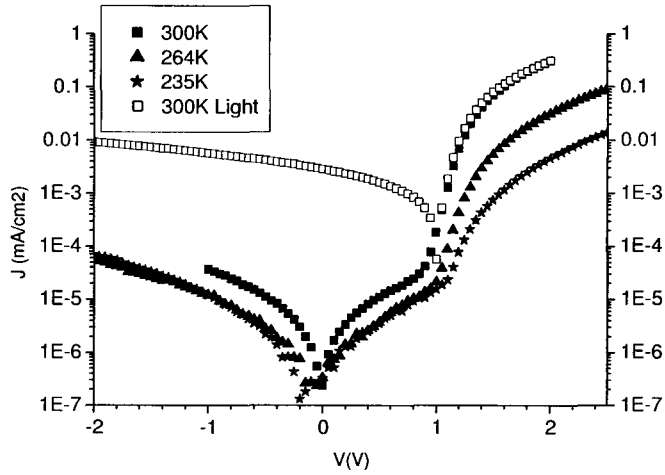

Figure V.1: *I-V measurements on PPV in light and dark for different temperatures. All measurements are on the same sample*

V.2: Capacitance

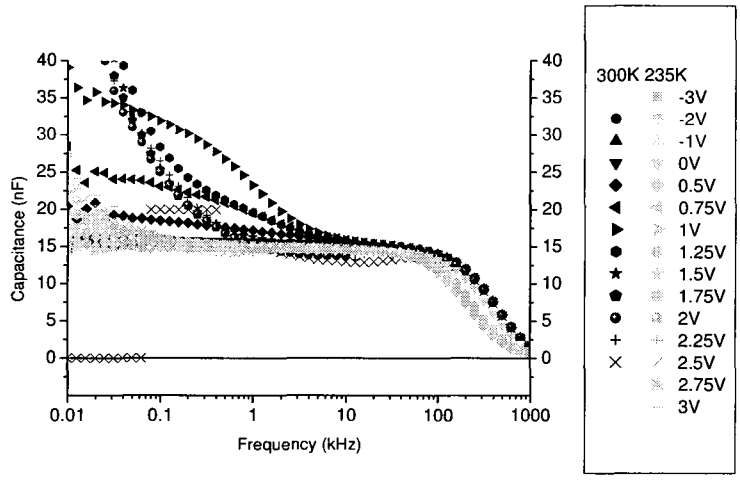

Figure V.2: *Capacitance of PPV in dark without LiF at different temperatures*

V.3: Conductance

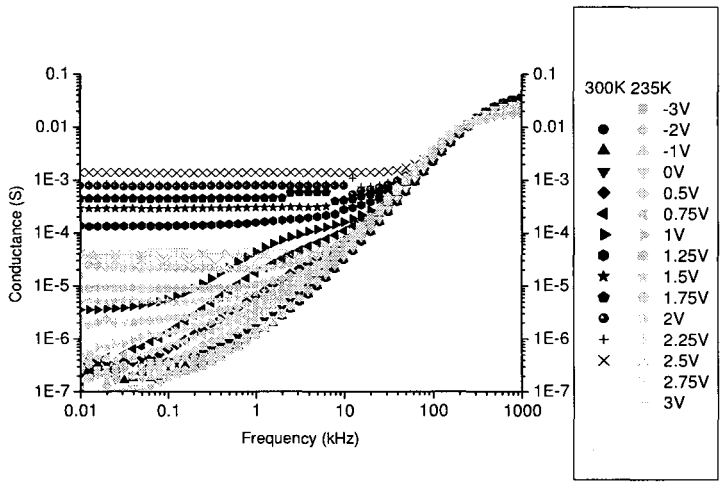

Figure V.3: *Conductance of PPV in dark without LiF at different temperatures*

Appendix VI: PCBM without LiF

All measurements were on the same sample of 18 November that has a surface of 0.90cm^2.

VI.1: IV-measurements

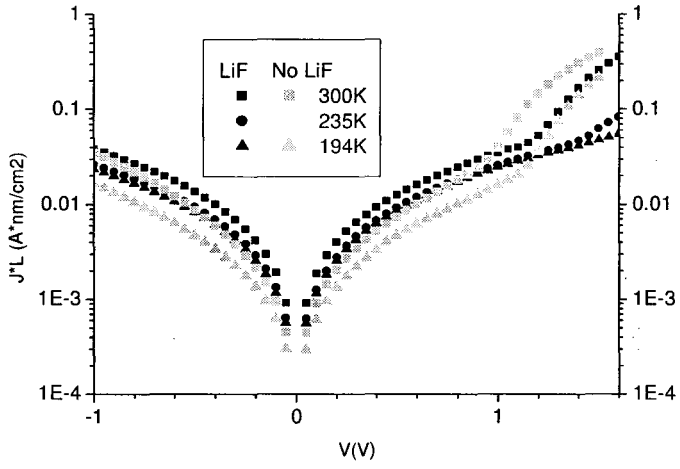

Figure VI.1: *I-V measurements on PCBM in dark for different temperatures*

VI.2: Capacitance

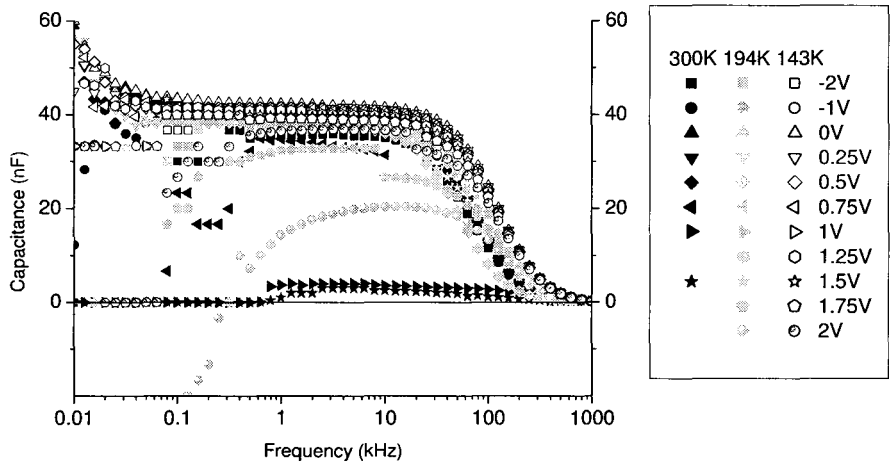

Figure VI.2: *Capacitance of PCBM in dark without LiF at different temperatures*

VI.3: Conductance

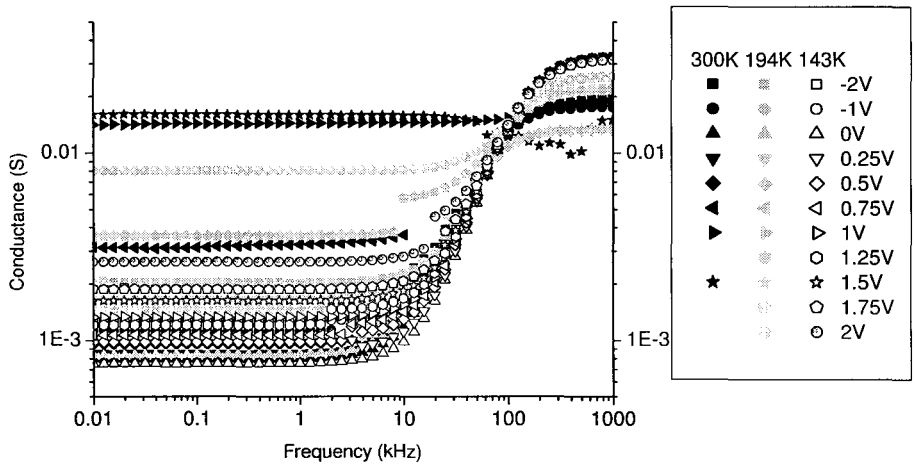

Figure VI.3: *Conductance of PCBM in dark without LiF at different temperatures*

Appendix VII: Blend without LiF

All measurements were on the same sample of 19 October.

VII.1: IV-measurements

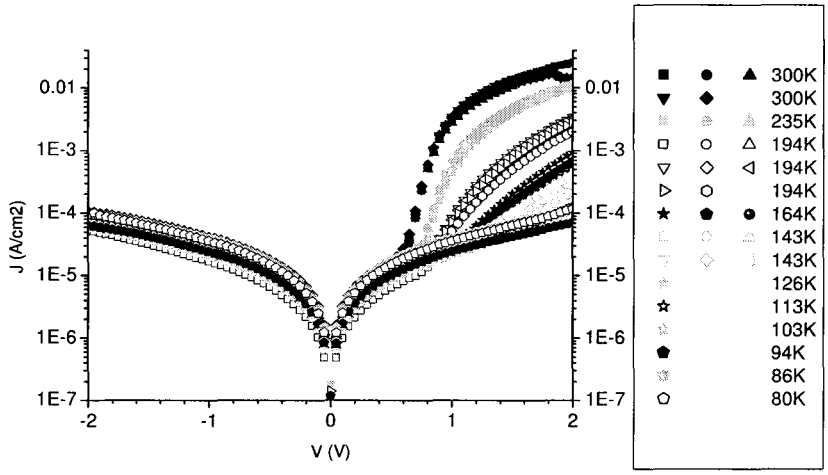

Figure VII.1: *I-V measurements on the blend in dark for different temperatures*

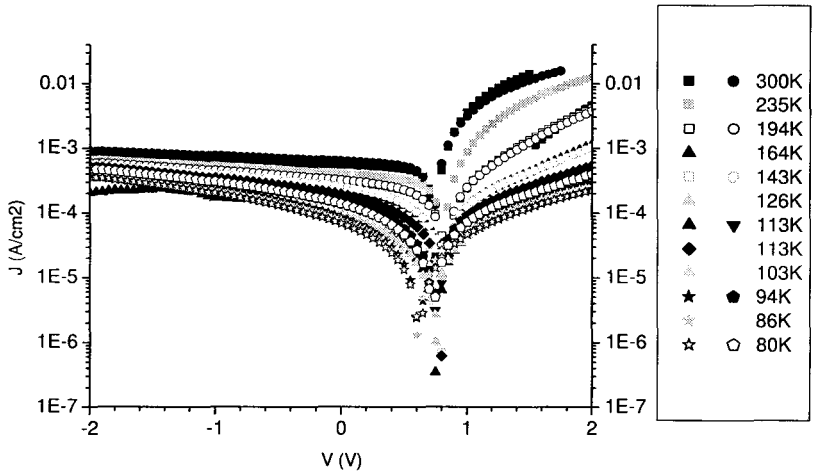

Figure VII.2: *I-V measurements on the blend in light for different temperatures*

VII.2: Capacitance

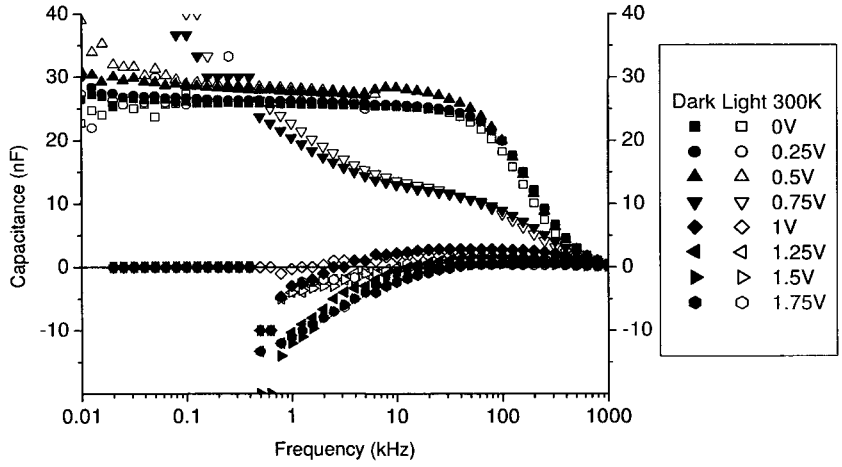

Figure VII.3: *capacitance in dark and light of the blend without LiF at 300K*

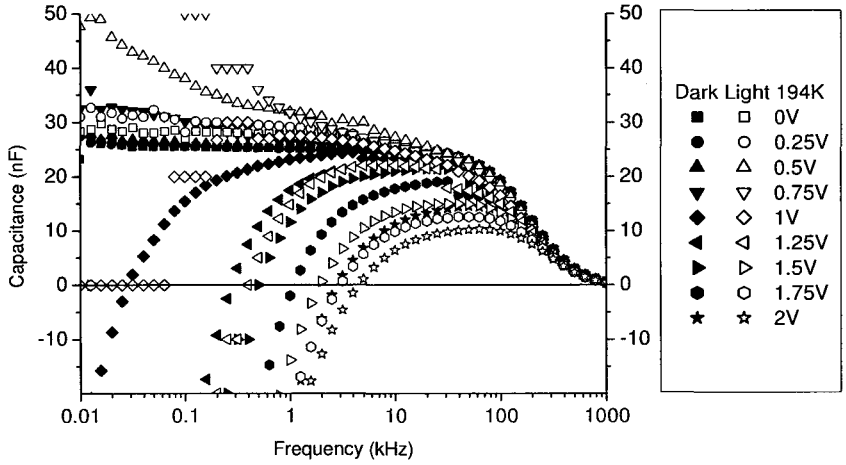

Figure VII.4: *capacitance in dark and light of the blend without LiF at 194K*

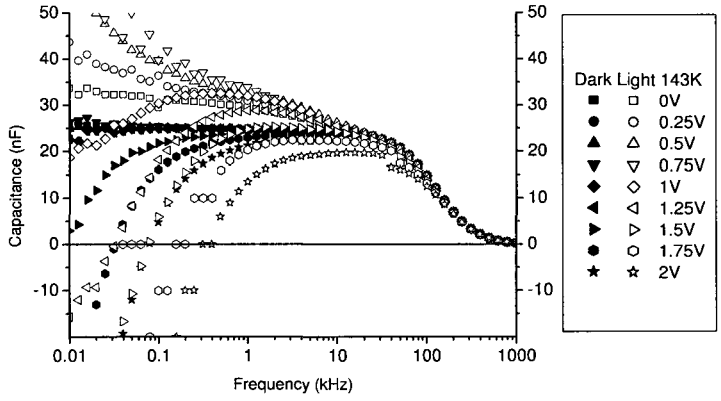

Figure VII.5: *capacitance in dark and light of the blend without LiF at 143K*

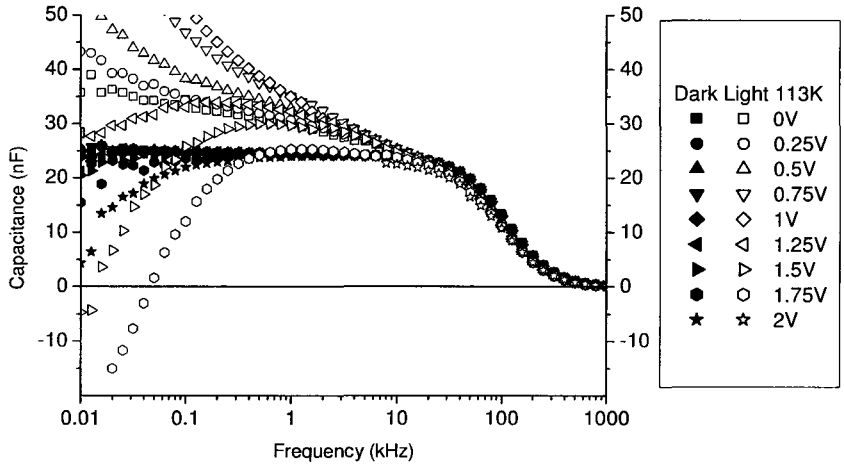

Figure VII.6: *capacitance in dark and light of the blend without LiF at 113K*

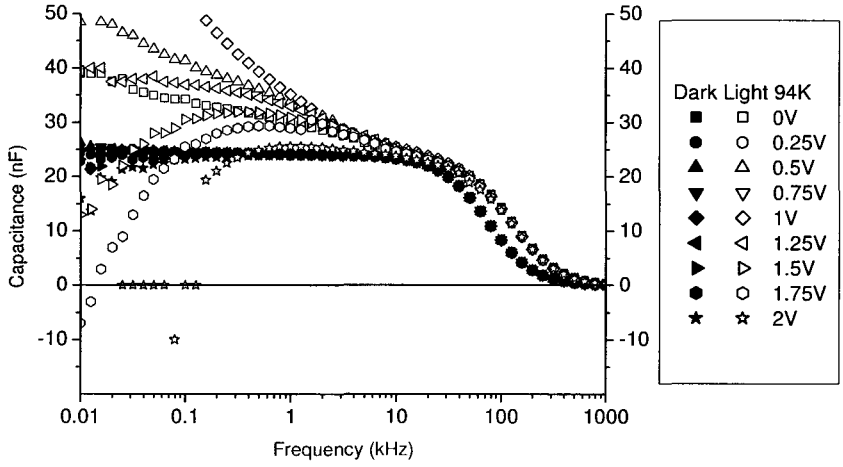

Figure VII.7: *capacitance in dark and light of the blend without LiF at 94K*

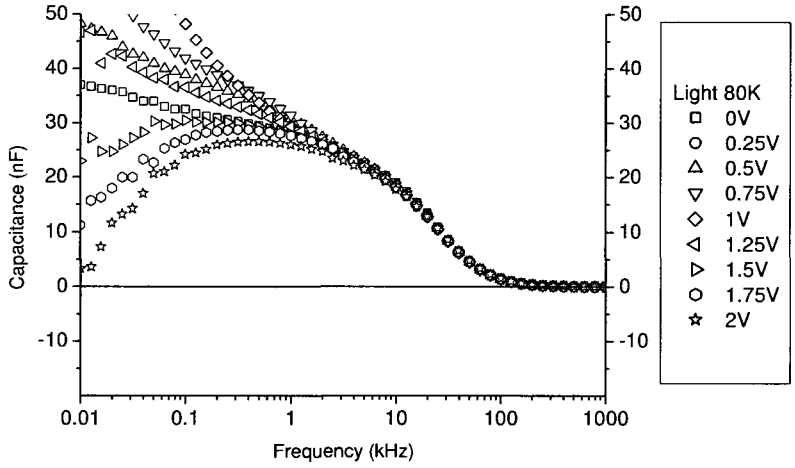

Figure VII.8: *capacitance in light of the blend without LiF at 80K*

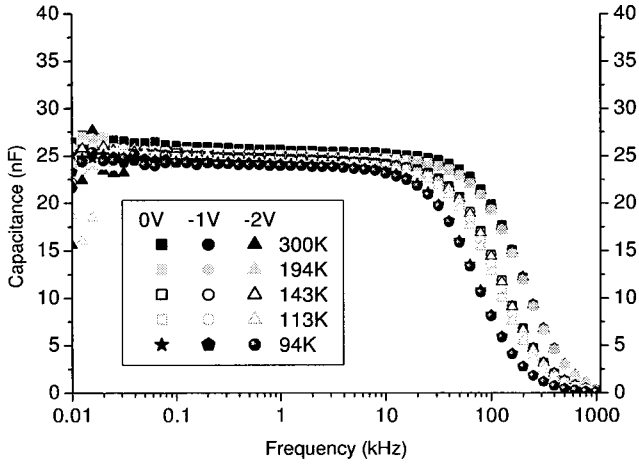

Figure VII.9: *capacitance in dark of the blend without LiF with negative voltages*

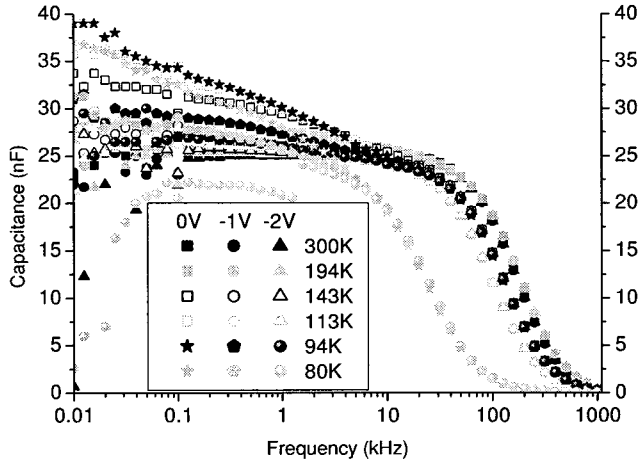

Figure VII.10: *capacitance in light of the blend without LiF with negative voltages*

VII.3: Conductance

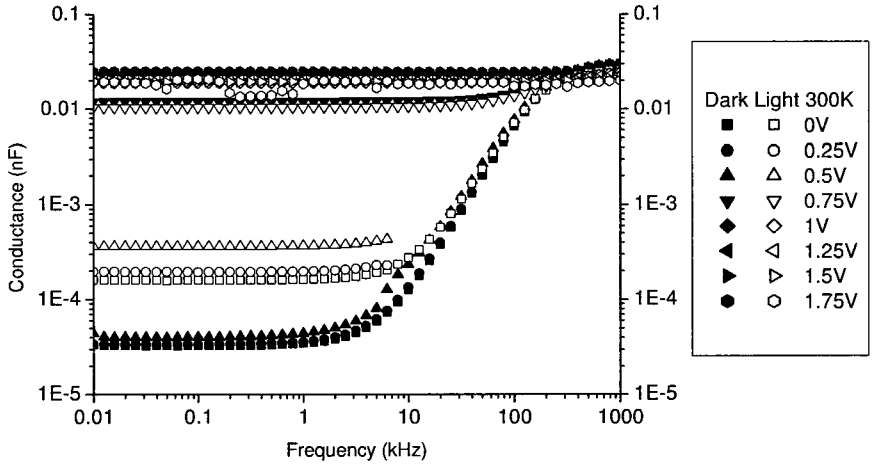

Figure VII.11: *conductance in dark and light of the blend without LiF at 300K*

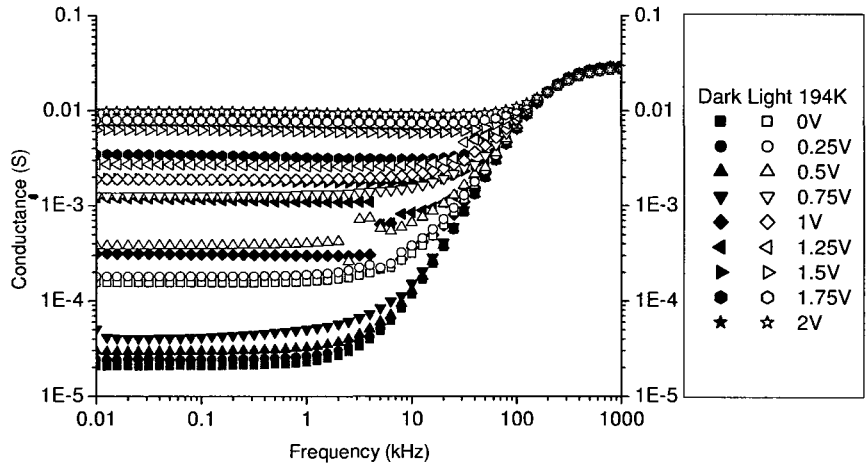

Figure VII.12: *conductance in dark and light of the blend without LiF at 194K*

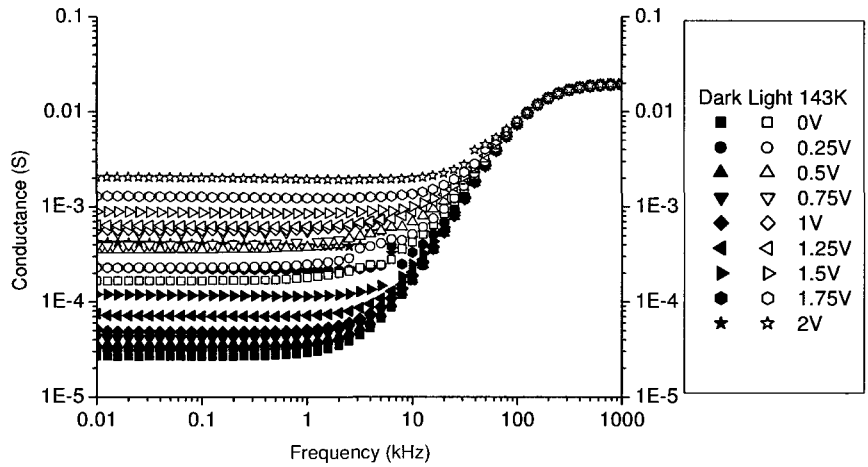

Figure VII.13: *conductance in dark and light of the blend without LiF at 143K*

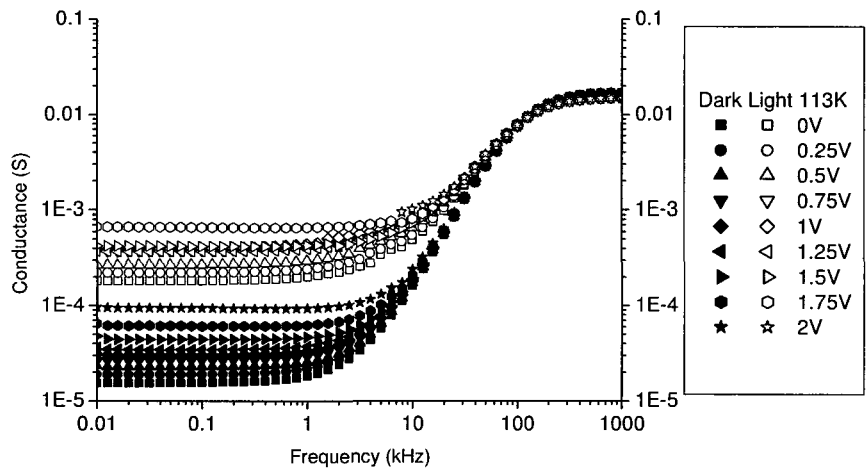

Figure VII.14: *conductance in dark and light of the blend without LiF at 113K*

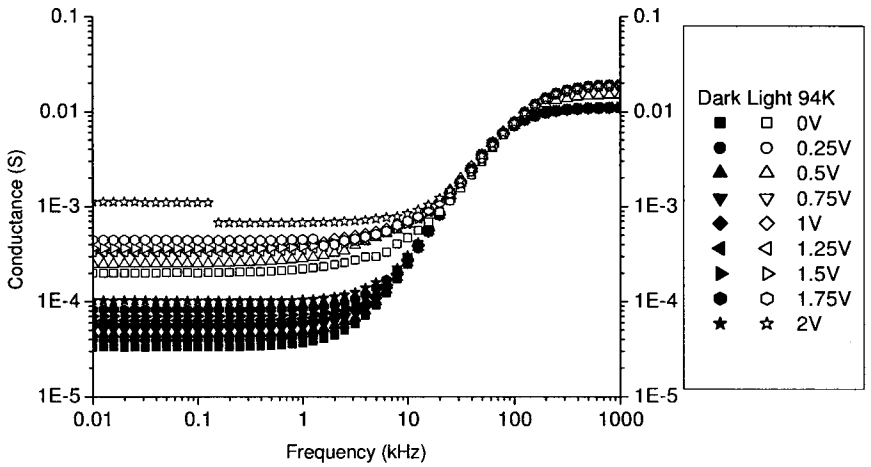

Figure VII.15: *conductance in dark and light of the blend without LiF at 94K*

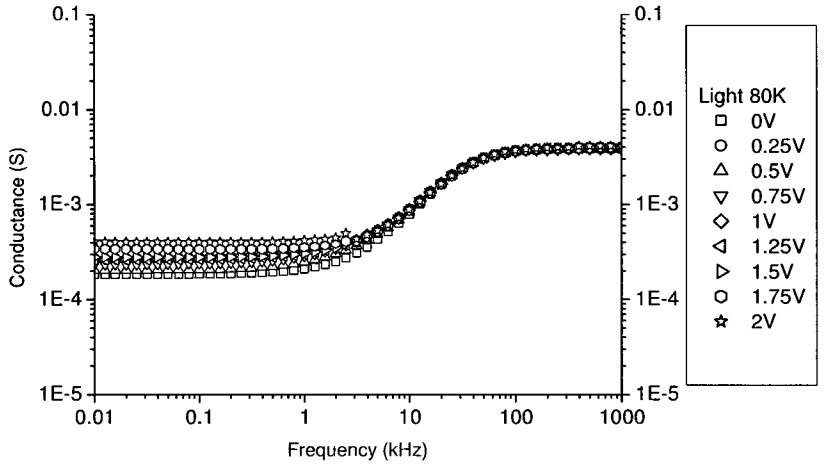

Figure VII.16: *conductance in light of the blend without LiF at 80K*

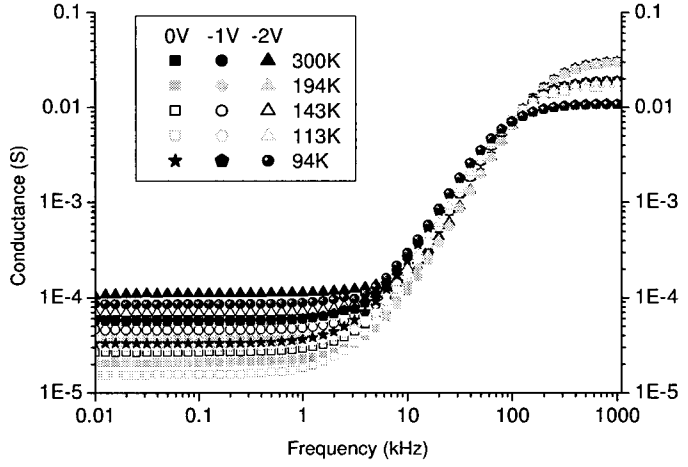

Figure VII.17: *conductance in dark of the blend without LiF at different voltages*

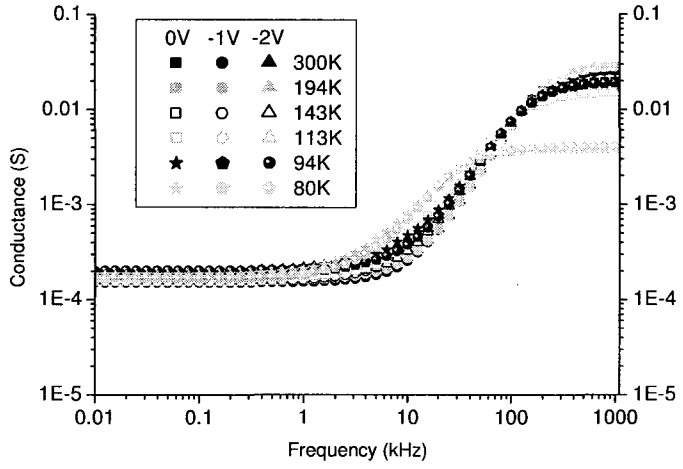

Figure VII.18: *conductance in light of the blend without LiF at different voltages*